STRUCTURE, MICROSTRUCTURE AND MAGNETO-DIELECTRIC PROPERTIES OF BARIUM TITANATE-FERRITE BASED COMPOSITES

A THESIS SUBMITTED IN PARTIAL FULFILLMENT
OF THE REQUIREMENT FOR THE DEGREE OF

Master of Technology (Research)

in

Ceramic Engineering

by

SREENIVASULU PACHARI

under the guidance of

Dr. Bibhuti B. Nayak and Dr. Swadesh K. Pratihar

Department of Ceramic Engineering
National Institute of Technology Rourkela
Odisha – 769 008, INDIA

December 2015

DEDICTAED TO

My parents

Date:

CERTIFICATE

This is to certify that the thesis entitled "Structure, microstructure and magneto-dielectric properties of barium titanate-ferrite based composites" submitted by Mr. Sreenivasulu Pachari, for the award of the degree of Master of Technology (Research), to the National Institute of Technology, Rourkela, is a record of bonafide research work carried out by him under our guidance and supervision at Department of Ceramic Engineering, NIT Rourkela.

In our opinion, the thesis has fulfilled all the requirements according to the regulations and has reached the standard necessary for submission. The results embodied in the thesis have not been submitted for the award of any other degree.

(**Bibhuti B. Nayak)**
Associate Professor
Head of the Department
Department of Ceramic Engineering
National Institute of Technology
Rourkela, ODISHA – 769 008, INDIA
Tel: 91-661-246 2209; Fax: 91-661-247-2926
Email: bbnayak@nitrkl.ac.in (or) bibhutib@gmail.com

(**Swadesh K. Pratihar)**
Associate Professor
Department of Ceramic Engineering
National Institute of Technology
Rourkela, ODISHA – 769 008, INDIA
Tel: 91-661-246 2206; Fax: 91-661-247-2926
Email: skpratihar@nitrkl.ac.in (or) skpratihar@gmail.com

Date:

DECLARATION

I hereby declare that the work presented in the thesis entitled **"**Structure, microstructure and magneto-dielectric properties of barium titanate-ferrite based composites**"** submitted for Master of Technology (research) Degree to the National Institute of Technology, Rourkela has been carried out by me at Department of Ceramic Engineering, National Institute of Technology, Rourkela under the supervision of Dr. Bibhuti Bhusan Nayak and Dr. Swadesh Kumar Pratihar. The work is original and has not been submitted in part or full by me for any degree or diploma to this or any other University/Institute.

Sreenivasulu Pachari
Department of Ceramic Engineering
National Institute of Technology, Rourkela
ODISHA – 769008, INDIA

ACKNOWLEDGEMENTS

It is with the most sincere thanks to who helped me to make this thesis possible.

I wish to express my deep sincere gratitude to my advisor prof. Bibhuti B. Nayak for his inspiring guidance, constructive criticism and valuable suggestion throughout the research work. I would also like to thank Prof. Swadesh Kumar Pratihar for his inspiring support and valuable suggestions.

I express my sincere thanks to Head of the Department, Ceramic Engineering for providing me all the departmental facilities required for the completion of the project work. I am also thankful to *Prof. Arun Chowdhury* and all other faculty members of the Department of Ceramic Engineering, NIT Rourkela for their constructive suggestions and encouragement at various stages of the work. My sincere thanks to all non-teaching staffs in Department of Ceramic Engineering for providing full of high- spirited delight in the lab and helping me throughout this project.

Last but not least, I would like thank to my senior research scholars and friends Subrat, Jayarao, Ganesh, Nadiya, Chandra Sekhar, Abhishek, Shubham, Raju, Venki, Abhi, Sowiji, Soumya and all other research scholars of the ceramic departments who have patiently extended all kinds of help for accomplishing this work.

Sreenivaslu Pachari
(Roll No: 613CR3001)

CONTENTS

ABSTRACT

Magneto-dielectric composites materials are those which perform both magnetic and dielectric properties in one single component. Due to the coupling between the ferroelectric and ferromagnetic, the magnetization can be controlled by an applied electric field, while the electric polarization can be controlled by applying a magnetic field. The phase connectivity and phase morphology plays an important role in the modifying the magneto-dielectric properties of the composites. Synthesis method is great tool to explore the microstructure and magneto-dielectric properties of the composites.

In present work three synthesis methods were adopted to prepare magneto-dielectric composites. They are combustion derived solid-state mixing, combustion derived in-situ synthesis method. $BaTiO_3$ selected for the ferroelectric phase which is having moderate properties of permittivity, loss, piezoelectric constant. $CoFe_2O_4$, ZnFe2O4 and $Co_{0.5}Zn_{0.5}Fe_2O_4$ are selected for ferrite phase, which are hard, soft and non-magnetic in nature respectively. Ferrite weight percentage was used in magneto-dielectric composites at 20%, 30%, 40%. Structure, microstructure and magneto-dielectric properties of composites were studied and analyzed. Dielectric, magnetic and magneto-dielctric properties of composites varied significantly by varying synthesis method. Traces hexagonal $BaTiO_3$ has been detected when tetragonal $BaTiO_3$ sintered along with ferrites. Plate like morphology of $BaTiO_3$ was evolved along with nearly spherical morphology of $BaTiO_3$ in solid-state derived composites, but no evidence of plate like $BaTiO_3$ in in-situ composites. Cobalt ferrite based composite shows negative magneto-capacitance response in both solid state and in-situ synthesis, which not in other ferrite systems of solid-state and in-situ derived composites.

Along with the solid-state and in-situ synthesis methods, ex-situ synthesis method was also adopted to explore in present magneto dielectric composites. Typical 30 wt% ferrite ($CoFe_2O_4$, $ZnFe_2O_4$ and $Co_{0.5}Zn_{0.5}Fe_2O_4$) composites were made in this method. Microstructural study shows large no of plate like $BaTiO_3$ exists in ferrite@BT composites than BT@ferrite composites. Cobalt and zinc ferrite based ex-situ composites show both positive and negative magneto capacitances in 7BT@3(CF/ZF) and 3(CF/ZF)@7BT composites respectively. Cobalt zinc ferrite based ex-situ composite show the positive magneto-capacitance in both 7BT@3CZF and 3CZF@7BT. Magneto-capacitance responses are dependent on both magnetostriction and magnetoresistance. Magneto-capacitance values of about -1.48%, -1.08%, 19.9% and -2.1% were observed in 7BT$3CZF, 7BT#3CZF, 7BT@3CZF and 3CZF@7BT composites respectively. Similarly 9.91%, 19.76% and 19.9% were observe in 7BT@3CF, 7BT@3ZF and 7BT@3CZF composites respectively.

Keywords: *Magneto-dielectric; Composite; Morphology; Magneto-capacitance; Ferroelectric; Ferrites; Combustion synthesis; Solid-sate mixing; In-situ; Ex-situ; Microstructure.*

List of Figures **Page No**

List of Tables **Page No**

Chapter 1

GENERAL INTRODUCTION

Technological advancements originate from the innovative research in the field of materials science based on materials physics and chemistry. Smart materials are those which perform multi functions at a time, which can save time and energy. Combining two different characteristic components to one object, it shows multifunctional properties. Multi functionality of material can be achieved and controlled by careful selection of individual components or compounds and combining them efficiently to appropriate scale and degree. Present work concentrates on the combining dielectric and magnetic materials to develop magneto-dielectric composite systems.

1.1 Magneto-dielectric materials:

Magneto-dielectric materials are those which perform both magnetic and dielectric properties in one single component. Due to the interaction between the ferroelectric and ferromagnetic, the magnetization can be modified by an applied electric field, while the electric polarization can be tailored by applying a magnetic field. Apart from the magneto-dielectric effect, these materials can also have permeability and permittivity in single material, in other words it can say as inductive and capacitive properties. Magneto-dielectric effect is kind of analogous to the multiferroic phenomenon where polarization can be controlled by magnetic field [1]. Large coupling effect results in the magneto-dielectric composites by large piezoelectric constant, large magnetostriction and large interfacial area between the phases. Though individual compounds in the composite systems have large piezoelectric and magnetostriction constant, lack of interaction in the composites may result in the poor magneto-dielectric effect. Microstructural development in the composite via different synthesis methods plays an important role in the resulting effect. In the history of magneto dielectric composite, first barium titanete-cobalt ferrite was made by the unidirectional solidification, which was done under precise control of composition of elements and temperature. [2] Small change in parameters can eventually change the resulting properties in those tough processes, and then scientists look for the better properties in the simple processes available. Many available synthesis methods used in different combinations of magnetic and dielectric phases gave the interesting results for further investigation in magneto-dielectric composites. [3]

Geometry of individual phases in composites plays an important role in deciding the final microstructure and properties of the composites. From the traditional classification of composites, it is easy to give the notations to the composites, which depend on the continuity of each phase in three dimensional spaces. [4,5] Most of the composites come under thin films, thick films or bulk composites. Except the bulk composites, remaining involves precise parameter controlling and heavy equipment handling. Bulk composites are mainly particulate category in which the composites are made up of particles (from nano to micro). Both compounds in the composite should maintain the homogeneity in nano or micro level. One of the properties such as magneto-dielectric or magneto-capacitance response of the composite is measured as the percentage change in the capacitance, in the presence of the DC magnetic field [6].

$$magneto - dielectric\ \% = \frac{\varepsilon(H) - \varepsilon(H=0)}{\varepsilon(H=0)} * 100$$

where Ɛ(H) - permittivity in magnetic field.

Ɛ(H=0) - permittivity without magnetic field

1.2 Ferroelectric phase:

In the magneto-dielectric composite, ferroelectric materials is used as the dielectric. Ferro electricity arises from the non-centro symmetry in the crystal systems and spontaneous polarization even in the absence of the electrical field, which leads to the hysteresis loop with the residue polarization (remanence). The unit cell shape reorientation according to the field with change in the dimension makes the phenomenon of piezoelectricity. [7] Perovskite (such as $BaTiO_3$) is the one highly studied ferroelectric compound which can stabilize in tetragonal (ferroelectric) phase at room temperature and changes to cubic (paraelectric or nonpolar phase) above Curie temperature (T_C). Large piezoelectric co-efficient is necessary to obtain large magneto-dielectric effect, because the magneto-dielectric coefficient is a mechanical coupling effect.

1.3 Magnetic phase:

Magnetic nature of compounds divided according to the responses of the materials in the magnetic field and their susceptibility to magnetic field and applied in different fields [8]. Ferromagnetic and ferrimagnetic have the net magnetic movements when compared to other categories. When the ferro/ferri-magnetic materials exposed to the magnetic field, it shows the hysteresis loop, with the remanence magnetic movements even in the absence of the magnetic field. Long range ferromagnetic phenomenon will be lost about certain temperature called Curie temperature. Above this Curie temperature magnets lost their net magnetic movements and become paramagnetic materials. According to the coercivity (H_C) (magnetic field required to bring the remanance to zero), magnets are divide in to two categories, which are soft and hard magnets. H_C < 10 A/Cm: soft magnetic; H_C > 300 A/Cm: hard magnetic (permanent magnets)

Soft magnets are easy to magnetize and demagnetize, where as hard magnets require very high magnetic field to demagnetize [9].The property of magnetostriction is change in the dimensions of the magnet when exposed to the magnetic field till the saturation magnetization. As the magneto-dielectric effect is a mechanical coupling phenomenon it demand for a large magnetostriction coefficients and large saturation magnetization of the magnetic phase.

Chemical stability at high temperature of the ferroelectric phase and magnetic phases play good role in stabilizing of the individual phases, otherwise impurity phases can hamper the final results. So, in this research work, $BaTiO_3$ as a ferroelectric and ferrites ($CoFe_2O_4$, $ZnFe_2O_4$ and $Co_{0.5}Zn_{0.5}Fe_2O_4$) have been used to develop magneto-dielectric composite systems.

1.4 Applications of magneto-dielectric materials:

Magneto dielectric materials have both permittivity and permeability, which can be used as the capacitor and inductor applications respectively. Some other applications towards the multi functionality of the magneto-dielectric composites are [2]

1. Magnetic sensors
    a. AC magnetic field sensors
    b. DC magnetic field sensors
2. Transformers and gyrators
3. Microwave devices
    a. Tunable devices
    b. Resonators
    c. Filters
    d. Phase shifters and delay lines

1.5: Organization of thesis

The thesis consists of seven chapters. Chapter 1 summarizes introduction to the magneto-dielectric composites. Chapter 2 provides detail literature review based on synthesis, microstructure, and properties of composites. Chapter 3 provides detail experimental techniques used to develop magneto-dielectric composites. Chapter 4 provides a detail description of individual powders (barium titanate and ferrites) preparation via combustion method and characterizing with different techniques. Chapter 5, 6 and 7 contains the composites preparation in three different methods namely conventional solid state mixing of combustion derived powders, combustion derived in-situ synthesis method and combustion derived ex-situ synthesis methods, respectively. Summarizing the results and discussion of $BaTiO_3$-ferrite based composite systems and conclude in the last chapter.

References

1. M. N. Ul-Haq, T. Yunus, A. Mumtaz , V.V. Shvartsman, Doru C. Lupascu, "*Magnetodielectric effect in relaxor/ferrimagnetic composites*", J. Alloy. Comp, **640**, (2015), 462–467.
2. C. Nan, M. I. Bichurin, S. Dong, D. Viehland and G. Srinivasan, "*Multiferroic magnetoelectric composites: Historical perspective, status, and future directions*", J. Appl. Phys. **103**,(2008), 031101.
3. J. S Andrew, J. D. Starr and M. A.K. Budi, "*Prospects for nanostructured multiferroic composite materials*", Scri. Mater, **74**, (2014), 38–43.
4. R.E. Newnham, D.P. Skinner and L.E. Cross, "*connectivity and piezoelectric-pyroelectric composites*", Mat. Res. Bull. Vol. 13, pp. 525-536, 1978.
5. J. P. Praveen, T. Karthik, A.R. James, E. Chandrakala, S. Asthana, D. Das, "*Effect of poling process on piezoelectric properties of sol–gel derived BZT–BCT ceramics*", J. Eur. Cer. Soc. **35**, (2015), 1785–1798.
6. M. Rafiquea, S. Q. Hassana, M.S.Awan, S. Manzoor, "*Dependence of magnetoelectric properties on the magnetostrictive content in 0–3 composites*", Cer. Inter, **39**, (2013), S213–S216.
7. R. Aepuru and H. S. Panda, "*Adsorption of Charge Carriers on Radial Zinc Oxide and the Study of Their Stability and Dielectric Behavior in Poly(vinylidene fluoride)*", J. Phys. Chem. C, **118**, (2014) ,18868−18877.
8. N.K. Prasad, Lucile Hardel, Etienne Duguet, Dhirendra Bahadur, "*Magnetic hyperthermia with biphasic gel of $La_{(1-x)}Sr_xMnO_3$ and maghemite*", J. Magn. Mag. Mat, **321,** (2009), 1490–1492.
9. D. S. Mathew, R. Juang, "*An overview of the structure and magnetism of spinel ferrite nanoparticles and their synthesis in microemulsions*", Chem. Eng. Jour, **129**, (2007), 51–65.

Chapter 2

LITERATURE REVIEW

2.1 Synthesis of $BaTiO_3$:

Barium titanate ($BaTiO_3$) stabilizes in the tetragonal phase at the room temperature and different synthesis methods have been explored to develop $BaTiO_3$ in the non-centro symmetric structure with the least possible steps and energy. Raw materials, precise parameters in process control will eventually leads to the change in the properties of the $BaTiO_3$. Conventional solid-state, sol gel, coprecipitation, combustion, hydrothermal, microwave hydrothermal, polymer precursor and spray pyrolysis are the some of the routes to synthesize the $BaTiO_3$.

Huan et al [1] had prepared the $BaTiO_3$ via hydrothermal synthesis method and sintered in two steps and produced the different grain size of $BaTiO_3$ ranging from 0.29μm to 8.61 μm. It was reported that lattice parameter '*a*' and '*b*' decreased (3.9992Å to 3.9926 Å) and '*c*' parameter increases. Piezoelectric coefficient d_{33} was raised (4.0296 Å to 4.0358 Å) with increase in grain size. Permittivity and polarization was also observed to increase with increase in the grain size, where permittivity reached ~12000 F/m near the Curie temperature. The problem was the lacking of Ba^{2+} ions during washing of hydrothermal synthesized powders. This could be compensated by the excess Ba^{2+} ions in the initial composition, as suggested by the Huarui Xu et al [2]. In this case, the Ba/Ti ratio was taken as 1.6 and $TiCl_4$ as well as $BaCl_2{\cdot}2H_2O$ are used as the initial raw materials. The synthesis was followed by precipitating with the NaOH. In this case, higher tetragonality was observed when excess NaOH added. The cubic phase was observed when the particles are fine in nature. Lee et al[3] came up with a solution for problem of leaching Ba^{2+} ions during washing by using of saturated $Ba(OH)_2$ solution. In this case, $BaTiO_3$was prepared by using barium acetate and hydrolyzed titanium acylate in the ratio of 1.0 to 1.8. Apart from the Ba/Ti ratio, it was reported that surface area increased with the increase in the KOH (which used during precipitation). Highest Ba/Ti ratio of 0.932 was noticed in the sample which was prepared using Ba/Ti ratio of 1.8. Chen et al[4]., reported that temperature during hydrothermal process was significantly effect the leaching of Ba^{2+} ions from the solution. Nearly 72% of Ba ions leaching reduced due to increase in the synthesis temperature from 120 °C to 200 °C, and the phase of $BaTiO_3$ was found to be cubic in nature. Effect of ammonia in the phase stabilization of $BaTiO_3$ was studied by Moon et al[5]. Significant effect in the particle size reduction and increase in the tetragonality was reported in this paper when the ammonia was used during hydrothermal process, but anatase phase was stabilized in the core of $BaTiO_3$ particles. Raw materials play an important role in the deciding the microstructure of the phases. Boulos et. al., [6] reported that abnormal grain growth in the $BaTiO_3$ when Ti source changed from TiO_2 to $TiCl_3$ along with the $BaCl_2$. In most of

the hydrothermal processes Ba/Ti ratio was varied during washing and phase stabilizes in cubic form.

In hydrothermal synthesis, conventional electric heating was used to generate heat during synthesis. But the polarity of the solvents can also be used to heat them in the presence of oscillating electromagnetic microwaves. Microwave heating uses the less power than the conventional heating and heat can be controlled very precisely. Jhunga et al., studied the effect of the Ba/Ti ratio, OH^-/Ti ratio and H_2O/Ti ratio using the $BaCl_2 \cdot 2H_2O$ and $TiCl_4$ as the precursor materials. It was reported that microwave heating results lower crystallite size than the conventional hydrothermal heating. Also, crystallite size increased with the increase in the reaction time. Size of the crystallite decreased with decrease in the Ba/Ti ratio. Also, water concentration had the significant effect on the crystallite size. Lower the water in the reaction lowers the crystallite size (15nm at $200H_2O$/Ti ratio and 25nm at $400H_2O$/Ti ratio). It was also reported that morphology of $BaTiO_3$ appears no much difference in both microwave and conventional heating.

Barium carbonate was one of the impurities that can be seen generally in hydrothermal synthesized powders and it was due to the dissolved carbon dioxide in the distilled water or carbon dioxide present in the autoclave chamber when reaction proceeds in the presence of air. Newalkar et al.,[8] studied the effect of the KOH and NaOH in the microwave hydrothermal synthesis of $BaTiO_3$ by using $BaCl_2 \cdot 2H_2O$ and $TiCl_4$ as main precursors. Traces of $BaCO_3$ in the powders were found even varying the temperatures using KOH and NaOH. Particle size of $BaTiO_3$ was found to be higher when KOH was used as a precursor. Auto combustion synthesis one of the energy and time saving technique used to produce the phase pure compounds using metal nitrates. Anuradha et al.,[9] synthesized the $BaTiO_3$ with different barium sources like BaO_2, $Ba(NO_3)_2$ and $Ba(CH_3COO)_2$ and $TiO(NO_3)_2$ as the titanium source. Carbohydrazide, citric acid and glycine are used as fuels. It was reported that citric acid and glycine gave the more gases and resulted in the great porosity.

2.2 Synthesis of Magnetic phases:

Spinal ferrite can be synthesized using the Coprecipitation method, solid-state method and gel-combustion method. Rathore et al [10] synthesized the $CoFe_2O_4$ nanoparticles via coprecipitation method using $CoCl_2 \cdot 6H_2O$ and $FeCl_3 \cdot 6H_2O$ with desired molar fractions in the solution. Finally ferrite particles formed in different particles sizes of 5.8 nm to 28.6 nm. Lower the particles size gave the higher dielectric constant and vice versa and permittivity decreases with the increasing frequency. Loss angle was also followed the trend of decreasing loss with the decreasing particles size and vice versa. Lowest loss was observed in lowest particle size of 5.8 nm with 0.055 (tan δ) at 300 K. Morphological images show clear cubic shape of the ferrite phases. Sol-gel, micro-emulsion

and coprecipitation are the wet chemical methods studied well individually by Sinko et al.,[11] and perform the comparative study of among these synthesis methods using chloride and nitrate as raw materials. Ethylene acetate, citric acid and Polydimethylsiloxane were used as surfactants. It was reported that microemulsion synthesis method gave the highest particle size 390-440 nm and lowest in the sol-gel method (size of 70-100 nm). Effect of surfactant is not much pronounced in the particle size. Hematite was traced in the cobalt ferrite particles which was prepared in the coprecipitation method and sol-gel method. Sharifi et al., [12] done the comparative study among the coprecipitation, reverse micelles and normal micelles synthesis of cobalt ferrite particles using $CoCl_2$ and $FeCl_3$. $CoCl_2.6H_2O$ and $FeCl_3.6H_2O$ used for the micelles method. Normal micelles formed by using the sodium dodecyl sulfate as surfactant and methylamine used to precipitate the compound. In reverse micelles process oils (petroleum oil, pyridine with water and alcohol) were used. Micelles and reverse micelles synthesis methods gave the crystallite size nearly half of co-precipitated synthesis method. Synthesis method had the significant effect on the magnetic properties of particles. Lower the particle size lesser the saturation magnetization was observed. Finer particles have lack of the domain wall, so saturation magnetization is less compared to the larger sizes. A comparative study between hydrothermal and co-precipitation was studied by Khorrami et al.,[13]. $(Co(NO_3)_2.6H_2O)$, and $(Fe(NO_3)_3 .9H_2O)$ were used as raw materials. Crystallite (33nm) of the hydrothermally prepared is half of the co-precipitate (15nm) method. Saturation magnetization has no affect on the particle size but coercivity is three fold in co-precipitated method when compared with hydrothermal method. Microwave synthesis gained its attention due to low energy consumption to synthesize the compounds. Bensebaa et al., [14] have synthesized the cobalt ferrite using cobalt (II) acetate tetrahydrate and iron (III) chloride as raw materials. Microwave along with the reflux set up was used to synthesize the particles at 160 °C. Temperature dependent magnetic properties show that saturation magnetization and coercivity increases by increasing temperature. 5nm is the average crystallite size obtained, which conformed by TEM and scherrer formula. TGA data reveals that total of 16% weight loss in the hating process due to evaporation of some organic matter. Temperature dependent magnetization measurement was done between low temperature to 300 K, which magnetization increased with the temperature till 250 K and then decreased. Comparative study among the different ferrite (Cobalt, Co-Zn and Ni-Zn) was performed by the Kima et al., [15] using microwave hydrothermal method. $NiCl_2 \cdot 6H_2O$, $ZnCl_2$, $FeCl_3 \cdot 6H_2O$ and $CoCl_2 \cdot 6H_2O$ used to obtain the required compound. All the samples (ferrite) gave the pure phases below 200 °C (microwave process). Increase in the lattice parameter with the increase in the Zn content was observed, which attributed to large cationic radius of Zinc. Narrow particle size distribution of ferrites was observed in the range of 80 to 12 nm.

In combustion synthesis technique, fuel is supplied with the raw materials and heat developed during the combustion of fuels useful to produce the compounds. This method is highly energy saving and time saving. One can select the fuel according the temperature required in the synthesis method. Heat produced in the synthesis proportionate to the type of fuel and percentage fuel in the composition. Hajarpour et al.,[16] synthesized the $Mg_{0.6}Zn_{0.4}Fe_2O_4$ soft ferrite using the combustion synthesis method. Author selected glycine as the fuel which has the high heat of combustion (-3.24Kcal/g). Fuel to nitrate ratio was taken 0.37 to 0.75. Lattice parameters observed to increase with fuel to nitrate ratio till 0.55 and decreased gradually with further increase in fuel. Saturation magnetization and coercivity increased with the increase in the fuel. Lower the fuel resulted in the lower crystallite size.

Cobalt ferrite is ferrimagnetic material and zinc ferrite is non-magnetic material with no magnetic movement. Combination of these magnets gave the ferrimagnetic material. Vaidyanathan et al.,[17] prepared the $Co_{1-x}Zn_xFe2O4$ ferrite with x=0 to 1. All metal chloride raw materials weighed to stoichiometric ratio and precipitated with the help of NaOH, followed by washing and drying. Lattice constant increased (8.385Å to 8.45 Å) with the increasing zinc concentration, which author attributed that Zn has the more ionic radius than the Co. Crystallite size reduced (12nm to 7nm) with increasing the Zn substitution. Saturation magnetization (45.30 Am^2/kg to 7.82 Am^2/kg), remanence magnetization (10.973 Am^2/kg to 0.014 Am^2/kg) and coercivity (27.076 kA/m to 0.014 kA/m) decreased with the increase in the Zn substitution. Being Zn is a diamagnetic atom, substitution can make magnet towards nonmagnetic. Raut et al.,[18] used the combustion synthesis to synthesize the Co_xZn_{1-x} Fe_2O_4 with varying zinc percentages at 0.0, 0.2, 0.4, 0.6, 0.8 and1. Nitrates (Fe $(NO_3)_39H_2O$, Co $(NO_3)_26H_2O$ and Zn $(NO_3)_2$ were used for the combustion synthesis along with citric acid($C_6H_8O_7$) as fuel of 1:3 (1 mole of compound/3 moles of citric acid). Authors reported that at 150 °C water evaporated and large loss in weight at 350 °C due to the decomposition of NO_3. Zn substitution made the unit cell dimensions to increase along with the percentage Zinc, but the crystallite decrease with the addition of Zinc. Saturation magnetization, coercivity and remanance decreased with the substitution of Zinc. Sivakumar et al., [19] also used the combustion synthesis method to used produce the $NiFe_2O_4$; along with calculated citric acid. Authors used the ethylene glycol and polyvinyl alcohol (PVA) in the combustion. Amount of 0.5 and 0.25g of PVA variations in the combustion was taken for the study. Crystallite sizes were reported as 24 nm and 30 nm for the higher and lower PVA weights. Saturation magnetizations of the samples were reported as 47.323 emu/g and 51.3 emu/g for higher and lower PVA weights. Bahadur et al., [20] had synthesized the $BaFe_{12}O_{19}$ in the auto combustion synthesis using $Ba(NO_3)_2$ and $Fe(NO_3)_3 \cdot 9H_2O$ as raw materials. Citric acid as fuel was taken at 1, 2 and 3 times to the metal

ions in the composition. Among the three fuel ratios, one with double citric acid to the metal ions gave the highest values of saturation magnetization (55emu/g), remanence (28 emu/g). Authors had claimed that 1:2 metal to fuel ratio is suitable for $BaFe_{12}O_{19}$ synthesis and giving better magnetic properties.

2.3 Synthesis of magneto-dielectric composites:

Any composite materials are designed to enhance the properties of the individual constituents in the composites. In some composites a new effect (product property) was arrived due to the mutual interaction between the constituents. Mathematical calculations could give the ideal geometry of composite that can give large effects, but chemistry involved in the synthesis method restrict the geometry to some extent. Synthesis method and constituents play an important role in development of the geometry and microstructure of composite. Composite structures broadly divided in the two categories, which are bulk, films and nano structures.

2.3.1 Inorganic Films on substrates:

Chemical deposition method, pulse laser deposition method, electro phoretic deposition technique are the some of the methods used to produce the magneto-dielectric composites films. Chemical deposition method involves the dispersion of compound in a solvent and applying the films using spin coating, dip coating and spray coating methods. These methods can be used to coat the composite compound directly or coating individual compound layer by layer.

2.3.1.1 Chemical deposition method:

Dai et al., [21] synthesized the $BaTiO_3$ (BTO)–$CoFe_2O_4$ (CFO) multilayer film on $Pt/Ti/SiO_2/Si$ (100) substrate using the chemical deposition method. Barium acetate and titanium phthalic acid n-butyl were used as precursors the $BaTiO_3$. Iron nitrate nona hydrate and cobaltous acetate were used as the precursors for the precursors for the $CoFe_2O_4$. 2-Methoxyethanol and acetic acid were used as the solvents along with the Ethanolamine which used for adjusting viscosity. Authors used spin coating technique to lay the films. Alternative BTO and CFO layers were coated by firing individual layers to control the diffusion. Author reported that strain and lattice constants decreased with the increasing BTO layer thickness, but in the case of CTO it has behaved in reverse. Author attributed that phase relaxation can be happened with increase in thickness (BTO). PE loop characteristics like saturation polarization, coercivity and romance increased with the molarity in the precursor solution. Magnetic saturation was high for the sample with 0.2M solution. Author reported that sample with 0.3M has micro cracks, so it showed less response. Highest magneto-dielectric response was reported for the samples 0.1M of 0.45% at 1MHz.

2.3.1.2 Electro phoretic deposition technique:

Electro phoretic deposition technique was used to produce the films. Charged particles may be attracted to the opposite charged electrodes. Thickness depends on the voltage deference, time of deposition and concentration of ions in the solution. Any organic solvent could be used instead of water. Water produces the hydrogen and oxygen gases during the process. As the chemical solution deposition method, this method can also use to produce layers of different compounds by changing the suspension.

Zhang et al.,[22] produced the $CoFe_2O_4$–$BaTiO_3$ thick layers via electro phoretic deposition method, by varying cobalt ferrite percentage 0.2 to 0.8 volume fraction. Individual powders were mixed in desired molar ratio and dispersed with a solvent. Due to unsmooth surface, thick films pressed at 200 Mpa for 5 minutes followed by firing at 1100 °C for 30 minutes. Higher the percentage higher the cracks in the composite were observed. Temperature dependent dielectric constant showed no Curie temperature hump due to highly porous structure influenced the interactions of $BaTiO_3$ with the temperature and also ferrite phase has influence on the phase transition $BaTiO_3$. Increases in the dielectric constant with increase in ferrite as well as loss increasing with temperature were due to the Maxwell-Wagner interfacial polarization effect. Author reported that poor responses from the composite were due to the uncompact and disproportionate deposition of composite.

In the EPD suspension, problem of agglomeration of magnetic particle give the different composition than expected. Solvent plays important role in the sedimentation of individual compounds. Zhou et al., [23] studied the influence of the suspension concentration, deposition time and voltage on the thickness of the film. Nearly 14 solvents were examined by the group to find the suitable one; authors came up with acetylacetone as the better among the examined solvents to sediment less amount in standard time. Thickness of the layer decreased with the time, because electrodes become more resistive if the thickness increased. Surfactant has no significant effect on the sedimentation and thick ness of the layer. PE loop saturated hardly and saturation polarization was found to be ~15μc/cm^2. Reported saturation magnetization, remanent and coercivity are 148.7 emu.cm−3, 70.2 emu.cm−3 and 2412 Oe respectively. Jian et al.,[24] investigated the electrical and magnetic properties of $BaTiO_3$/$CoFe_2O_4$ films. $BaTiO_3$ was prepared by using barium acetate, titanate butoxide in sol-gel method, ferrite phase was prepared via co-precipitating using chloride salts. Acetylacetone and ethanol used as solvent. Final composite films annealed at 600 for 20 min. Multi ferroic property like ME coefficient reported to have 3.9 mV/cmOe at 2245 Oe. PE loops shows saturated hardly. Saturation magnetization, remanence and coercivity were reported as 25 μc/cm^2, 20.4 μc/cm^2 and 240 kV/cm, respectively.

2.3.1.3 Pulse laser deposition technique:

Pulse laser deposition is the technique to grow the compounds on a substrate. High energy laser beam strikes the dense target and evaporated molecules and will condense on nearer substrate.

Aguesse et la.,[25] produce the multi-layer thin films of the $BaTiO_3$(BTO)-$CoFe_2O_4$(CFO) by using dense samples of $BaTiO_3$ and $CoFe_2O_4$ at target place, and calcined finally at 1100 °C for 5h. Ba $(Fe_{10}Ti_2)O_{19}$ along with the cubic phases of barium titanate (cubic phase due to dopants in the barium titanate structure) and cobalt ferrite was detected. Number of bi layers strongly affected the magnetic properties of the film. Lesser the layers more the magnetic response observed, author explained that distribution of cobalt in the tetrahedral and octahedral sites disturbed due to the thermal annealing and leads to the poor response. Authors faced the problem of decrease in the saturation magnetization with increasing the bilayer stack, so this leads to reduce he response of the ME coefficient. $SrTiO_3$ layer between the BTO and CFO layers reduced the diffusion between BTO and CFO layers, because $SrTiO_3$ was chemically stable with CFO than the BTO. This technique gave the 20 % increase in the magnetic properties. Kim et al.,[26] grown the thin films of the $0.6BaTiO_3$-0.4 $CoFe_2O_4$ by using the pre-prepared composite in the solid state method. Authors found that low pressure deposition of phases gave poor results, high pressure deposition made the compounds to deposit slowly and distinctly.

2.3.2 Particulate composites:

Particulate synthesis is easiest among the available synthesis methods for development of composites. Making the compounds individually in different synthesis methods and mixing them to require composition gives the good control over the percentage of constituents using in the composites. Leonel et al., [27] studied the different synthesis methods in making $BaTiO_3$: $CoFe_2O_4$ composite system. Two synthesis methods mainly used for the making of composite, one mixing the individual powders and another one is to disperse the pre calcined ferrite powder in the $BaTiO_3$ precursor solution. Hexagonal and orthogonal phases detected in the barium titanate phase which fired alone for solid state synthesis. In composite hexagonal phase detected. Ferrite crystallite sizes lower in the composite when compared with the ferrite which fired alone. Barium titanate has higher the crystallite size when used in the composite, particularly in composites which made by dispersing the ferrite particles in to the barium titanate precursor solution. Khamkongkaeo et al.,[28] studied the magneto electric properties of the barium titanate-cobalt ferrite composites made by simple grinding and mixing of solid state derived powders. Barium titanate varied at 30, 40, 50 and 60 volume percentages. $Ba_2Fe_2O_5$ phase detected as impurity in all compositions. Due to prolonged sintering time of composites for 4 hours at 1200 °C gave the impurity phase. Author explained that, diffusion of Fe^{2+} and Fe^{3+} ions in to the Ti^{3+} give the impurity. Magnetic responses are proportional

to the ferrite phase in the composite. Magnetic saturation decreased with the increasing barium titanete phase and coercivity increased with the increase in the barium titanate phase. ME coefficient was higher for the 0.5 volume percentage barium titanate composite, but 0.3 volume percentage barium titanate composite show ME coefficient near to the 0.3 volume fraction composite. ~7mV/A ME response achieved by the 0.3 volume fraction barium titanate composite. Agarwal et al., [29] synthesized the $BaTiO_3$(BTO)-$CoFe_2O_4$(CFO) composite in the solid state method, with variation of ferrite from 0.1 volume fraction to 0.6 volume fraction. Magnetic properties are proportional to the ferrite percentage in the composite. Ferrite gave the 80 emu/g saturation magnetization, but when used along with the barium titanate it decreased (to 32 emu/g) for 50 volume percentage of barium titanate. Maximum ME coefficient observed is 15.6 mV/cmOe (for 50 vol % BTO composite).

Fina et al., [30] studied the magneto-capacitance response in the $BaTiO_3$–$CoFe_2O_4$ composites (thin films made by sputtering). Nearly 2% change in the magneto capacitance observed in the composites and the measured resistance did not change much with the magnetic field. Loss of the composite varied sinusoidally with the magnetic field. Results show ME response is frequency dependent, which has highest response at lower frequency. Rafiquea et al., [31] studied the ME response with respect to the magnetostriction properties of the composite, synthesized mixing of sol-gel derive powders. Magneto-capacitance of the composite increased with the increase in ferrite content and response saturated at lower frequency, but increased with the magnetic field. ~8 mV/cmOe was the highest reported ME response in the 50 mol% composite.

Change in dielectric constant and permittivity was observed by Yang et al.,[32] in the $BaTiO_3$/$Ni_{0.8}Zn_{0.2}Fe_2O_4$ composite prepared by solid state method. X-ray diffraction pattern revealed the hexagonal barium titanate in the composites, which increased with the increase in the ferrite content. Barium titanate appeared in rod like morphology. Diffusion of Fe^{3+} ions in the $BaTiO_3$ structure leads to the hexagonal structure. Author reported that interfacial polarization between two phases in the composite gave the high dielectric constants. Loss in the composites followed the percentage of ferrite. Higher the ferrite gave the higher loss and loss increased with the frequency. Zheng et al.,[33] prepared $BaTiO_3$ and $Ni_{0.5}Zn_{0.5}Fe_2O_4$ composites in solid state mixing of sol-gel ($BaTiO_3$) and combustion ($Ni_{0.5}Zn_{0.5}Fe_2O_4$) synthesized powders, followed by sintering at 1220 °C for 3hours. Hexagonal barium titanete formed in the composite, which author attributed to lower charged cation substitution at Ti^{3+} sites. Ferrite lattice constants decreased with the increase in barium titanate concentration. $Ni_{0.5}Zn_{0.47}Fe_2O_4$ and $BaTiO_3$ composites prepared by Zhenga et al.,[34] using combustion technique and sol gel method, respectively by varying ferrite percentage. Hexagonal barium titanate with rod like structure formed in the all compositions, which

substitution of lower charged Fe^{3+}, Zn^{2+} and Ni^{2+} ions at the higher charged Ti^{4+} sites. Frequency dependent permittivity measure and observed to decrease with the frequency and loss is proportional to the ferrite percentage in the composite. Densities of composites increased with increase in the ferrite percentage also increased with the sintering temperature, but at higher ferrite percentage density decreased with the increasing temperature.

2.3.2.1 In-situ and ex-situ synthesis methods:

The technique of producing compounds in single step, called as the in-situ synthesis methods. Molten salt synthesis, combustion synthesis and one pot method are some of the synthesis methods to produce compounds in in-situ method.

Nie et al.,[35] used the molten salt synthesis method to produce the $CoFe_2O_4$–$BaTiO_3$, using oxides as raw materials. High dielectric constants observed in the lower frequencies due to the space charge polarization and Max-Well interfacial polarization. Large area enclosed in PE loop for 0.65 volume fraction barium titanate indicates that loss is higher. 2.531 % and 1.295 % are the losses for the 0.65 and 0.5 volume fraction (barium titanate) composites. ME- coefficient of maxium 17.04 mV/cmOe was reported for 0.5-0.5 composite. One pot method is also a kind of in-situ method to produce the magneto-dielectric composites. In this method all the nitrates according to the stoichiometry will be dissolved in distilled water along with the stabilizer and chelating agent. Ren et al., [36] prepared the (BTO) $BaTiO_3$/(CFO) $CoFe_2O_4$ composites in the one pot method in the volume ratio of 4:1 (BTO:CFO). All the raw materials (except titania source, which took in $Ti(OC_4H_9)_4$ form) in the nitrate form are dissolved in the water along with the EDTA as solution stabilizer with citric acid. Viscous gel was formed due to continuous stirring under heating (70 °C), gel was the dried and calcined to develop phases. Authors prepared another composite in the solid state mixing for comparison. Microstructure difference reported by the authors when compare between solid state synthesis and one pot method. Ferrite particles in solid state method look agglomerated and in one pot method ferrite particles divided individually. Maximum ME effect reported in one-pot method synthesis composite is 2540mV/cmOe. Authors reported that agglomerated ferrite particles in solid-state synthesis make the channels for conductivity and make them hard for poling and finally decrease ME coefficient. Deng et al., [37] produced feather like $CoFe_2O_4$–$BaTiO_3$ composites using hydrothermal method and polymer-assisted deposition method. Reported Saturation polarization (P_s) and remanent polarization of composite are 10.5μC/cm^2 and 5.6μC/cm^2 respectively. Saturation magnetization (M_s), remanent magnetization (M_r) and coercivity (H_c) values of composite reported as 21 emu/g, 10.4emu/g and 560 Oe respectively. Ahmed et al.,[38] prepared the composites in two different methods one is by insitu sol-gel method and other one is by solid state mixing of individual compounds. Microstructure show clear and distinct

difference between the microstructures which in-situ method synthesized composite has better distribution. Solid-state method shows better magnetic properties than in-situ. Iordan et al., [39] prepared the $CoFe_2O_4$–$Pb(ZrTi)O_3$(PZT) composite in the in-situ process. Composite formed by dispersing the PZT particles (already prepared and calcined) in the combustion synthesis of cobalt ferrite. PZT crystallite size did not change much in the presence of the ferrite phase and remained in between 150-180nm. Author attributed high loss at lower frequencies to the space charge at hetro interfaces and giving raise to the Max well-Wagner polarization. Dielectric constant values reported are 550, 200 and 200 for the pure PZT, 0.1 and 0.3 vol % ferrite composites, which indicated that permittivity decreases with the frequency. Ferrite phase percentage dependent magnetic properties noticed which saturation magnetization from 40 emu/g to 30 emu/g when ferrite volume fraction changes from 0.3 to 0.1. Harnagea et al., [40] studied (0.7) $BaTiO_3$–(0.3) $Ni_{0.5}Zn_{0.5}$) Fe_2O_4 composite prepared in the dispersing the $BaTiO_3$ powders in the co-precipitation synthesis of $(Ni_{0.5}Zn_{0.5})Fe_2O_4$ (NZF). Dielectric constant study of the composite made the existence of the Maxwell-Wagner mechanism which conformed by the increasing dielectric constant with the temperature, author attributed that response to the thermally activated relaxation and conductivity.

Buscaglia et al., [41] prepared the Fe_2O_3@$BaTiO_3$ Core-Shell particles in the combination of sol-gel method and soft chemical method and sintered using spark plasma sintering. $BaTi_2O_5$, $BaFe_{12}O_{19}$, $Ba_{12}Fe_{28}Ti_{15}O_{84}$ formed as impurity, with undisturbed core and shell structure. Presence of impurities in the composites made composite M-H loop look double hysteresis. High dielectric response at low frequency attributed to the Maxwell-Wagner interfacial polarization.

Apart from the $BaTiO_3$- ferrite (maximum cobalt based ferrites) systems, researches also studied PZT (lead zirconate titanete) - $NiFe_2O_4$ [42], PZT- $CoFe_2O_4$ [43, 44], BZT (barium zirconate titanate) [45], BZT-BCT (barium calcium titanate) [46], ST (strontium titanate)- $NiFe_2O_4$ [47] were also investigated. Synthesis method was followed were solid state mixing and sintering [42, 44-46], SPS (spark plasma sintering) [43, 47] of as received powders, combination of sol-gel and co-precipitation method. $SrCO_3$ observed by Mojić-Lanté at al., [47] in ST- $NiFe_2O_4$ system. Dielectric properties of the composite was measure again its frequency to observed the dielectric relaxation[44] of available polarizations and how they behave in the presence of ferrite. Also dielectric measurement against temperature gives the phase transitions temperature of crystal structures. Authors described [46] the decreasing dielectric constant and loss with the frequency as (i) polarizations (ionic, space charge [43] and electronic) contribution at higher frequency ceases with increasing frequency, (ii) Hoping mechanism[44] between Fe^{2+}, Fe^{3+}, Co^{2+} and Co^{3+} (and other metallic ions) leads to oriental polarization and (iii) Maxwell–Wagner polarization theory [44,45] and Koops phenomenological model [44,45]. Rani et al.,[46] measured the dielectric constant against the frequency at room

temperature which reported to have highest permittivity of ~650 for the 0.1 volume fraction of ferrite and decreased with further addition of ferrite. Same phenomenon observed by the Rahman et al.,[45] in which permittivity for the pure ferroelectric BZT ranges at > 20×10^3 and decrese drastically with the increasing ferrite phase. Temperature dependent dielectric constant and loss studies performed on magneto-dielectric composites to study the transition temperatures (e.g.,curie temperature T_c[44], magnetic transition temperature[46]). PE loop characterizations in the magneto dielectric composite tuned by the percentage of ferrite and dielectric phase and used to study ferroelectric nature of composite. Authors described the increased coercivity in PE loop with the addition of ferrite due to pining of ferro electric phase by magnetic phase, which ceases the domain wall motion [46].

2.4 Statement of the problem:

From the critical review on various literatures, it may conclude that the combustion synthesis technique is advantageous for developing magneto-dielectric composite systems and very few literatures are available which are based on combustion derived in-situ and ex-situ synthesis. In addition, composites based on ferrites including $CoFe_2O_4$, $ZnFe_2O_4$ and $Co_{0.5}Zn_{.05}Fe_2O_4$ along with $BaTiO_3$ prepared via combustion derived in-situ and ex-situ synthesis have not been explored. Microstructural evolution of two phases ($BaTiO_3$ and ferrites) via these synthesis methods as well as magneto-dielectric properties of these composite have also not been explored.

2.5 Objective:

The objective of this research work focuses a comparative study of structure, microstructure and magneto-dielectric properties of $BaTiO_3$: ferrite ($CoFe_2O_4$, $ZnFe_2O_4$ and $Co_{0.5}Zn_{0.5}Fe_2O_4$) composites prepared via three different routes such as (i) conventional solid-state method using auto-combustion derived individual powders, (ii) auto-combustion derived in-situ composites and (iii) auto-combustion derived ex-situ composites.

Chapter 3

EXPERIMENTAL WORK

3.1: Introduction

Magneto-dielectric composites have been prepared using solution combustion synthesis method, which also called as self-propagating high temperature synthesis (SHS). This is one of the most promising techniques to produce variety and wide range of nanoparticles. Tailoring of properties according to the application can be possible due to available parameters in synthesis method. Conventional soli-state synthesis of powders includes high energy and time consumption.

.3.2: Raw materials:

For $BaTiO_3$ (barium titanate) synthesis, raw materials like $Ba(NO_3)_2$(Barium Nitrate), $TiO(NO_3)_2$(Titanyl nitrate), $C_6H_8O_7$ (citric acid), NH_4NO_3 (ammonium nitrate) $C_{10}H_{16}N_2O_8$ (EDTA) were taken in the 1:1:1.5:12:0.1 molar ratio. Similarly for $CoFe_2O_4$ (cobalt ferrite) synthesis $Fe(NO_3)_2.9H_2O$ (Ferric Nitrate nona hydrate), $Co(NO_3)_26H_2O$ (Cobalt nitrate hexa hydrate) and $C_6H_8O_7$ (citric acid) are taken in the 2:1:3 molar ratio. For $Co_{0.5}Zn_{0.5}Fe_2O_4$ (Cobalt Zinc ferrite) synthesis $Fe(NO_3)_2.9H_2O$ (Ferric Nitrate nona hydrate), $Co(NO_3)_2.6H_2O$ (Cobalt nitrate hexa hydrate), $Zn(NO_3)_2.6H_2O$ (Zinc nitrate hexa hydrate), $C_6H_8O_7$ (citric acid) are taken in the 2:0.5:0.5:3 molar ratio. For $ZnFe_2O_4$ (Zinc ferrite) synthesis $Fe(NO_3)_2.9H_2O$ (Ferric Nitrate nona hydrate), $Zn(NO_3)_26H_2O$ (Zinc nitrate hexa hydrate) and $C_6H_8O_7$ (citric acid) are taken in the 2:1:3 molar ratio.

3.2.1: Preparation of $TiO(NO_3)_2$ solution

Amount of 40 grams of $(NH_4)_2SO_4$ was dissolved in 120 ml of concentrated H_2SO_4 with under constant heating and stirring (glass rod). When it gets clear solution, 5 grams of TiO_2 was added slowly by vigorous stirring with glass rod. After it got dissolved, cool the solution to room temperature. The prepared $TiO(SO_4)$ solution was added to 500 ml chilled distilled water (because reaction is exothermic). Now set up cold bath on a stirrer and place 2lt beaker contain diluted $TiO(SO_4)$ solution. Chilled NH_4OH was added slowly under magnetic stirring till the solution reached pH ~10. Meanwhile it get precipitates with $TiO(OH)_2$. The precipitates were washed with hot distilled several times to reach pH ~ 7. The paste of $TiO(OH)_2$ was collected in beaker after decanting the water solution. Nearly 500 ml of 1:1 (v/v) HNO_3 solution was prepared. Cold bath was set up and the beaker containing HNO_3 solution was kept in that and then $TiO(OH)_2$ paste was slowly added to it under magnetic stirring. Finally $TiO(NO_3)_2$ solution obtained. Reaction mechanism in the formation of $TIO(NO_3)_2$ as follows

$$TiO_2 + H_2SO4 = TiO(SO_4) + H_2O$$

$$TiO(SO_4) + 2NH_4OH = TiO(OH)_2\downarrow + (NH_4)_2SO_4$$

$$TiO(OH)_2 + HNO_3 = TIO(NO_3)_2 + 2H_2O$$

3.2.1.1: Estimation TiO_2 in $TiO(NO_3)_2$ (gravimetric method)

Measure the 10 ml of solution in 50 ml beaker and precipitate that with the help of ammonia at pH 10. Then filter the precipitate in No: 42 Watman filter paper followed by drying and calcination of filter paper (using platinum crucible) in a chamber furnace at 1000 °C /2 hours. The strength of solution can be calculated as follows

W1: weight of empty platinum crucible; W2: weight of platinum crucible after calcination

$$\text{Molarity of } TiO(NO_3)_2 \text{ solution: } \frac{w2-w1}{molecular\ weight\ of\ TiO_2} * 100$$

Molar value obtained from the formula should be used for further calculation in preparation of $BaTiO_3$.

3.3: Combustion synthesis

Solution combustion synthesis proceeds due to heat evolved during the combustion of the fuel in the precursor solution, which useful to dissociate nitrate and formation of compound. The amount and type of fuel controls the reaction temperature of combustion synthesis. Fuel used for the combustion synthesis can be categorized in to fuel rich, fuel lean and stoichiometry. The optimized amount of fuel can be categorized by following formula [48].

$$\varphi_e = \frac{\sum(coefficient\ of\ oxidising\ elements\ in\ specific\ formula\ X\ valency)}{(-1)\sum(coefficient\ of\ reducing\ elements\ in\ specific\ formula\ X\ valency)}$$

For the preparation of required compound, appropriate raw materials selected and weighed according to the stoichiometry and dissolved in distilled water. Under continuous stirring ammonia was added to the precursor solution to reach pH: 7, then slowly temperature rose to 80 °C and let all the water evaporated. Then we can identify the viscous gel formation, take out the magnetic bead and raise the temperature 350 °C. Spontaneously gel starts combustion with lot of gases out of beaker. At the end of experiment combustion residue will be remained. Collected residue was grinded in agate mortar and proceeded by calcination in chamber furnace at required temperature.

3.4: Palletization and sintering:

After weighing calcined powders for required composite, they are thoroughly mixed in an agate mortar by adding 3wt% PVA solution. After drying the mixed batch under sodium lamp for few minutes and again powder grinded for homogeneity. Pellets were pressed under uniaxial pressing machine at the load of 4 tons, with 90 seconds dwell time. Pellets were dried at 80 °C for 1 hour. Sintering was done in the chamber furnace according to optimizes temperature schedule.

3.5 Silver coating for dielectric measurements:

For dielectric characterization of the pellets a thin silver (conducive) coating is used to electrode the pellet. Polished and cleaned pellets were taken to apply the silver coating. A thin Ag conductive paste coated on either surfaces of pellets and kept in oven for curing at 600 °C/0.5h.

3.6: Characterization techniques

3.6.1: Bulk density

Density of sintered pellets was measured by Archimedes principle using kerosene as immersion media using ASTM standard C20. The value density/porosity reported in this work was calculated with an error of ± 1 %. The formula for the calculation of bulk density were as follows

$$Bulk\ density = \frac{W_d}{W_s - W_{su}} X\ density\ of\ kerosene$$

W_d, W_S and W_{Su} are dry weight, soaked weight and suspended weights respectively. The theoretical density (TD) of a biphasic composite material can be calculated as follows

TD of composite = ∑(Volume fraction of the phase × Theoretical density of the phase)

The relative density of the composites can be calculated according to the following formula.

$$Relative\ densit\ of\ composite = \frac{bulk\ density\ of\ composite}{calculated\ theritical\ density\ of composite}$$

3.6.2: X-ray diffraction

Phase formation in different composite systems was studied using the room temperature powder X-ray diffraction technique (Cu-Kα radiation) performed with Rigaku Ultima-IV, Japan. Samples are scanned in a continuous mode from 10° – 90° using a step size of 0.02.

3.6.3: Field emission Scanning electron microscope (FE-SEM)

The morphology the powders and surface microstructure of sintered pellets were studied using FESEM (model: NOVA Nano SEM/FEI 450). The powders, sintered pellets are coated with Au. These samples are used for microscopy.

3.6.4: Particle size measurement:

Crystallite size (D_X): The size corresponds to the mean value of the crystalline domain size of the particles is determined from the X-ray line broadening using Scherrer formula[49] with correction factor as given below.

$$D_x = \frac{0.9\lambda}{\beta cos\theta}$$

Where D_X is average crystalline size, λ is the X-ray wavelength used, β the angular line width of half maximum intensity and θ the Bragg's angle in degree.

3.6.5: Dielectric measurements:

Pellets were electrode with silver coating to perform dielectric characterization Dielectric measurements were carried out using HIOKI 3532-50 LCR Hitester at room temperature, in the frequency range of 42Hz to 1MHz.

Relative permittivity (ε_r) of the sample were calculated from the following relation between capacitance and relative permittivity

$$C_p = \frac{\varepsilon_0 \varepsilon_r A}{t}$$

C_p, $\mathcal{E}_0$, $\mathcal{E}_r$, A, *and* t are capacitance, permittivity of the vacuum ($(8.854 \times 10^{-12}$ F/m), relative permittivity, electrode area of pellet and thickness of pellet.

3.6.6: M-H loop measurements:

M-H loop of the magneto-dielectric pellets were measure using M-H loop tracer (make: MAGNETA, INDIA). Characterizations were carried out at room temperature. Magnetization (M) response of the applied magnetic field (H) gives the hysteresis loop. Before proceeding for testing instrument was calibrated using standard sample. Test executes by giving the area and thickness data of test sample to the programmed instrument.

3.6.7: P-E loop measurement:

Prior to experiment pellets were electrode with silver coating. Test carried out using the P-E loop traces (make: Marine India, Electronics). Polarization response to the given electrical field gives the hysterics loop. Tests executes by placing the sample in silicon oil and giving the thickness and area values. Measurement carried out at room temperature.

3.6.8: Magneto-dialectic measurement:

Percentage capacitance change without and with DC magnetic field gives the % magneto-capacitance of the sample. Electromagnet (make: GMW magnet system, USA) was used to produce 0 to 2.68 kOe of DC field. Capacitance was measured using HIOKI 3532-50 LCR Hitester. Test carried out by placing the sample between DC magnetic poles. Measurement carried at room temperature. Magneto capacitance was calculated using following formula.

$$magneto - dielctric\ \% = \frac{\varepsilon(H) - \varepsilon(H=0)}{\varepsilon(H=0)}\ X\ 100$$

$\mathcal{E}(H)$*and* $\mathcal{E}(H=0)$ are permittivity in DC magnetic field and permittivity without DC magnetic field respectively.

RESULTS AND DISCUSSION

CHAPTER 4

Phase analysis and powder morphology of auto-combustion derived pure BT, CF, ZF and CZF powders

In this chapter, pure BT, CF, ZF and CZF powders have been prepared using auto-combustion synthesis method. Phase analysis and powder morphology of these auto-combustion derived powders are characterized using XRD and FESEM, respectively.

4.1: Introduction

One of our objectives is to develop barium titanate: ferrite composites via solid state method using the auto-combustion derived powders. In this work, individual compounds such as BT, CF, ZF and CZF in powder form were prepared using auto-combustion method, before proceeding to develop solid-state derived BT: ferrite composites. Phase analysis and powder morphology of these auto-combustion derived powders are characterized using XRD and FESEM, respectively.

4.2: Experimental

$Ba(NO_3)_2$ (Barium Nitrate), $TiO(NO_3)_2$ (Titanyl nitrate), $C_6H_8O_7$ (citric acid), NH_4NO_3 (ammonium nitrate) and $C_{10}H_{16}N_2O_8$ (EDTA) are the raw material selected for the synthesis of $BaTiO_3$ via auto-combustion route and are taken in the 1:1:1.5:12:0.1 ratio respectively. Further, all these reagents were dissolved in distilled water to form a precursor solution. Under continuous stirring, ammonia was added to the precursor solution in order to achieve pH ~ 7. At the same time, temperature of the solution was increased to around ~ 80 °C. After certain time, a viscous gel was formed which proceeded by self-ignition, leaving residue. The collected residue was grounded in agate-mortar and further calcined in chamber furnace at 1000 °C for 6h. Similarly, $Fe(NO_3)_3.9H_2O$ (Ferric Nitrate nona hydrte), $Co(NO_3)_26H_2O$ (Cobalt nitrate hexa hydrate), $Zn(NO_3)_2.6H_2O$ (Zinc nitrate hexa hydrate) and $C_6H_8O_7$ (citric acid) were selected as raw materials for the synthesis of ferrite compounds such as $CoFe_2O_4$, $Co_{0.5}Zn_{0.5}Fe_2O_4$ and $ZnFe_2O_4$ via auto combustion method. Citric acid of 3 moles was added for the mole of ferrite synthesized. Also, nitrates were weighed as per the moles required in the ferrite compound. Similar combustion procedure (as followed in $BaTiO_3$) was followed to synthesize $CoFe_2O_4$, $Co_{0.5}Zn_{0.5}Fe_2O_4$ and $ZnFe_2O_4$. After auto-combustion, the ferrite powders were calcined at 900 °C for 4 h. Phase analysis and morphology of the calcined BT and ferrite powders were further analyzed using X-ray diffraction and FESEM, respectively.

4.3: Results and discussion

4.3.1: Phase analysis of auto-combustion derived BT and ferrite powders

Auto-combustion derived powders are calcined at 1000 °C for 4h and phase analysis was performed using X-ray diffraction. Fig. 4.1 shows XRD pattern of auto-combustion derived BT powders calcined at 1000 °C. All the peaks are identified with phase pure $BaTIO_3$ having tetragonal structure, as per the JCPDS file number: 79-2265. The crystallite size of calcined BT powders was found to be around 40 nm, as determined from the Scherrer's formula.

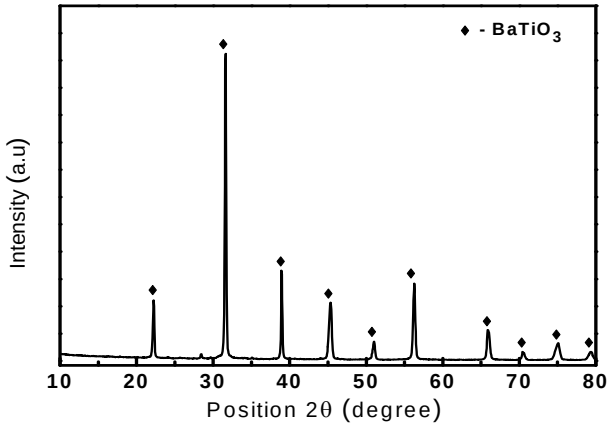

Fig. 4.1: XRD pattern of auto combustion derived BT powder calcined at 1000 °C for 4h.

In a similar way, ferrites powders such as CF, ZF and CZF were prepared separately using auto-combustion route. The individual ferrite powders were calcined at 900 °C and phase analysis was performed using XRD. Fig. 4.2 shows XRD patterns of calcined CF, ZF and CZF powders. All the peaks are well matched with cubic phase ferrite, as confirmed from JCPDS file numbers: 22-1086 and 22-1012. The crystallite size of CF, ZF and CZF were found to be 34.4 nm, 63.4 nm and 70.7 nm, respectively as determined from Scherrer's formula.

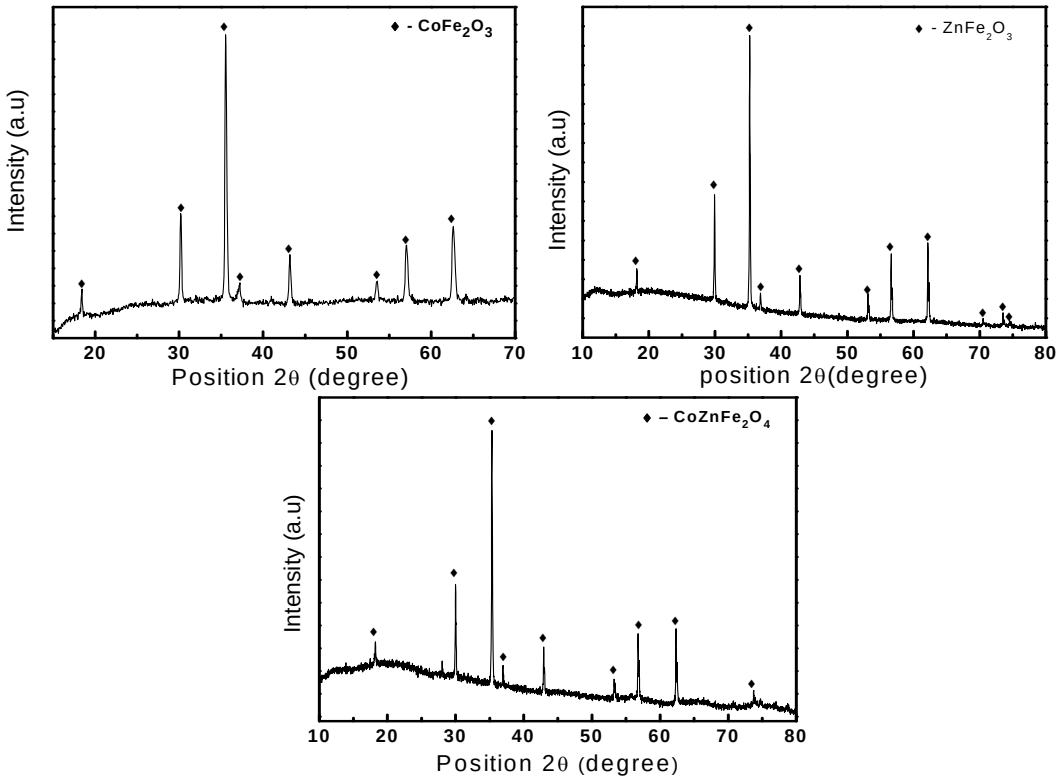

Fig. 4.2: XRD patterns of auto combustion derived CF, ZF and CZF powder calcined at 900 °C.

4.3.2: Powder morphology of auto-combustion derived BT and ferrite powders

In order to understand the powder morphology of auto-combustion derived BT and ferrite powders, FESEM was performed on the calcined powders. In case of auto-combustion derived BT sample, FESEM was performed on both calcined (i.e. 1000 °C/6h and 1200 °C/4h) BT powders. Fig. 4.3 (a) and (b) show FESEM micrographs of BT powder calcined at 1000 °C and 1200 °C, respectively. In both FESEM micrographs, the particles are agglomerated and porous in nature. [9] It is well understood that the particle size of lower temperature calcined powders is smaller than the higher temperature calcined powders. The average agglomerated particle size was around 1-2μm at 1000 °C, whereas, the particle size grows to larger in size at 1200 °C. The average agglomerated particle size at this temperature was around 2-4μm.

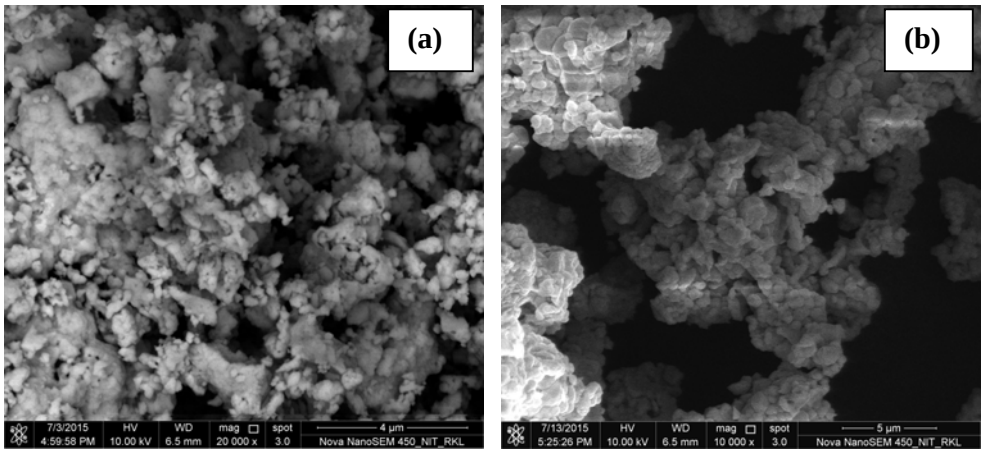

Fig. 4.3: FESEM micrographs of auto combustion derived BT powders, calcined at (a) 1000 °C (b) 1200 °C.

In a similar way, all ferrite powders were calcined at 900 °C for 4h and 1200 °C for 4h. Fig. 4.4 (a), (b) and (c) show FESEM micrographs of calcined (900 °C) CF, ZF and CZF powders, respectively. In all cases, the powders are agglomerated in nature. The particles of ferrites are also porous in nature. The average particle size of ferrite at 900 °C was found to be around 1 μm. When these ferrite powders are calcined at 1200 °C, the particles became polyhedral in shape. At this temperature, all the particles are agglomerated in nature and also the particles are polyhedral with flake like morphology. The average particle size of CF and ZF at 1200 °C was found to be 1-3μm. However, the average particle size of CZF calcined at 1200 °C seems to be larger (3-4μm) in size as compared to CF and ZF powders.

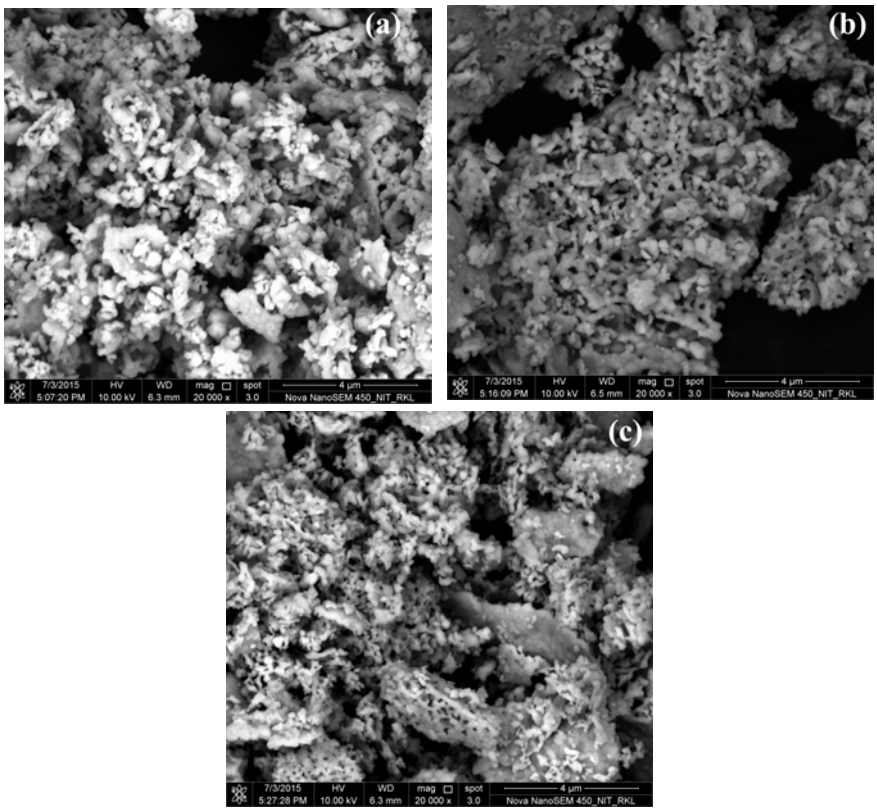

Fig. 4.4: FESEM micrographs of auto-combustion derived calcined (900 °C) (a) CF, (b) ZF and (c) CZF powders.

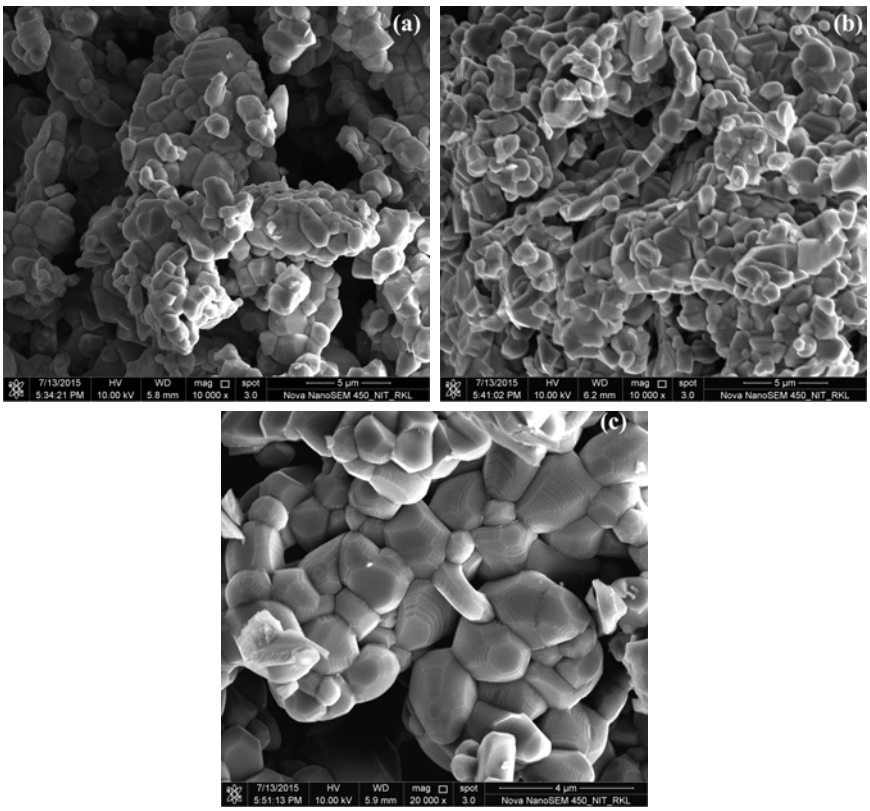

Fig. 4.5: FESEM micrographs of auto-combustion derived calcined (1200 °C) (a) CF, (b) ZF and (c) CZF powders.

4.3.3: Microstructure of sintered BT: ferrite composite pellet

In this research work, one of the objectives is to prepare BT: ferrite composite pellets using the auto-combustion derived powders. So, it is necessary to understand the FESEM micrograph of BT: ferrite composite pellet before preparing the BT: ferrite composites having different composition. In this context, one of the ferrite (ZF) was chosen and mixed with BT powders having a composition of 70 BT and 30 ZF. The pellet has been prepared and sintered at 1200 °C for 4h. FESEM micrograph with elemental mapping was performed on this particular composite pellet. Fig. 4.6 show FESEM micrographs with elemental mapping of typical BT: ZF composite pellet. From FESEM micrograph, it was well understood that the composite morphology was completely different as compared with the powder morphology of individual powders. From elemental analysis, it was clear that BT have two types of morphology such as elongated larger size (plate-like) and fine size with nearly spherical in type. However, the ferrite morphology was polyhedral in nature.

.

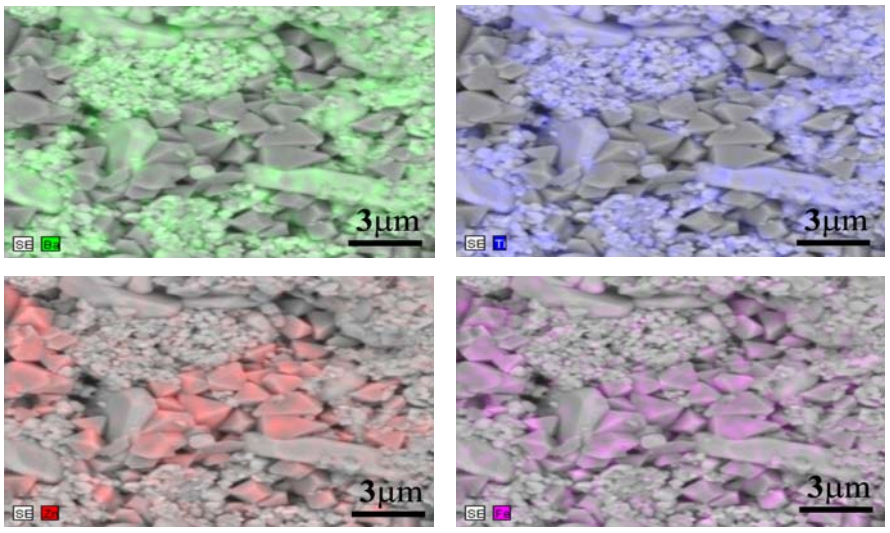

Fig. 4.6: FESEM micrographs of BT: ferrite composite pellets with mapping.

4.4: Remarks

Phase pure BT and three different ferrites were successfully prepared using auto-combustion route. Individual powders of BT and ferrites were agglomerated in nature either at lower or higher calcination temperature. However, the two different types of morphology of BT and one type of morphology of ferrite arrangements in BT: ferrite composite pellet may be interesting and in the same time, it may lead to modify the magneto-dielectric properties of BT: ferrite composites. So, structure, microstructure and magneto-dielectric properties of BT: ferrite composites, prepared via different ways, were analyzed in detail in next three chapters.

CHAPTER 5

Structure, microstructure and magneto-dielectric properties of solid-state derived BT: ferrite composites

In this chapter, BT: ferrite composites have been prepared using auto-combustion derived BT and ferrite powders (CF, ZF and CZF) via conventional solid state mixing. Structure, microstructure along with magneto-dielectric properties of different BT: ferrite composites are studied and analyzed in detail.

5.1: Introduction

Two different types of morphology of BT and one type of morphology of ferrite in BT: ferrite composite, as observed from FESEM micrographs and elemental mapping in Fig. 4.6, motivate to study the structure, microstructure and magneto-dielectric properties of BT: ferrite composites. So, in this context, one of the methods such as conventional solid-state mixing was explored to develop BT: ferrite composites using auto-combustion derived BT and ferrite powders.

5.2: Experimental

From Chapter 4, it was found that phase pure BT was formed at 1000 °C for 6h and the ferrite phase were developed at 900 °C for 4h. So, these calcined powders were used as the starting material to develop BT: ferrite composites via solid-state mixing method. Three different ferrite powders such as CF, ZF and CZF were used as the ferrite phase for preparing BT: ferrite composites. Additionally, three different compositions of 20, 30 and 40 wt % of ferrite powders have also been used for preparing BT: ferrite composites. All the powders were weighed according to the weight percentage required in the composite and mixed in agate mortar using 3wt % PVA solution as binder. Further, these dried powders were compacted in uniaxial pressing machine at load of 4 tons. Finally, the prepared pellets were then sintered at 1250 °C for 4 h. Phase analysis, microstructure, magneto-dielectric measurements were performed using different instruments and results are analyzed. In this chapter, samples are specified with notation such as XBT$Yferrite, where X stands for wt % of BT phase, $ stands for solid-state mixing and Y stands for wt % of ferrite phase (CF/ZF/CZF).

5.3: Results and discussion

5.3.1: Phase analysis of BT: ferrite composites

Phase analysis of the sintered pellets of BT: CF, BT: ZF and BT: ZCF were analyzed using XRD and are shown in Fig. 5.1. All the peaks are identified with either tetragonal BT (marked as *) or cubic ferrite (marked as ♦) as per the JCPDS data file (for BT: JCPDS file no: 75-2116 and for ferrite: JCPDS file no: 22-1086, 73-1963). In addition to these phases, minute amount of barium hexa-ferrite ($BaFe_{12}O_{19}$) was also observed in all composites due to diffusion of Fe^{2+} or Fe^{3+} ions in to Ti^{3+} site. [28,34] It was also observed that the phase (BT, CF, ZF and CZF) peak intensity of ferrite phase increases with increase in ferrite percentage in all composites. [53] The crystallite size of BT phase was found to be comparatively larger in size than the crystallite size of ferrite in BT: ferrite composites. The crystallite size of BT phase was in the range between 26 nm to 34 nm, whereas, the crystallite size of ferrite was found to be in between 18 nm to 32 nm.

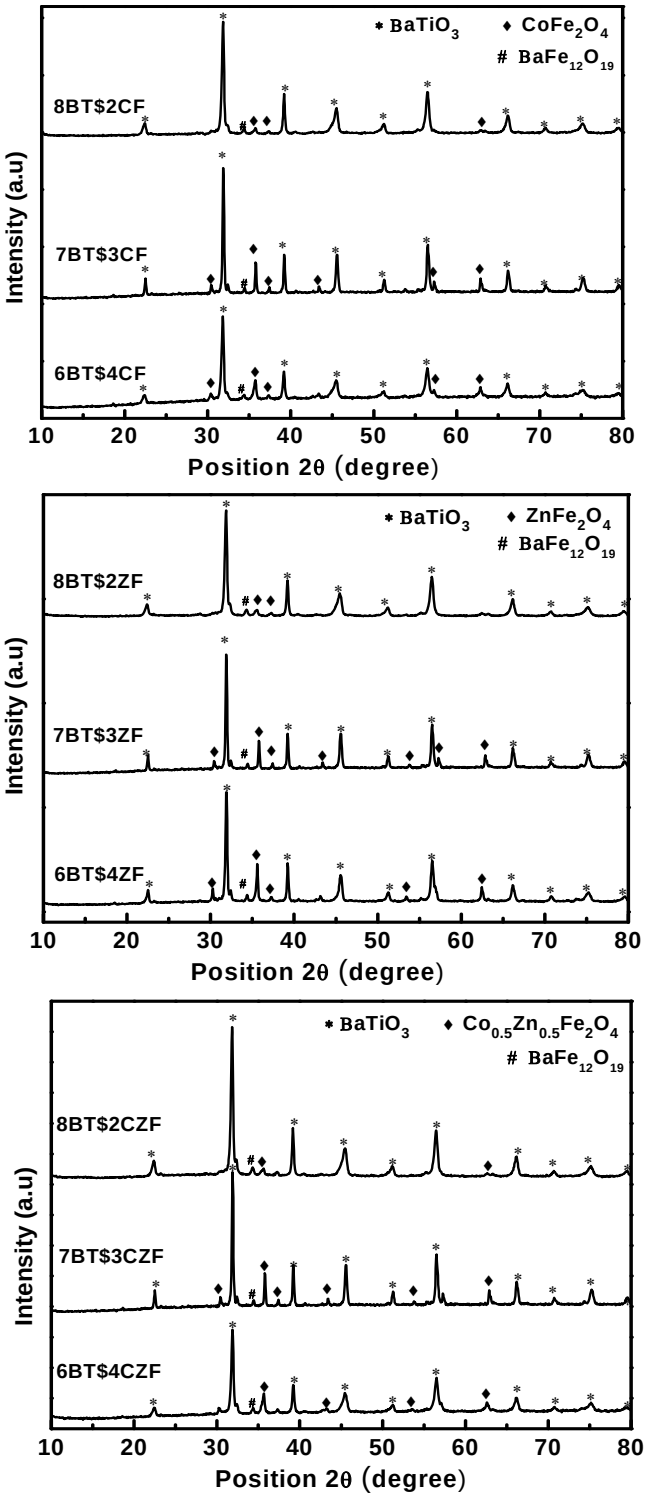

Fig. 5.1: X-ray diffraction patterns of solid-state derived BT: ferrite composites

5.3.2: Microstructure of BT: ferrite composites

In order to study the microstructure, FESEM was performed on all sintered solid-state derived BT: ferrite composites. Fig. 5.2 show FESEM micrographs of solid-state derived BT: CF composite having three different compositions (such as 20, 30 and 40 wt % of CF). In all three compositions of BT: CF composites, BT phase having two different types of morphology including elongated plate-like and agglomerated nearly spherical shape, but, CF phase exits in polyhedral in shape. Plate like BT in 30wt% ferrite composite oriented in a random way. However in 20 and 40wt% ferrite composites they oriented in unidirectional. Ferrite growth has been increased with its percentage in the composite and which is quite enough to orient the plate like BT in the 30wt% ferrite composites but in 20wt% ferrite composite ferrite growth is relatively low to orient the plate like BT. However In 40wt% composites ferrite covers and suppresses the randomness of BT and orient them directionally. The distribution of ferrite phase is not much homogeneous in nature (like ant-colony) in BT matrix. Grain size of BT varies from 1 μm to 5 μm, whereas particle size of CF was around 0.5 to 2 μm. Both BT and CF were well packed and seem to be highly dense. The theoretical density of 8BT$2CF, 7BT$3CF and 6BT$4CF were found to be around 92 %, 91 % and 90 %, respectively.

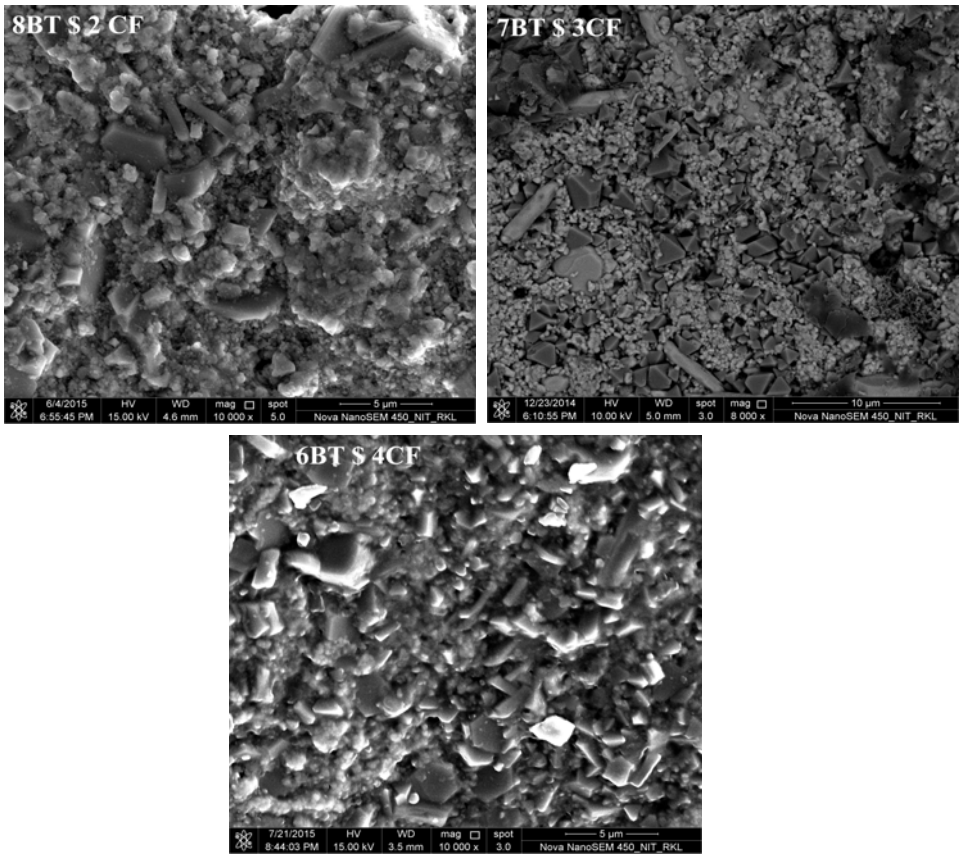

Fig. 5.2: FESEM micrographs of solid-state derived BT: CF composite having three different compositions.

Similarly, FESEM was performed on all sintered solid-state derived BT: ZF composites. Fig. 5.3 show FESEM micrographs of solid-state derived BT: ZF composite having three different compositions (such as 20, 30 and 40 wt % of CF). In all three compositions of BT: ZF composites, BT phase having two different types of morphology including plate-like and agglomerated nearly spherical shape, but CF phase exits in polyhedral in shape. But, in this particular composite, elongated and plate-like BT is more prominent in 7BT$3ZF as seen the 7BT$3CF composite. However, plate-like shape of BT phase is also visible in both 8BT $ 2ZF and 6BT $ 4ZF bur got oriented directionally according to the phenomenon as observed in the BT$CF composites, but the population of plate like morphology of barium titanate is relatively higher than the 7BT$3CF. In this composite, the distribution of ferrite phase is less homogeneous in nature (like ant-colony) in BT matrix. The particle size of BT varies from 1 μm to 5 μm, whereas particle size of CF was around 0.5 to 2μm. Both BT and CF were well packed and seem to be highly dense. The theoretical density of 8BT$2ZF, 7BT$3ZF and 6BT$4ZF were found to be around 90 %, 89 % and 89 %, respectively.

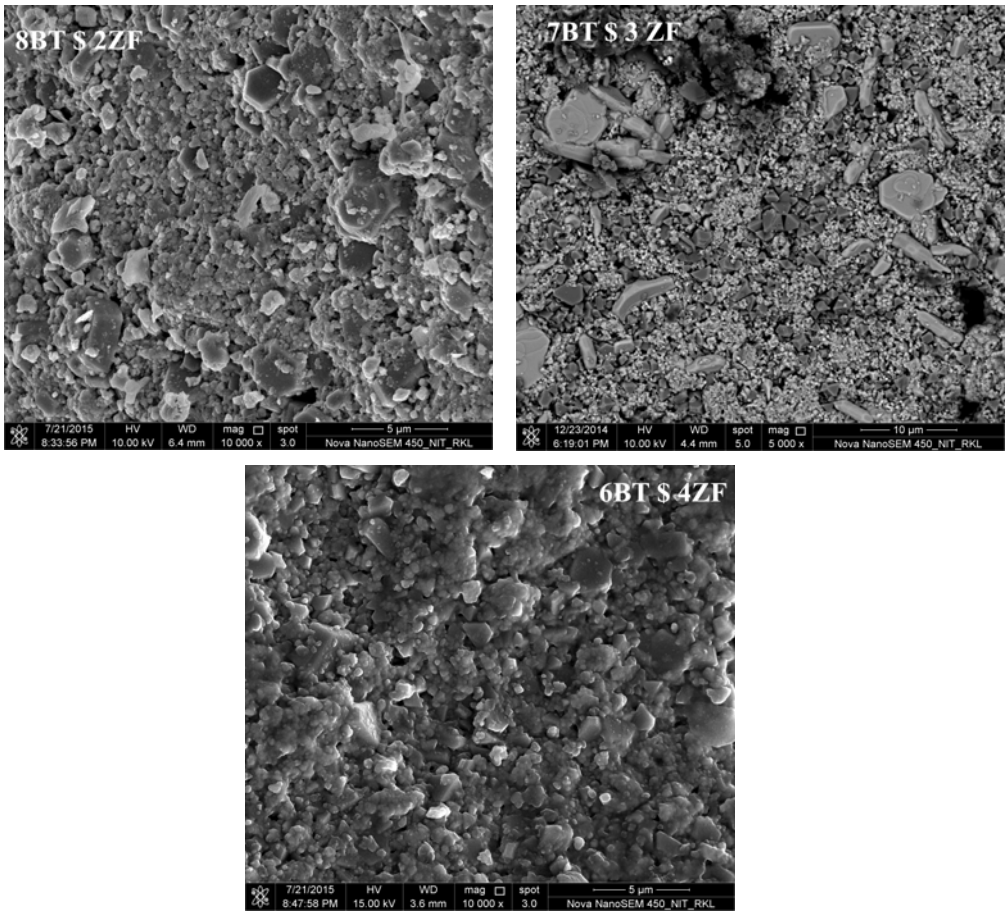

Fig. 5.3: FESEM micrographs of solid-state derived BT: ZF composite having three different compositions.

In addition, FESEM was performed on all sintered solid-state derived BT: CZF composites. Fig. 5.4 show FESEM micrographs of solid-state derived BT: CZF composite having three different compositions (such as 20, 30 and 40 wt % of CF). In all three compositions of BT: CZF composites, BT with two different morphologies (elongated plate-like and agglomerated nearly spherical shape) are much more prominent in 7BT $ 3CZF sample. However, Plate-like BT phase was also visible in both 8BT $ 2CZF and 6BT $ 4CZF. The random orientation of the plate like BT in observed in the 7BT $ 3CZF. The orientation of depend in the percentage of ferrite in the composite which is also responsible for the growth of ferrite in the composite. So eventually the growth of ferrite in the 20wt% ferrite composite is lower and not sufficient to orient the plate like BT. However in 30wt% ferrite composite sufficient growth of ferrite led to orient the plate like BT. Finally in 40wt% ferrite composite relatively higher percentage of ferrite partially covers plate like BT and its orientation. Similar behavior was also observed in the BT$CF and BT$ZF composite also. Plate like barium titanate is prominent in the CZF based composite, than CF and ZF based composites. The particle size of BT varies from 1 μm to 5 μm, whereas particle size of CF was around 2 μm. Both BT and CF were well packed and seem to be highly dense. The theoretical density of 8BT$2CZF, 7BT$3CZF and 6BT$4CZF were found to be around 90 %, 89 % and 89 %, respectively.

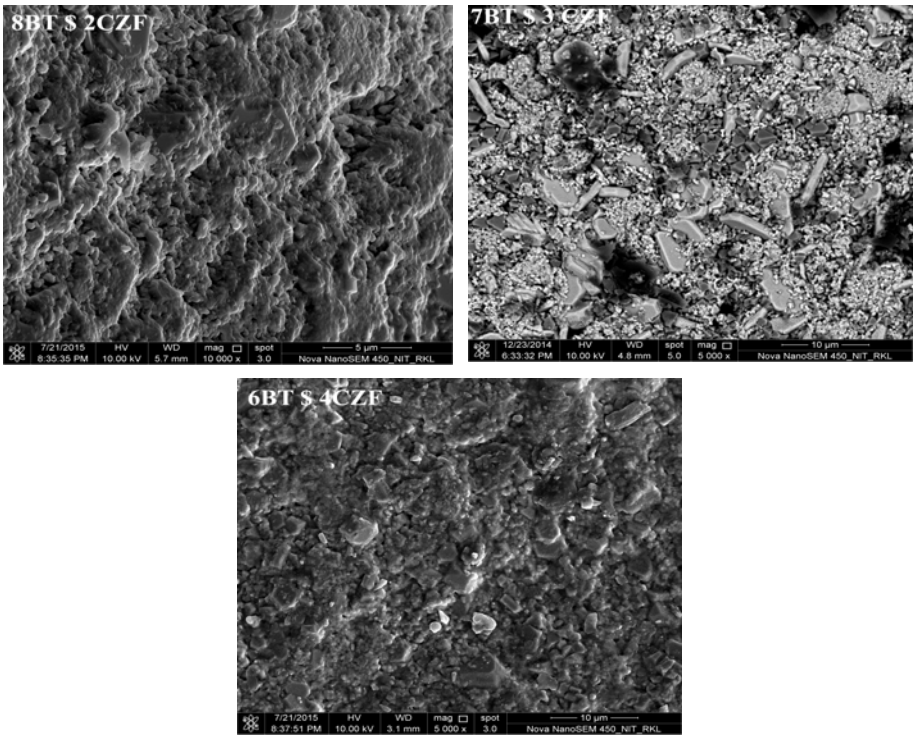

Fig. 5.4: FESEM micrographs of solid-state derived BT: CZF composite having three different compositions.

5.3.3: Dielectric and magnetic properties of BT: ferrite composites

The variation of microstructure of BT: ferrite systems may lead to modify the dielectric and magnetic properties of these composites. So, one of the dielectric properties such as permittivity as a function of frequency of all solid-state derived composites was analyzed at room temperature and are shown in Fig. 5.5. Generally, for this type of composites, the permittivity decreases with frequency. [34] In this current composite system, it was observed that the permittivity was nearly independent with frequency for the composites having 20 wt % ferrite. However, the permittivity was dependent on frequency for the composites having 30 and 40 wt % ferrite. In addition, higher permittivity was observed at lower frequency than at higher frequency. Sharply grown up permittivity at lower frequency may be due to Maxwell-Wagner interfacial [32, 53, 54], space charge polarization [34, 54] or electrical charge depletion between two phases having different permittivities [51], some of the authors attributed the high permittivity in high ferrite composites due to the hopping mechanism. Al lower frequency the permittivity response cannot be attributed to the dielectric phase because of interfacial effects, so at higher frequency permittivity response can be from the dielectric phase. So that composites at higher frequency follow the ascending order of increase in permittivity with increase in dielectric phase. [33, 53] In BT: CF composites, the permittivity of 7BT$3CF at 42 HZ is 2279 and at 1 MHz is 184. Similarly, In BT: ZF composites, the permittivity of 6BT$4ZF at 42 HZ is 9423 and at 1 MHz is 409, in BT: CZF composites, the permittivity of 7BT$3CZF at 42 HZ is 676 and at 1 MHz is 250.

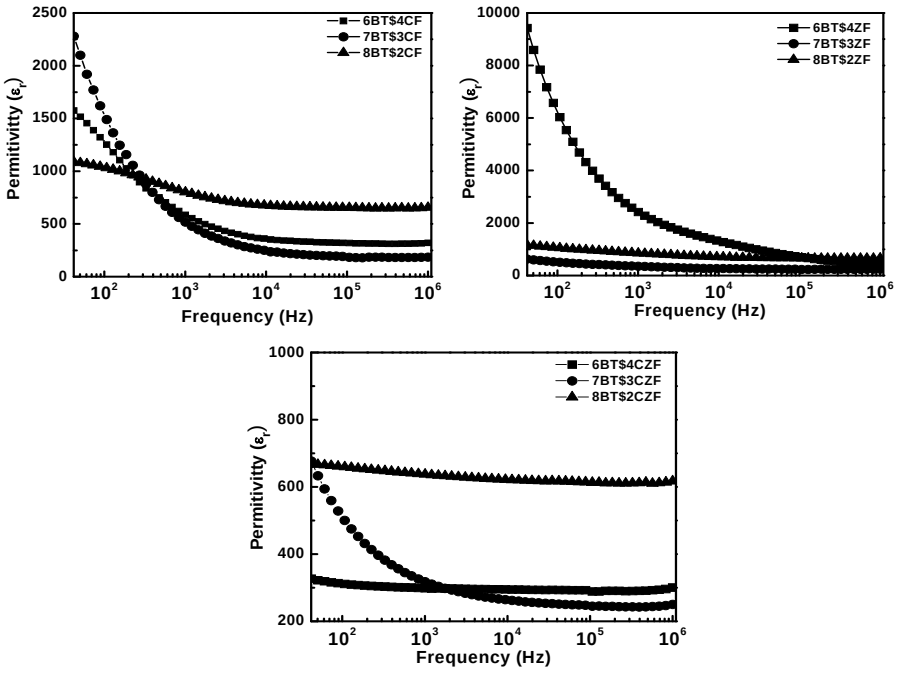

Fig. 5.5: Permittivity as a function of frequency for solid-state derived BT: Ferrite composites.

Dielectric loss is also one of the important parameter and thus was studied for the current magneto-dielectric composite systems at room temperature. Fig. 5.6 shows the loss (tan δ) response with frequency for all BT: ferrite composites. Dielectric loss is usually dependent on the dielectric phase and percentage of dielectric phase in the magneto-dielectric composites. In addition loss is also dependent on the connectivity of the dielectric phase. Also, loss is inversely proportional to the dielectric percentage in the magneto-dielectric composite [52]. In this composite system, proportionality was observed in the particular BT: ZF composites. Hump type of loss response in the composite can be attributed to the resonance of applied frequency with the hopping mechanism [34] between Fe^{2+} and Fe^{3+} ions, also humps can be seen prominently in cobalt and zinc based composite systems and also can be attributed to the Maxwell-wagner models [52] In this system, the loss of 1.27, 0.56 and 0.23 was observed in 40, 30 and 20 wt % ZF composites, respectively at 42 Hz. However, highest loss of about 1.37 was observed for 30 wt % CF in BT: CF composites and loss of about 0.83 was observed in 30 wt % CZF in BT: CZF composites at 42 Hz. Composites having 20 wt % ferrite has the least loss relatively to the 30 and 40 wt % of ferrite composites. Loss of around 0.03, 0.11 and 0.23 was observed in 20 wt% of cobalt-zinc, cobalt and zinc ferrite composite systems, respectively at 42 Hz. In addition, BT: CZF composites have the lowest loss among the BT: CF and BT: ZF composites.

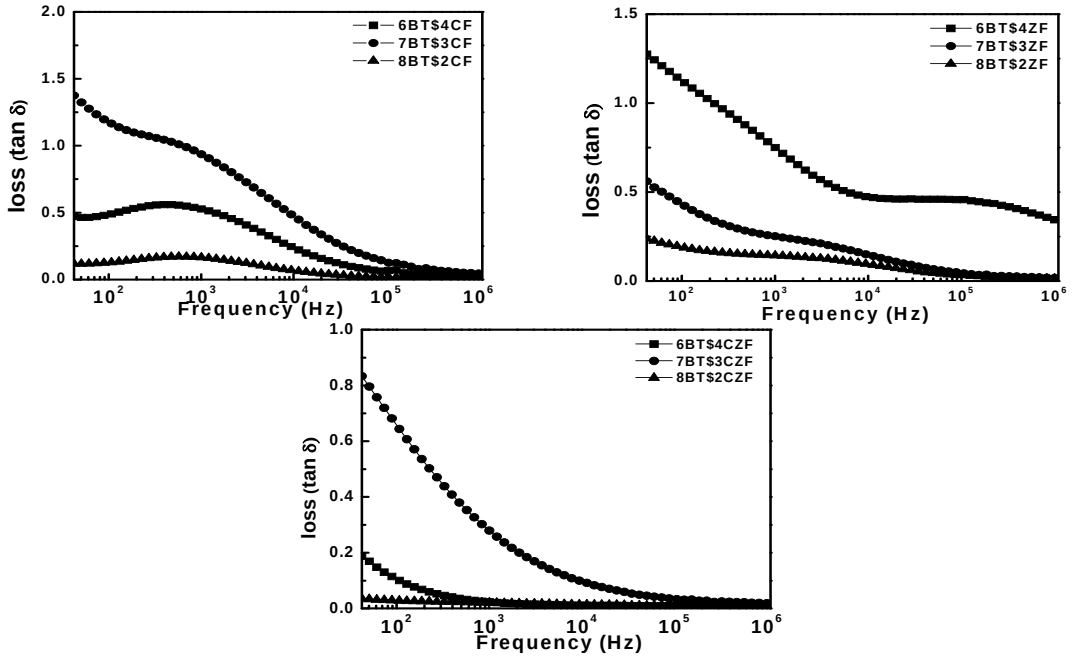

Fig. 5.6: Dielectric loss as a function of frequency for solid-state derived BT: ferrite composites

Polarization response as a function of applied field is shown in Fig. 5.7. In present magneto-dielectric composite system, percentage dielectric phase has the significant effect in the polarization response. Polarization in the material generally comes from the dielectric phase. Composites having higher ferrites show the higher polarization in the present composite system which may have raised die to magnetic dipoles like Fe^{2+} and Fe^{3+}. It was observed that the responses of PE loop of the present BT: ferrite composites deviated from the ideal ferroelectric loop. The particular 30 and 40 wt % ferrite based composites appear in oval shape indicating lossy capacitor phenomena due to field discharge by conductive ferrite phase [28]. However, all 20 wt % ferrite based magneto-dielectric composites shows near ferroelectric behavior due to maximum dielectric phase in the composite, also it can be true that it has less loss compared with 30 and 40wt% ferrite composites, which can be said by area enclosed in PE loop. Polarization (at maximum field), remanent polarization and coercivity of all composites are given in Table 5.1

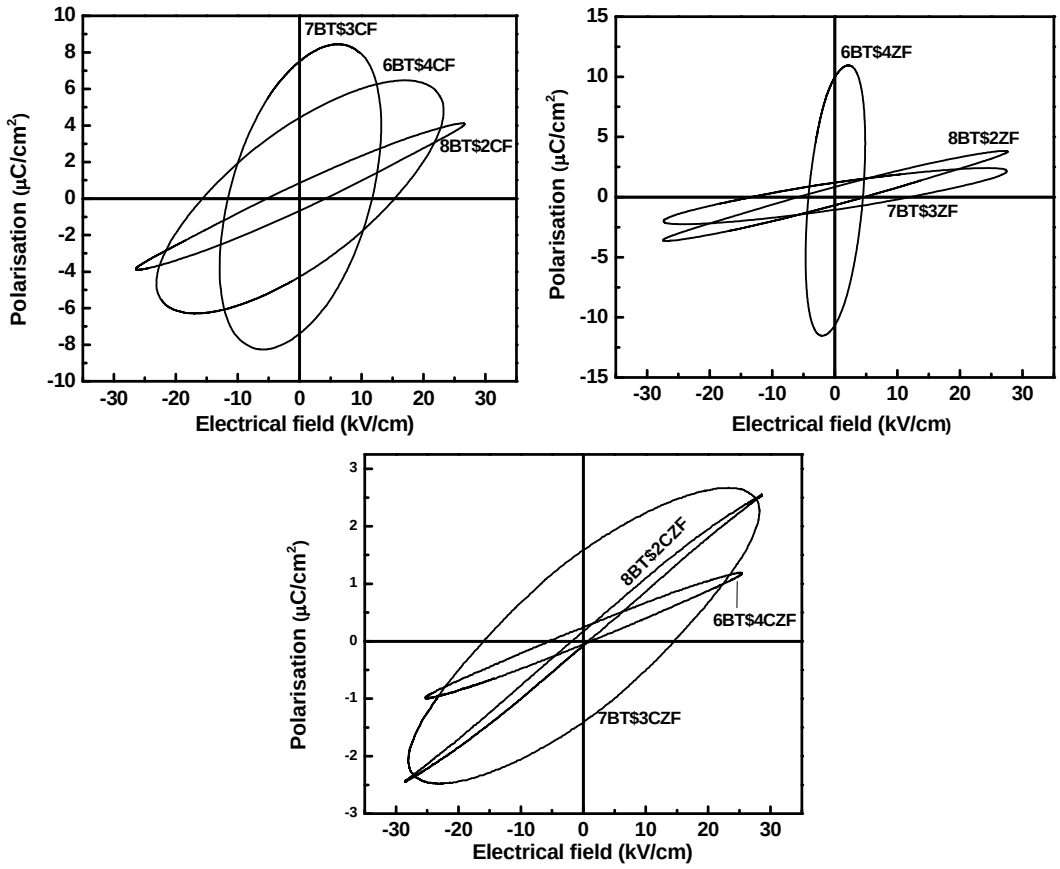

Fig. 5.7: polarization as function of electric field for solid-state derived BT: Ferrite composites

Table 5.1: Remanent polarization, coercivity and polarization (at maximum field) of solid-state derived BT: ferrite composites.

Composites	Remanent Polarization $P_r(\mu C/cm^2)$	Coercivity Ec(kV/cm)	Polarization at maximum field $P(\mu C/cm^2)$
6BT$4CF	4.39	11.5	6.49
7BT$3CF	7.6	16	8.4
8BT$2CF	0.8	5	4.4
6BT$4ZF	10	4	10.8
7BT$3ZF	1.2	13	2.3
8BT$2ZF	0.8	5	3
6BT$4CZF	0.2	5	1.2
7BT$3CZF	1.59	16	2.6
8BT$2CZF	0.17	1.7	2.54

The magnetic nature and parentage of ferrite in the composite has the significant effect on the total magnetization response of the composites. Fig. 5.8 shows the magnetization as function of magnetic field for solid-state derived 30 wt. % ferrite composites. The ferromagnetic behavior of the composite is due to the magnetic phase in the composite. Cobalt and cobalt-zinc ferrites are magnetic in nature and saturated hardly. Though zinc ferrite is a nonmagnetic compound, it shows the magnetic characteristics because of the magnetic impurity in the composite which originated in the sintering of composite, which can be confirmed by X-ray diffraction pattern shown in fig.5.1. Magnetization (at 4.5 kOe) of the composites decreased with the increase in $BaTiO_3$ addition, which can be attributed to the reduced magnetic moments per unit volume [28,29,54,55]. Cobalt-zinc ferrite composite represents soft magnetic nature when compared to cobalt ferrite composite by showing comparatively lower coercivity, increase in coercivity [29, 28] of composite (compared to pure ferrite) with addition of $BaTiO_3$ due to wall pining of ferrite by the surrounding nonmagnetic (ferroelectric or piezoelectric) phases, which indicates the interfacial mechanical interaction between the magnetic and non-magnetic phases present in the composites. Remanence magnetization increases with increasing ferrite percentage due to increasing contact between the ferrite particles in composite [29, 31]. Magnetization (M) ay 4.5 kOe, remanent magnetization (M_R) and coercivity (H_C) of the 30 wt% cobalt ferrite composites are 89.85emu/g, 8.45emu/g and 0.305 kOe respectively. Similarly 84emu/g, 5.23emu/g and 0.17kOe are the magnetization (M) (at 4.5 kOe), remanent magnetization (M_R) and coercivity (H_C) of the 30 wt % cobalt-zinc ferrite composites. Magnetic responses of the cobalt-zinc ferrite composites are relatively lower than the cobalt based composites.

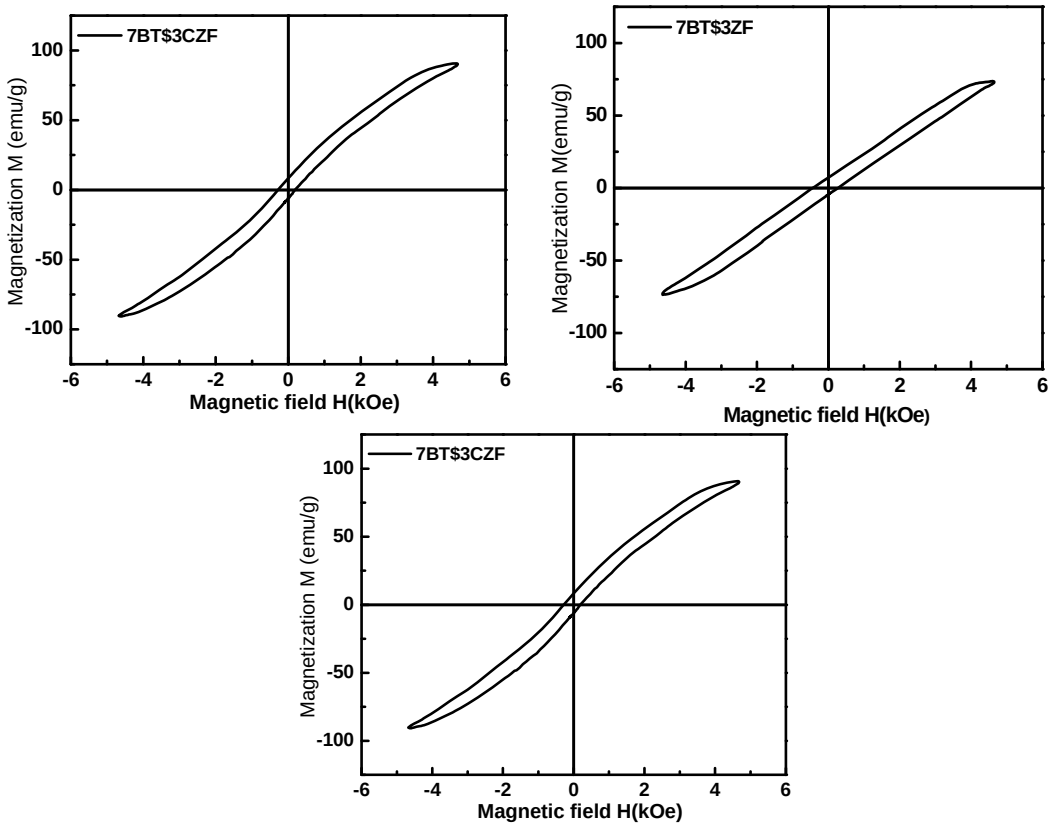

Fig. 5.8: M-H loop of solid-state derived 30 wt % ferrite based BT: ferrite composites.

Table 5.2: Ramanent magnetization, coercivity and magnetization (at 4.5 kOe) of solid-state derived BT: ferrite composites.

Composites	Remanent magnetization Mr(emu/g)	Coercivity Hc(kOe)	Magnetization M (emu/g)
6BT$4CF	8.89	0.325	91.74
7BT$3CF	8.45	0.305	89.85
8BT$2CF	7.07	0.26	69.56
6BT$4ZF	5.00	0.315	73
7BT$3ZF	4.20	0.31	65
8BT$2ZF	3.20	0.29	64
6BT$4CZF	5.99	0.18	90.81
7BT$3CZF	5.23	0.17	84
8BT$2CZF	4.66	0.23	70

Magneto-capacitance response in the BT: ferrite composites can be originated from the mechanical coupling between ferromagnetic and ferroelectric phases in the composites. Extrinsic parameters like magnetic/ferroelectric percentage and microstructure plays a significant role for magneto-capacitance response. [56] Fig.5.9 shows the magneto-capacitance as function of magnetic field for BT: ferrite composites prepared via solid-state mixing of auto-combustion derived powders. It was observed that the magneto-capacitance increases with increase in magnetic field and saturate at around 1.5 K Oe. Both cobalt and zinc ferrite based composites followed the trend of increasing magneto-capacitance response with increase in percentage of ferrite. In addition, cobalt and zinc ferrite based composites shows negative magneto-capacitance response for all ferrite weight percentages, but cobalt-zinc ferrite based composites shows both negative (for 30 wt % ferrite) and positive (for 20 and 40 wt % ferrite) magneto-capacitance response. The response of magneto-capacitance in the present BT: ferrite composite systems can be explained in two different ways: first, induced strain in the magnetic material due to applied magnetic field can modify the capacitance of the composite by mechanical coupling. The positive or negative capacitance may depend on the sign of the magnetostriction of magnetic phase used in the composite. Second, according to the Catalan, the interfacial polarization effect in this composite system can also give the magneto-capacitance due to change in the resistance of the grain boundary or conducting grain with application of magnetic field [57,51]. In addition, the microstructure and morphology of BT/ferrite may also effect the direction of the magneto-capacitance which can be varied depend on the interfacial interaction between the dielectric and magnetic phases present in the composite.[57-59] The observed negative magneto-capacitance response in both cobalt-ferrite and zinc-ferrite based composite systems are well correlated with the available literatures.[59] The negative magneto-capacitance behavior was also partially due to interface dominated magneto-resistance.[51] However, both positive and negative magneto-capacitance response in BT: CZF composites are due to the involvement of magnetostriction and microstructural morphology.

In general, cobalt-zinc ferrites possess a negative value of in-plane magnetostriction.[25,28] Therefore, it is expected that permittivity increases with increase in applied magnetic field and thus shows positive magneto-capacitance for the particular 20 and 40 wt % cobalt-zinc ferrite based composites. But, the 30 wt% cobalt-zinc ferrite based composite shows negative response. This can be attributed due to the magnetostriction, Maxwell-Wagner polarization along with microstructural effect, where the plate-like morphology of BT modifies the magneto-capacitance response. [51] The magneto-capacitance values are higher in the present composite systems comparing with literatures.[57,59,60] The observed enhanced magneto-capacitance values in BT: CF, BT: ZF and BT:

CZF composites were due to strong mechanical interaction of plate-like BT phase with polyhedral ferrite phase.

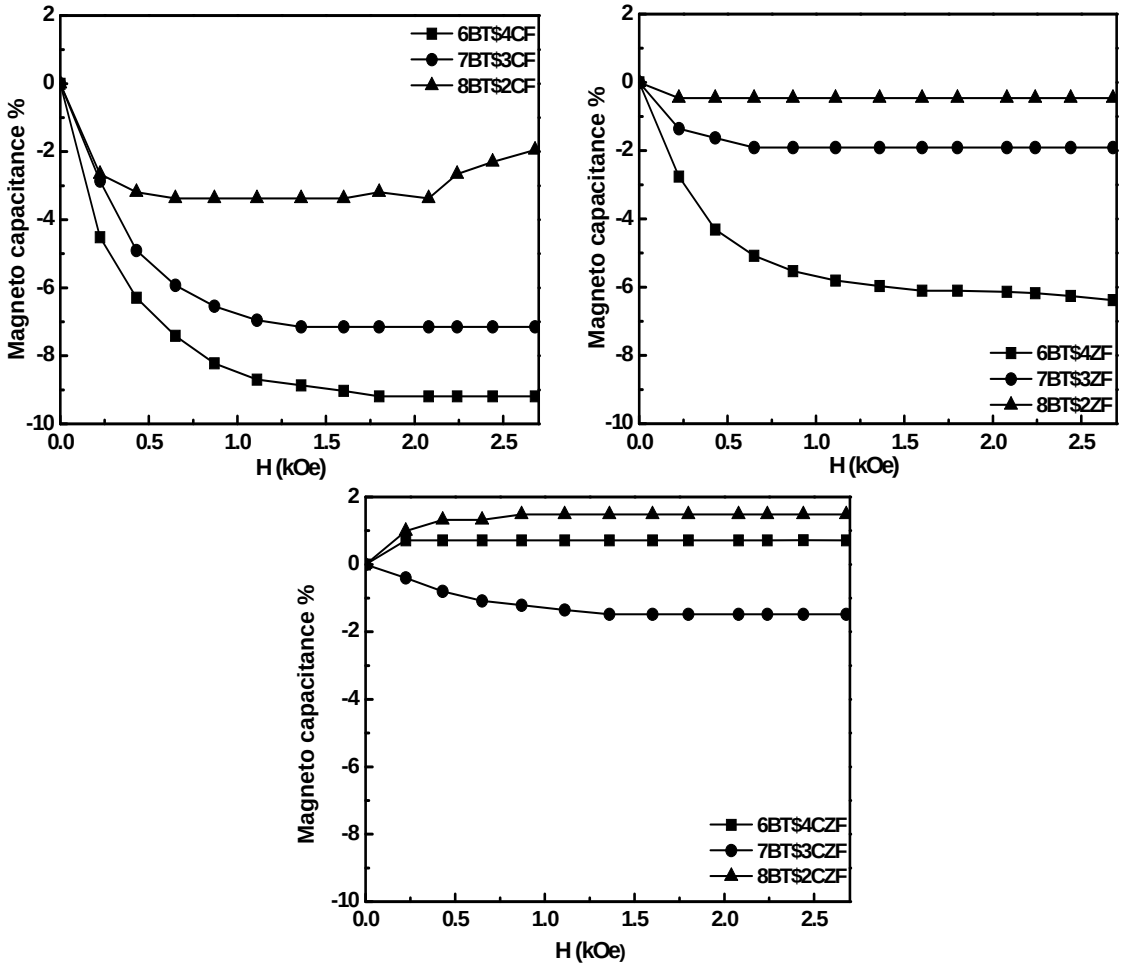

Fig. 5.9: Magneto-capacitance as function of magnetic field for solid-state derived BT: Ferrite composites

A simplified graph also plotted to understand the nature of magneto-capacitance with respective magnetic phase percentage at 1.6 KOe. Fig. 5.10 shows the magneto-capacitance as function of magnetic phase percentage for solid-state derived composites. The effect of ferrite phase can be clearly understood by behavior of BT: ferrite composite under magnetic field. Cobalt and zinc ferrite based composites show the negative response in all the three selected ferrite weight percentages. However in cobat-zinc based ferrite, the magneto-capacitance response is positive in both 20 and 40 wt % and negative response in 30wt% ferrite. Among three ferrite cobalt based composites shows the highest response.

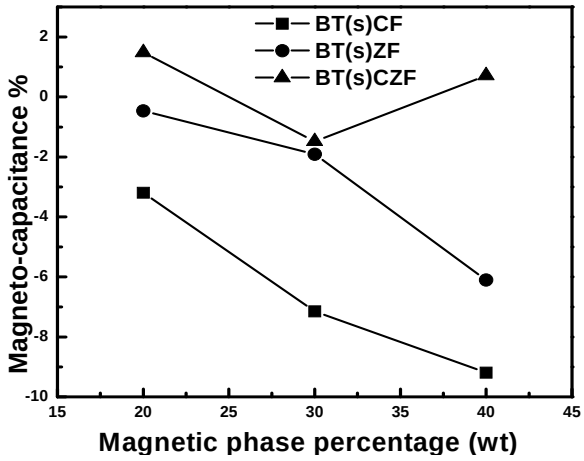

Fig. 5.10: Magneto-capacitance as function of magnetic phase percentage for solid-state derived composites

5.4: Remarks:

$BaTiO_3$ with ferrite based composites has been prepared via auto combustion derived solid state method. XRD pattern shows existence of $BaTiO_3$, $CoFe_2O_4$, $ZnFe_2O_4$, $CoZnFe_2O_4$, as major phase in their respective composites along with $BaFe_{12}O_{19}$ in all composite. $BaTiO_3$ exists in plate-like and agglomerate nearly spherical morphology along with ferrite which exists in only polyhedral morphology. Frequency independent permittivity and loss found in all 20 wt% ferrite composites and also 20 Wt% ferrite composites found have typical ferroelectric behavior in PE loop response, but 30 and 40 wt% ferite shows the loss loop behavior. CF and CZF ferrite composites show the ferromagnetic nature in MH Hysteresis loop. Negative magneto capacitance response found in CF and ZF based composites, but CZF based composites has both negative and positive magneto capacitance response. Magneto capacitance response found to be increase with increasing ferrite percentage in CF and ZF based composites.

CHAPTER 6

Structure, microstructure and magneto-dielectric properties of auto-combustion derived in-situ BT: ferrite composites

In this chapter, BT: ferrite composites have been prepared via in-situ auto-combustion method. Three different compositions of 20, 30 and 40 wt % of Ferrites such as CF, ZF and CZF have been used for preparing BT: ferrite composites. Structure, microstructure along with magneto-dielectric properties of different BT: ferrite composites are studied and analyzed in detail.

6.1: Introduction

In the previous chapter, auto-combustion derived powders were used for preparing BT: ferrite composites via solid-state mixing process and structure, microstructure and magneto-dielectric properties were studied. In this context, magneto-dielectric properties of BT: ferrite composites strongly depend on the distribution of BT and ferrite phases in composite. Different way of distribution of ferrite in BT matrix is also possible via in-situ way of combustion synthesis. Additionally, structure, microstructure and magneto-dielectric properties may alter for BT: ferrite composites. So, in this chapter, in-situ combustion process was explored to develop BT: ferrite composites. Structure, microstructure along with magneto-dielectric properties of different BT: ferrite composites are studied and analyzed.

6.2: Experimental

Raw materials such as Ba $(NO_3)_2$ (Barium Nitrate), $TiO(NO_3)_2$ (Titanyl nitrate), $C_6H_8O_7$(citric acid), NH_4NO_3 (ammonium nitrate) and $C_{10}H_{16}N_2O_8$ (EDTA) were selected for $BaTiO_3$ phase in composite. Similarly, $Fe(NO_3)_3.9H_2O$ (Ferric Nitrate nona hydrte), $Co(NO_3)_26H_2O$ (Cobalt nitrate hexa hydrate), $Zn(NO_3)_2.6H_2O$ (Zinc nitrate hexa hydrate) and $C_6H_8O_7$(citric acid) were selected for the ferrite ($CoFe_2O_4$, $Co_{0.5}Zn_{0.5}Fe_2O_4$ and $ZnFe_2O_4$) phase. All the raw materials weights calculated for required stoichiometric and weight ratio (each ferrite at 20, 30 and 40 wt %) in the composite. All the nitrates along with the required fuel for each compound dissolved in the distilled water to make precursor solution along with ammonia addition to make pH~7. Under constant stirring temperature was raised to 80 °C to evaporate water in the precursor solution. Slowly gel formation initiated and became very thick gel. Heater temperature was slowly raised to initiate ignition for combustion. Spontaneous combustion was observed, which stood for few seconds and left residue in combustion beaker. Carefully collected residue was grinded in agate mortar and calcined at 800 °C for 4 hours followed by sintering the 4 ton compacted 10 mm pellets at 1150 °C for 6 hours.

6.3: Results and discussion

6.3.1: Phase analysis of BT: ferrite composites

Phase analysis of in-situ combustion derived sintered pellets of BT: CF, BT: ZF and BT: CZF were analyzed using XRD and are shown in Fig. 6.1. All the peaks are identified with either tetragonal BT (marked as *) or cubic ferrite (marked as ♦) as per the JCPDS data file (for BT: JCPDS file no: 75-2116 and for ferrite: JCPDS file no: 22-1086, 73-1963). In addition to these phases, minute amount of barium hexa-ferrite [34] ($BaFe_{12}O_{19}$) was also observed in all composites due to diffusion of Fe^{2+} or Fe^{3+} ions in to Ti^{3+} site [28]. It was also observed that the peak intensity

of ferrite phase increases with increase in ferrite percentage in all composites [53]. The crystallite size of BT phase was found to be comparatively larger in size than the crystallite size of ferrite in BT: ferrite composites. The crystallite size of BT phase was in the range between 26 nm to 34 nm, whereas, the crystallite size of ferrite was found to be in between 18 nm to 32 nm.

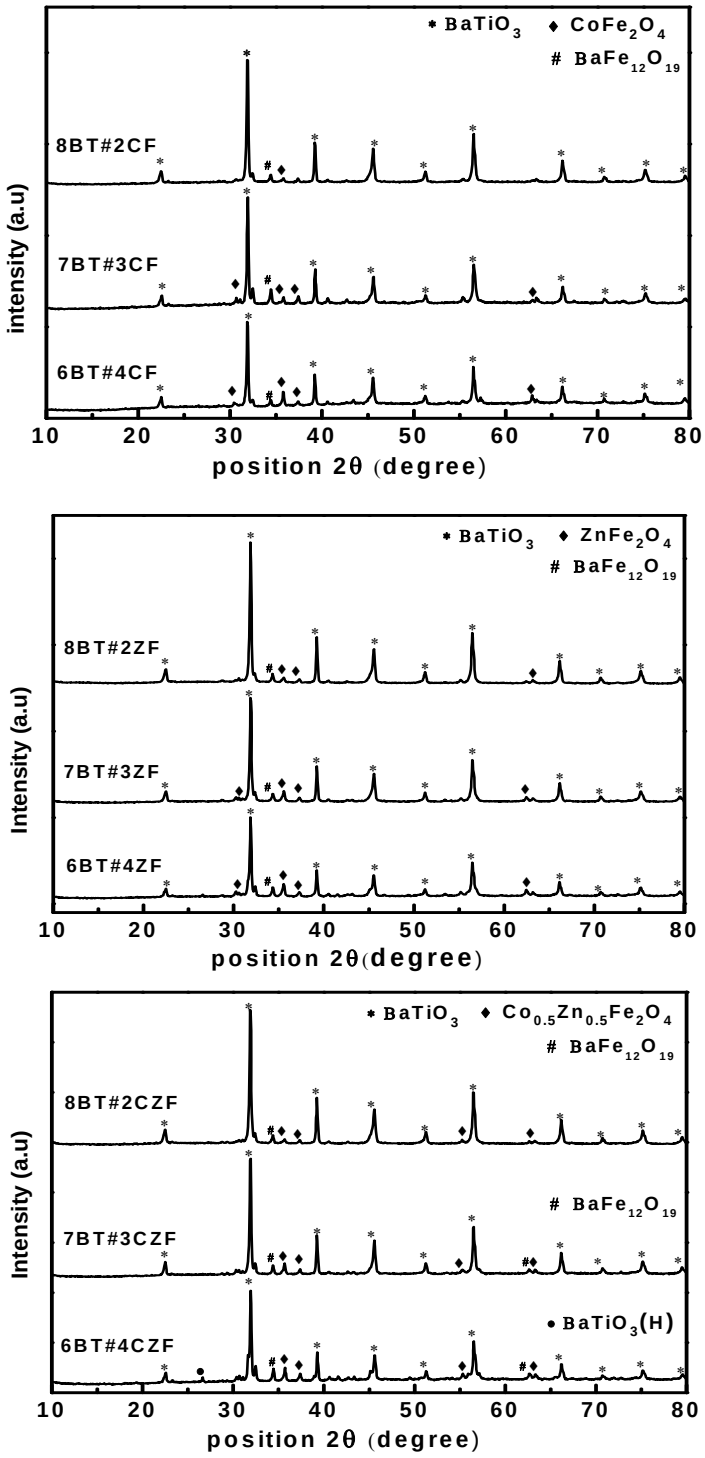

Fig. 6.1: X-ray diffraction patterns of auto-combustion derived in-situ BT: ferrite composites

6.3.2: Microstructure of BT: ferrite composites

In order to study the microstructure, FESEM was performed on all sintered combustion derived in-situ BT: ferrite composites. Fig. 6.2 show FESEM micrographs of in-situ combustion derived BT: CF composite having three different compositions (such as 20, 30 and 40 wt % of CF). In all three compositions of BT: CF composites, BT and CF grains were uniform in size, but bigger grain with polyhedral shape are seems to be BT phase as discussed in EDAX in section 4.3.3. Phases of BT and CF are well connected and distributed in narrow size. The grain size of BT varies from 1 μm to 5 μm, whereas particle size of CF was around 2 μm. Both BT and CF were well packed and seem to be highly dense. The theoretical density of 8BT#2CF, 7BT#3CF and 6BT#4CF were found to be around 92 %, 91 % and 93 %, respectively.

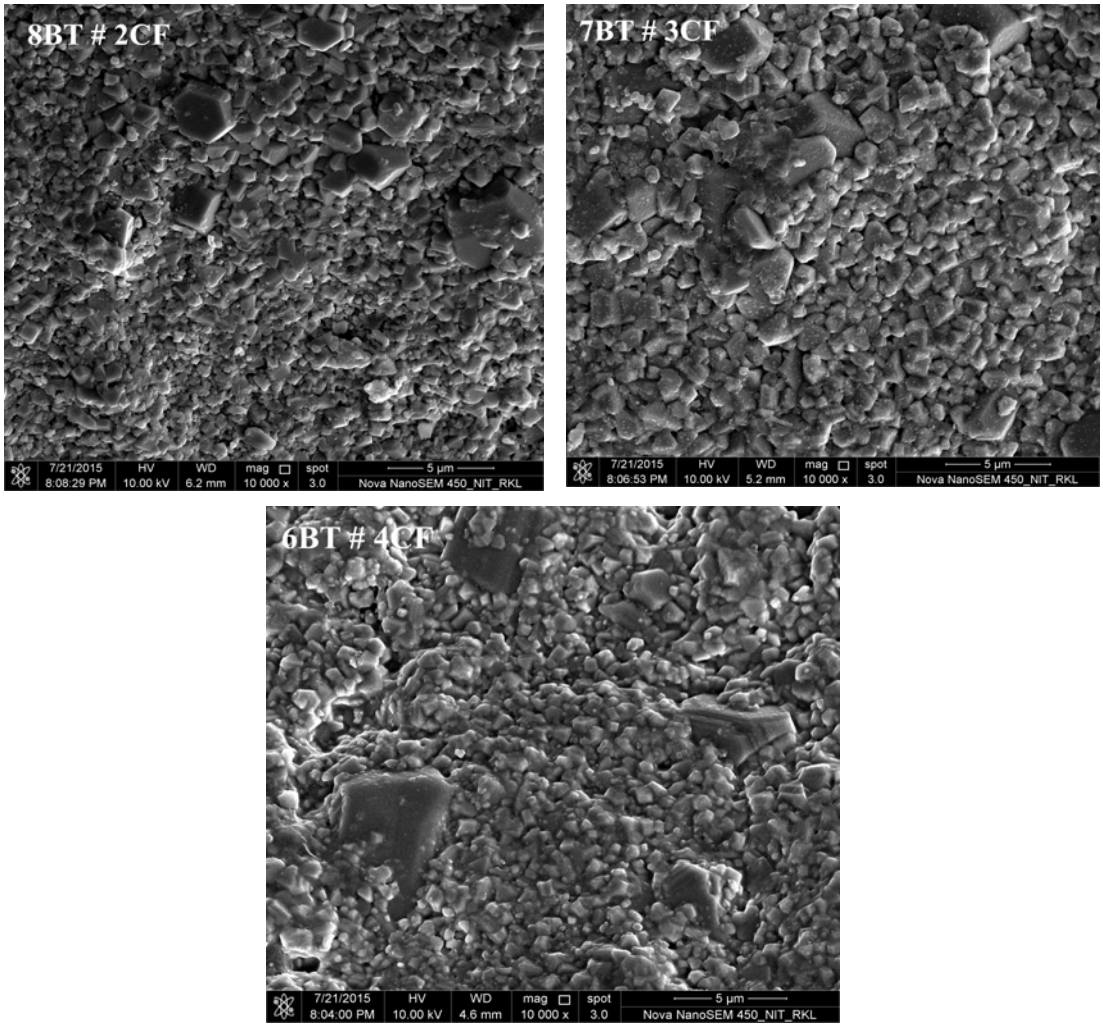

Fig. 6.2: FESEM micrographs of combustion derived in-situ BT: CF composite having three different compositions.

Similarly, FESEM was performed on all sintered combustion derived in-situ BT: ZF composites. Fig. 6.3 show FESEM micrographs of combustion derived in-situ BT: ZF composites having three different compositions (such as 20, 30 and 40 wt % of ZF). In all three compositions of BT: ZF composites, BT and ZF grains were uniform in size, but bigger grain with polyhedral shape are seems to be BT phase (from the EDAX in section 4.3.3) and having less number compared to solid state composites. Phases of BT and ZF are well connected and distributed in narrow size as similar to BT: CF composites. The grain size of BT varies from 1 μm to 5 μm, whereas particle size of CF was around 2 μm. Both BT and CF were well packed and seem to be highly dense. The theoretical density of 8BT#2ZF, 7BT#3ZF and 6BT#4ZF were found to be around 92 %, 92 % and 94 %, respectively.

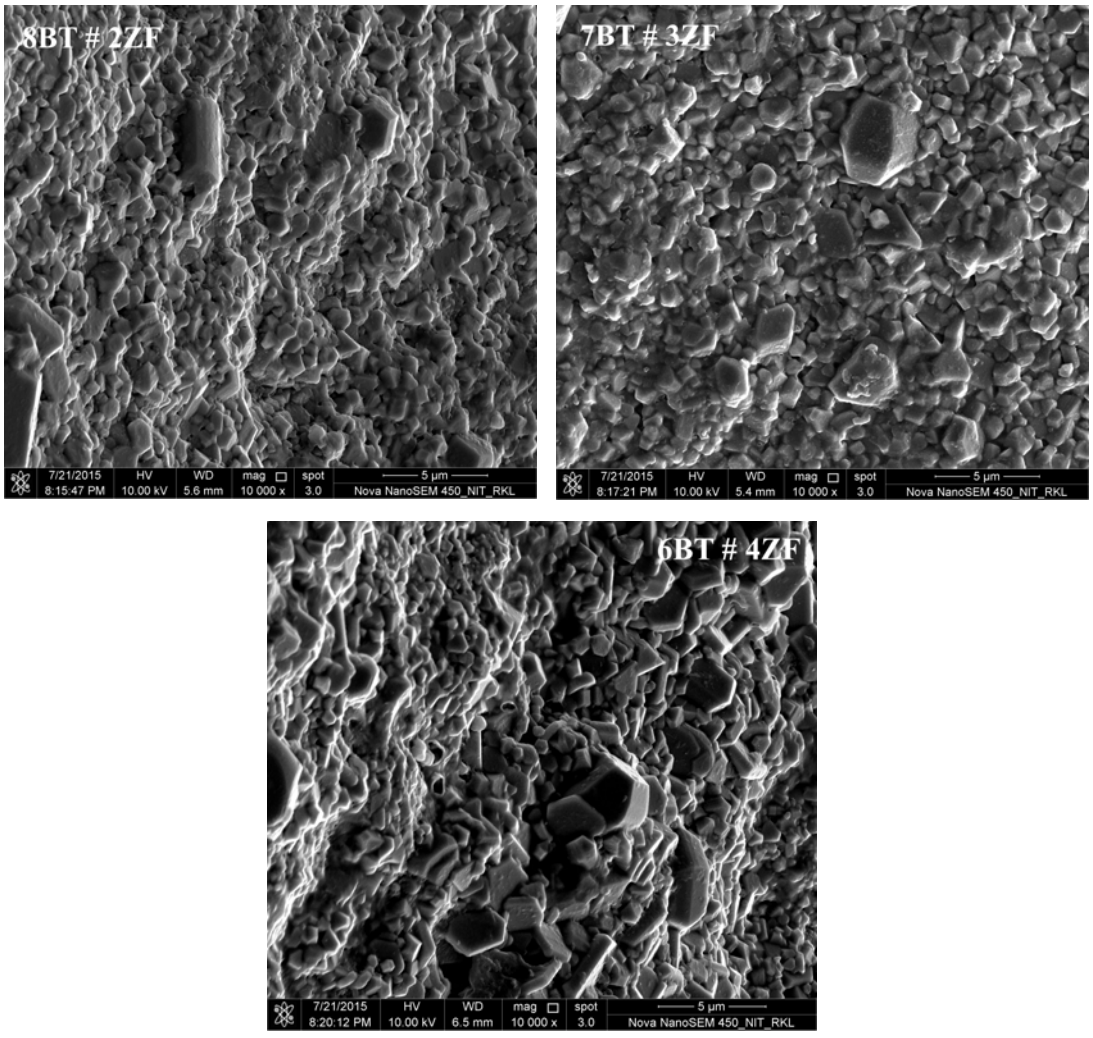

Fig. 6.3: FESEM micrographs of combustion derived in-situ BT: ZF composite having three different compositions.

In addition, FESEM was performed on all sintered combustion derived in-situ BT: CZF composites. Fig. 6.4 show FESEM micrographs of combustion derived in-situ BT: CZF composites having three different compositions (such as 20, 30 and 40 wt % of CZF). The microstructure of these composites was found to be nearly similar type as observed in BT: CF or BT: ZF system. However, the grains of BT and CF were smaller than BT: CF or BT: ZF system. Also, larger size of polyhedral BT phase was not prominent as observed in case of BT: CF and BT: ZF systems. The grain size of BT varies from 1 μm to 4 μm, whereas particle size of CF was around 2 μm. Both BT and CZF were well packed and seem to be highly dense. The theoretical density of 8BT#2CZF, 7BT#3CZF and 6BT#4CZF were found to be around 90 %, 91 % and 91 %, respectively.

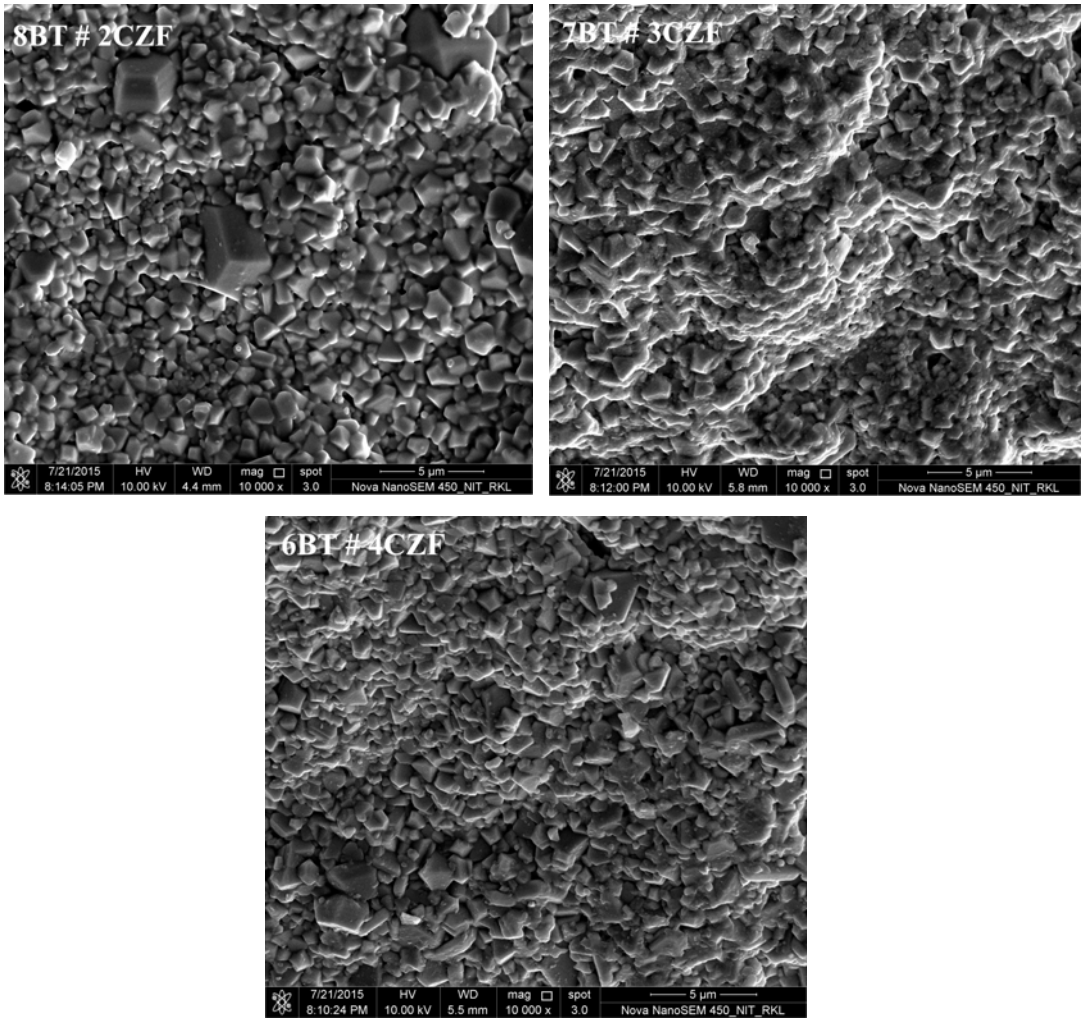

Fig. 6.4: FESEM micrographs of combustion derived in-situ BT: CZF composite having three different compositions.

6.3.3: Dielectric and magnetic properties of BT: ferrite composites

The combustion derived in-situ BT: ferrite composites have different microstructure than the solid-state derived composites prepared using combustion derived powders. The change in microstructure of BT: ferrite systems may lead to modify the dielectric and magnetic properties of these composites. So, the permittivity as a function of frequency of all combustion derived in-situ composites was analyzed at room temperature and is shown in Fig. 6.5. It was observed that the permittivity decreases with frequency. However, the permittivity of all composites derived from in-situ way was dependent on frequency, which was slightly deviated from the permittivity data of solid-state derived composites. In addition, higher permittivity was observed at lower frequency than at higher frequency [31]. Higher permittivity at lower frequency can be attributed to the space charge [54] and Maxwell-Wagner interfacial polarization [32, 34, 54] or due to hopping mechanism in ferrite phase [33] which is prominent after percolation limit [34]. In these type of composites material true dielectric characteristic can only be seen at higher frequency, which high BT composites has high dielectric constant at high frequency[33,53]. In BT: CF composite, the permittivity of 6BT#4CF at 42 HZ is 2278 and at 1 MHz is 689. Similarly, In BT: ZF composites, the permittivity of 6BT#4ZF at 42 HZ is 3873 and at 1 MHz is 954, in BT: CZF composites, the permittivity of 8BT#2CZF at 42 HZ is 1864 and at 1 MHz is 1302.

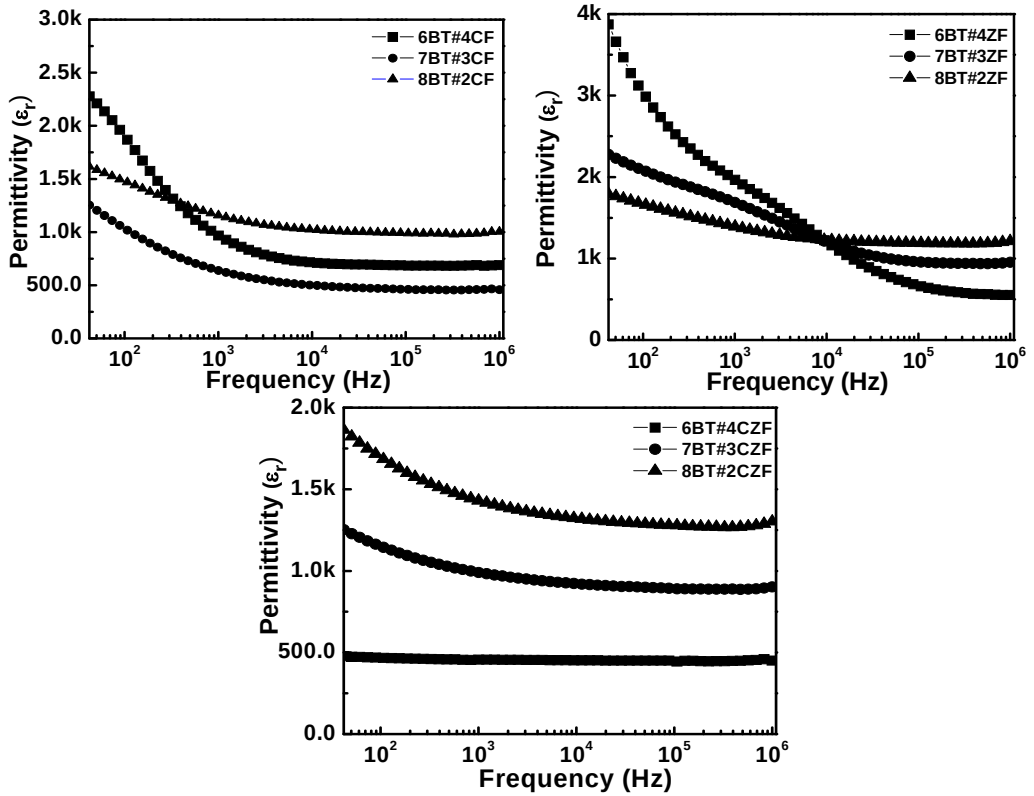

Fig. 6.5: Permittivity as a function of frequency for combustion derived in-situ composites.

Dielectric loss is also one of the key parameter in magneto-dielectric composites and thus was studied for the current composite systems at room temperature. Fig. 6.6 shows the loss (tan δ) response with frequency for all BT: ferrite composites. Dielectric loss is typically dependent on the dielectric phase and percentage of dielectric phase in the magneto-dielectric composites. In addition loss is also dependent on the connectivity of the dielectric phase which ferrite phase gets as continuous phase after percolation limit [34]. In present composite system loss is inversely proportional to the dielectric phase percentage in the BT: CF and BT: ZF magneto-dielectric composite and decrese exponentially with frequency in all three BT: CF, BT: ZF and BT: CZF composite systems. In cobalt zinc ferrite based composite loss varied linearly with the percentage of in the composite, which less loss observed in the composite having highest $BaTiO_3$. However in BT: CF and BT: ZF composite system has the hump type of response, but not in BT: CZF composite. loss humps can be attributed to the frequency resonance with hopping mechanism of Fe^{2+} and Fe^{3+} ions[34],which is prominent in high ferrite (only in CF and ZF) composites. In BT: CZF composite there is no evidence of such hump response, due to which cobalt-zinc ferrite may has less or no conductive behavior compared to cobalt and zinc ferrites. In this system, the loss of 0.08, 0.19 and 0.21 was observed in 40, 30 and 20 wt % CZF composites, respectively at 42 Hz. However, highest loss of about 1.05 was observed for 40 wt % ZF in BT: ZF composites Loss of around 0.19, 0.15 and 0.08 was observed in 20 wt% of cobalt, zinc and cobalt-zinc ferrite composite systems, respectively at 42 Hz. In addition, BT: CZF composites have the lowest loss among the BT: CF and BT: ZF composites.

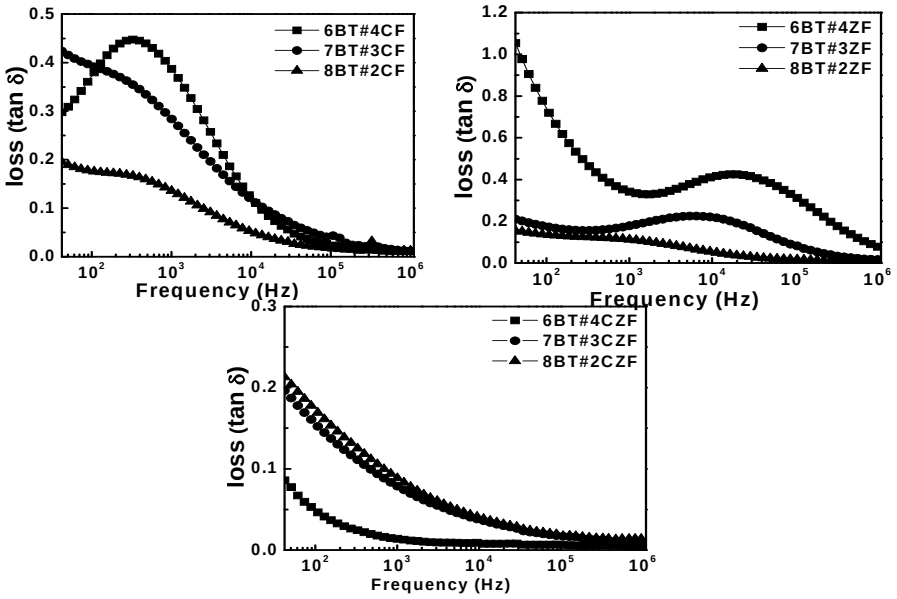

Fig. 6.6: Dielectric loss as a function of frequency for combustion derived in-situ BT: ferrite composites

Polarization responses in the composite arise from the dielectric phase. Fig. 6.7 shows the polarization response as s function of applied field of In-siut derived BT: ferrite composites. In present magneto-dielectric composite system, percentage dielectric phase has the major effect in the polarization response. It was observed that the responses of PE loop of the present BT: ferrite composites deviated from the ideal ferroelectric loop. Particularly 30 and 40 wt % ferrite based composites appear in oval shape indicating lossy capacitor phenomena in BT: CF and BT: ZF composites due to conductive ferrite phase [28]. However, all 20 wt % ferrite based magneto-dielectric composites shows near ferroelectric behavior due to less ferrite percentage. BT: CZF ferrite composites responded differently when compared to BT: CF and BT: ZF composite. Polarization, remanent polarization and coercivity increased with increasing ferrite percentage in BT: CF and BT: ZF composites, which rose from the magnetic dipoles like Fe^{2+} and Fe^{3+}. In BT: CZF composite polarization and remanent are proportional to the dielectric phase in the composites. Polarization, remanent polarization and coercivity of all composites are given in Table 6.1. It was observed that all these parameters increase with the magnetic percentage, which can be attributed to the magnetic dipoles (due to Fe^{2+} and Fe^{3+}) response to the electric field. From the appearance of PE loos in solid state and in-situ composites it can confirm that dielectric properties are prominent in the in-situ synthesis method.

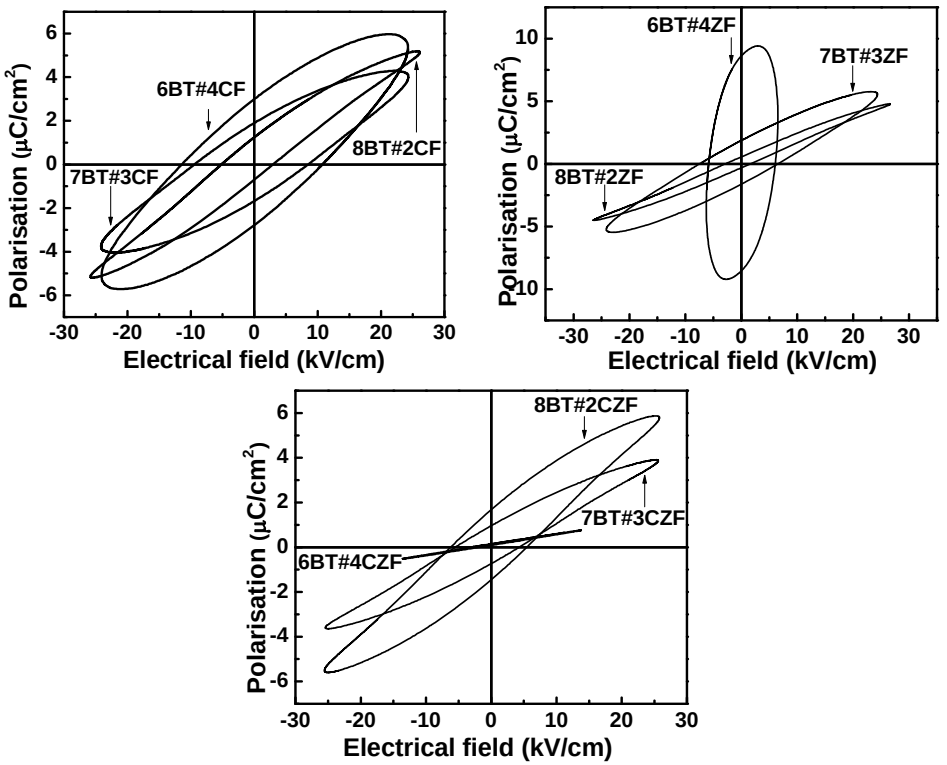

Fig. 6.7: polarization as function of electric field for combustion derived in-situ composites

Table 6.1: Remanent polarization, coercivity and polarization (at maximum field) of in-situ derived BT: ferrite composites.

Composites	Remanent Polarization $P_r(\mu C/cm^2)$	Coercivity Ec(kV/cm)	Polarization $P(\mu C/cm^2)$
6BT#4CF	2.9	11	6
7BT#3CF	1.9	9	4.2
8BT#2CF	1.2	5	5.2
6BT#4ZF	8.5	6	9.3
7BT#3ZF	1.7	7	5.7
8BT#2ZF	0.55	2	4.8
6BT#4CZF	0.2	1.7	0.7
7BT#3CZF	0.9	5.5	3.9
8BT#2CZF	1.69	6.2	5.8

The nature and parentage of magnetic phase in the composite has the significant effect on the magnetic response of the composite. Fig. 6.8 shows the magnetization as function of magnetic field for typical solid-state derived 30 wt. % ferrite composites. Composite magnetization responses in the applied magnetic field are nearly same as responses noticed in the auto combustion derived solid-state composites .The ferromagnetic behavior of the BT: CF and BT: CZF composites are due to the magnetic phase in the composite. BT: CF and BT: CZF composites saturated hardly because of pining effect from the non-magnetic $BaTiO_3$ in the composite. Zinc ferrite based composite are responding like magnetic material, due to magnetic impurity $BaFe_{12}O_{19}$ in the composite which originated in the sintering of composite, presence of $BaFe_{12}O_{19}$ can be confirmed from the Fig. 6.1. Cobalt-zinc ferrite composite represents soft magnetic nature when compared to cobalt ferrite composite by showing slightly lower coercivity, but not prominent as it was in combustion derived solid state composites. Magnetization (M) at 4.5 kOe, remanent magnetization (M_R) and coercivity (H_C) of the 30 wt% cobalt ferrite composites are 70emu/g, 4.67emu/g and 0.35 kOe respectively. Similarly 67emu/g, 4.24emu/g and 0.31kOe are the magnetization (M), remanent magnetization (M_R) and coercivity (H_C) of the 30 wt % cobalt-zinc ferrite composites. Magnetic responses of the cobalt-zinc ferrite composites are relatively lower than the cobalt based composites. Remanent magnetization, coercivity and magnetization of in-situ composites in detailed in tabulated in table no 6.2

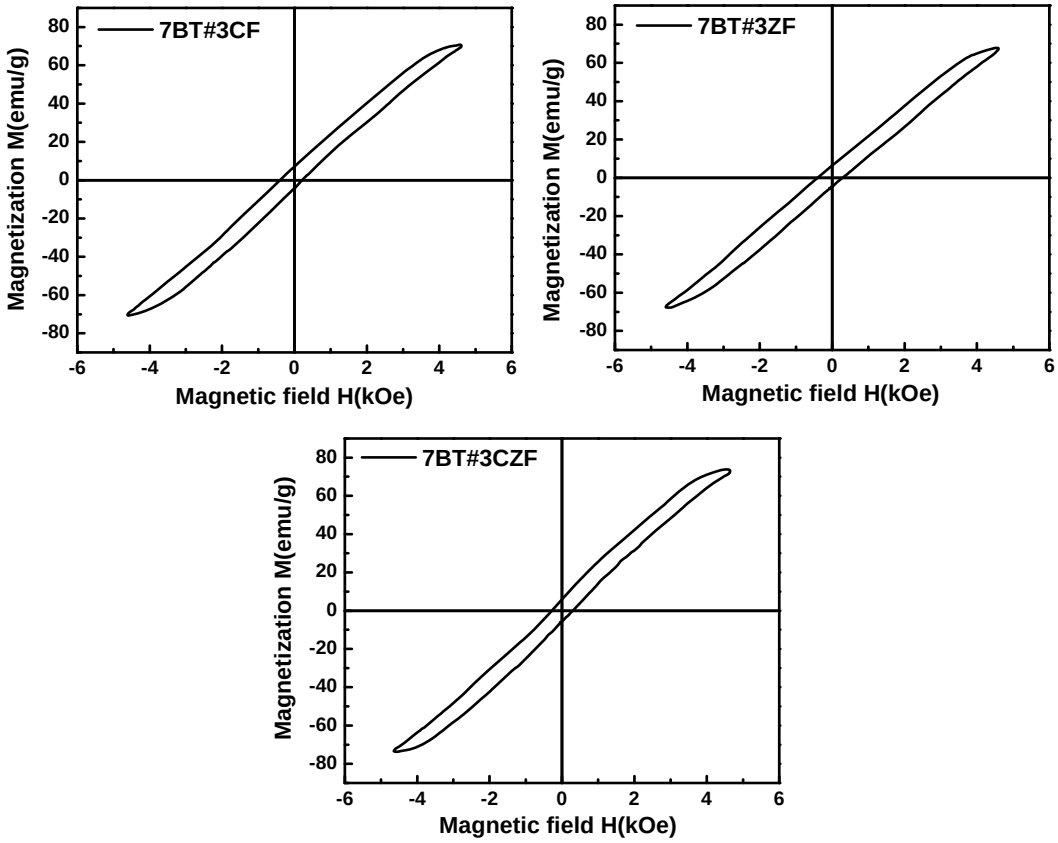

Fig. 6.8: M-H loop of In-situ derived 30 wt % ferrite based BT: ferrite composites.

Table 6.2: Ramanent magnetization, coercivity and magnetization (at 4.5 kOe) in-situ derived BT: ferrite composites.

Composites	Remanent magnetization Mr (emu/g)	Coercivity Hc (kOe)	Magnetization M (emu/g)
6BT#4CF	7.01	0.29	86
7BT#3CF	4.67	0.35	70
8BT#2CF	4.5	0.29	67
6BT#4ZF	3.78	0.25	76
7BT#3ZF	3.78	0.19	73
8BT#2ZF	3.78	0.28	69
6BT#4CZF	4.01	0.27	67
7BT#3CZF	4.24	0.31	67
8BT#2CZF	4.22	0.27	65

Magneto-capacitance response in the composites can be originated from the mechanical coupling between ferromagnetic and ferroelectric phases in the composites, so extrinsic parameters like magnetic percentage and microstructure plays a significant role in magnet-dielectric response [56]. Fig.6.9 shows the magneto-capacitance as function of magnetic field for in-situ derived composites. Significant response can be seen from the composites due to the magnetic field. Cobalt and cobalt-zinc based composites shows the negative capacitance response. In cobalt zinc ferrite based composites both negative and positive responses are observed. As discussed in previous chapter the cause of magneto-capacitance in the composite arises from two sources. Magnetostriction and magnet resistance and either of the mechanisms are strongly dependent on the microstructure and morphologies of phases present in the composites.[57,51] Cobalt and cobalt-zinc ferrite composites followed the trend of increasing capacitance response with respective to percentage of ferrite in composite. Also Zinc and cobalt zinc ferrite based composite shows the both negative and positive magneto-capacitance response. Magnetostriction and magneto resistance of ferrites along with phase morphological complexes are responsible for the present divergent results [57,51] 9.19 %, 7.15% and 1.95% are the responses from the 40 wt%, 30 wt% and 20 wt% cobalt ferrite composite systems respectively and 6.38%, 1.91% and 0.46% capacitance responses are from 40 wt%, 30 wt% and 20 wt% zinc ferrite composite systems respectively. 30 wt % cobalt zinc composite gave the negative response. Highest magneto resistance among the solid-state composites observed in 40% cobalt ferrite composite with 9.19% change in capacitance

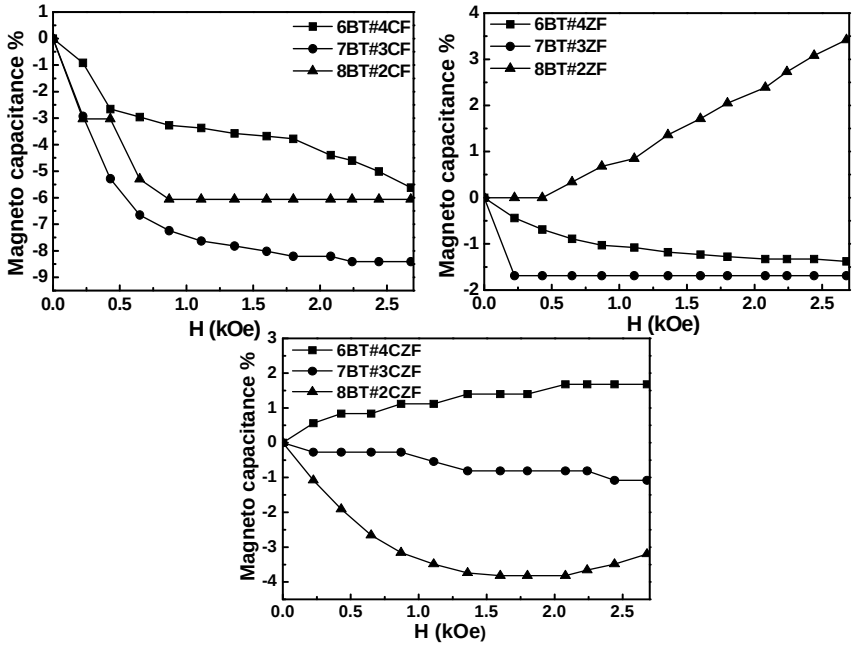

Fig.6.9: Magneto-capacitance as function of magnetic field for combustion derived In-situ composites

Magneto-capacitance response of the composite shows the divergent results due to change in the synthesis method. To under the nature of magnetic phase as function of its percentage has been studied. Fig. 6.10 shows the magneto-capacitance as function of magnetic phase percentage for In-situ derived composites. In comparison to the magneto-capacitance data obtained from solid state derived composites, ex-situ composites have different nature. At 20 and 30 wt % region magneto-capacitance is higher in the in-situ composites, whereas in 40wt % ferrite region in-situ synthesis method has the higher value. The homogeneity in the in-situ composites has supported the composite to have higher magneto capacitance at 20 and30 wt% ferrite composite, but at 40 wt% percentages the even distribution of ferrite among the $BaTiO_3$ made the composite not to react much to the magnetic field. In solid state composite system the availability of plate like $BaTiO_3$ has the significant effect. Though at 20wt% capacitance response is lower, 30 and 40 wt% composites has the capacitance response higher than the in-situ composites, due to which well-connected $BaTiO_3$ plate morphology supports much for magneto capacitance effect.

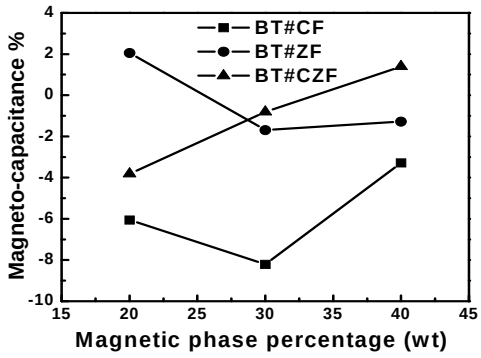

Fig. 6.10: Magneto-capacitance as function of magnetic phase percentage for In-situ derived composites

6.4: Remarks:

$BaTiO_3$ with ferrite based magneto-dielectric composites has been prepared using auto combustion derived in-situ synthesis method. XRD pattern shows the existence of $BaTiO_3$, $CoFe_2O$, $ZnFe_2O_3$ and $CoZnFe_2O_3$ as major phases along with traces of $BaFe_{12}O_{19}$ in all composites. Traces of hexagonal BT also found in the 40 wt% CZ ferrite bases composite. Homogeneity and narrow grain distribution are found in microstructures of composite. Permittivity and loss responses of composites found to be frequency dependent. PE loop characteristics of composites with 20wt% ferrite have the ferroelectric behavior, 30 and 40 wt% ferrite composite shows near ferroelectric behavior. CF and CZF based composite shows ferromagnetic behavior in HM hysteresis loop. ZF and CZF based composite shows the both positive and negative magneto-capacitance response, but CF based composite shown only negative response.

CHAPTER 7

Structure, microstructure and magneto-dielectric properties of auto-combustion derived ex-situ BT: ferrite composites

In this chapter, BT: ferrite composites have been prepared via ex-situ auto-combustion method. 30 wt % of Ferrite such as CF, ZF and CZF have been used for preparing BT: ferrite composites. Structure, microstructure along with magneto-dielectric properties of different BT: ferrite composites are studied and analyzed in detail.

7.1: Introduction

Microstructure of BT: ferrite based composites strongly dependent on the synthesis method, as observed from chapter 5 and 6 and this drives forward to explore different way of combustion synthesis i.e. ex-situ way. Combustion derived ex-situ synthesis method provides a new direction to explore the structure, microstructure and magneto-dielectric properties of BT: ferrite based composites. In this chapter, one typical composition of 30 wt % ferrite was chosen to explore ex-situ way of combustion synthesis to develop BT: ferrite composites. Structure, microstructure along with magneto-dielectric properties of different BT: ferrite composites are studied and analyzed

7.2: Experimental

Ex-situ synthesis method involves dispersing one of the composite compounds during combustion synthesis of another compound. Raw materials such as Ba $(NO_3)_2$ (Barium Nitrate), $TiO(NO_3)_2$ (Titanyl nitrate), $C_6H_8O_7$(citric acid), NH_4NO_3 (ammonium nitrate) and $C_{10}H_{16}N_2O_8$ (EDTA) were selected for evolution of BT phase during combustion synthesis (discussed in Chapter 4). Similarly, $Fe(NO_3)_3.9H_2O$ (Ferric Nitrate nona hydrte), $Co(NO_3)_26H_2O$ (Cobalt nitrate hexa hydrate), $Zn(NO_3)_2.6H_2O$ (Zinc nitrate hexa hydrate) and $C_6H_8O_7$(citric acid) as raw materials for evolution of ferrite ($CoFe_2O_4$, $Co_{0.5}Zn_{0.5}Fe_2O_4$ and $ZnFe2O_4$) phase during combustion synthesis. In addition, calcined ferrite powders (derived from combustion synthesis) of 30 wt% were dispersed in the precursor solution during combustion of BT. This composite is symbolically represented as 3(CF/ZF/CZF) @ 7BT. Similarly, calcined BT powder (derived from combustion synthesis) of 70 wt% were dispersed in the precursor solution during combustion of ferrite (CF/ZF/CZF). This composite is symbolically represented as 7BT @3(CF/ZF/CZF). The samples after combustion synthesis were calcined at 800 ^oC for 4 h. The calcined powders were compacted to pellets and finally sintered at 1150 °C for 6 h.

7.3: Results and discussion

7.3.1: Phase analysis of BT: ferrite composites

Phase of each composite after sintering of pellets was analyzed by XRD pattern. Fig. 7.1 indicates XRD patterns of auto-combustion derived ex-situ BT: ferrite composites. All the BT: Ferrite composite systems have major phases like BT, CF, ZF and CZF in their respective composites. Though the percentages of phases are same in composites, the particular ex-situ combustion synthesis method i.e. ferrite@BT plays an important role for forming additional hexagonal ($BaTiO_3$(H)) phase of BT along with the tetragonal $BaTiO_3$, which caused by oxygen vacancies due to the substitution of low charged Fe^{2+}, Co^{2+} and Zn^{2+} ions in the place of high charged Ti4+ ion.[32-34] However, no traces of hexagonal BT was found in case of ex-situ

combustion synthesis method i.e. BT@ferrite. Additionally, Barium hexa-ferrite ($BaFe_{12}O_{19}$) was observed in all ex-situ synthesized composites.

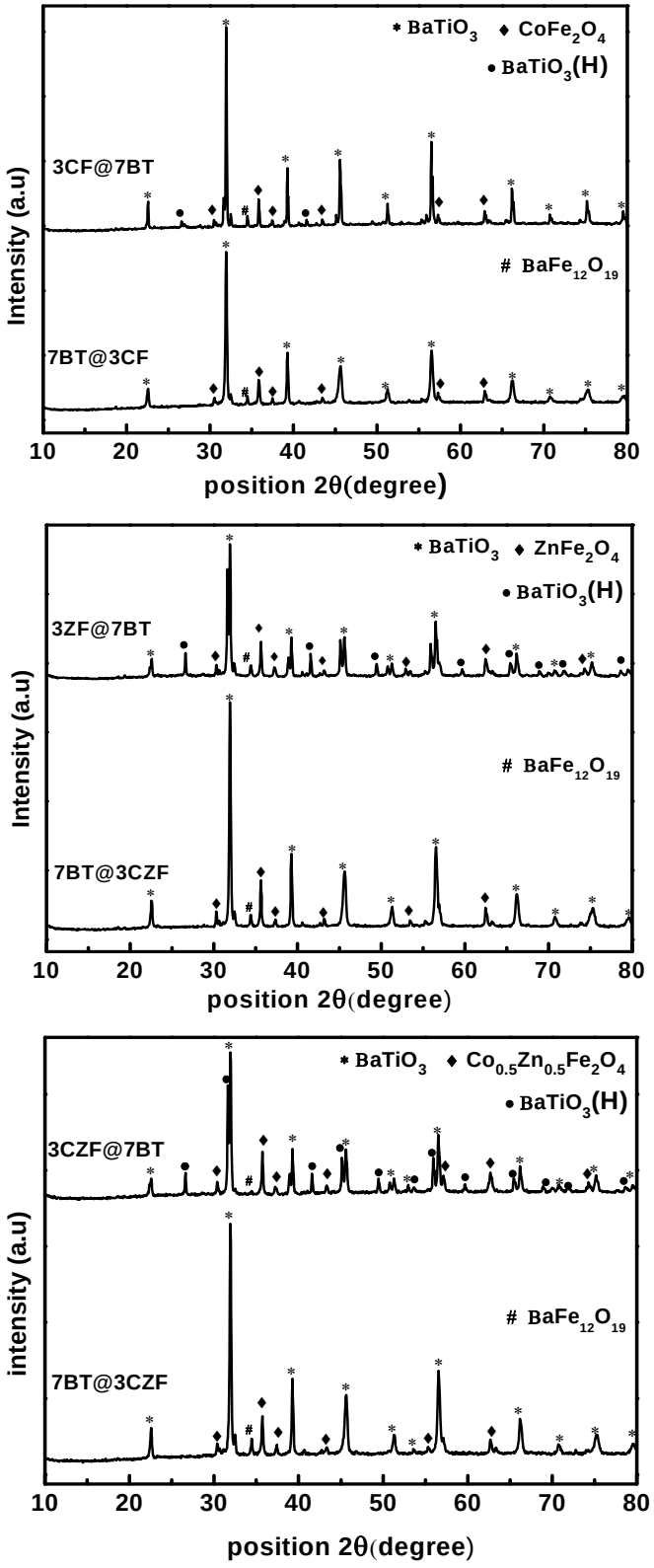

Fig. 7.1: X-ray diffraction patterns of auto-combustion derived ex-situ BT: ferrite composites

7.3.2: Microstructural analysis of BT: ferrite composites

Lower and higher magnified FESEM micrographs of 3CF@7BT and 7BT@3CF are shown in Fig. 7.2. Two morphologies as nearly spherical and plate like structure of BT and one morphology of ferrite in polyhedral form (as observed chapter 5 section 5.3.2) are also observed in both 3CF@7BT and 7BT@3CF composites. But, the BT morphology in the shape of plate-like are more prominent in 3CF@7BT composite than 7BT@3CF composites, as observed from lower magnified FESEM micrograph. The plates of BT are randomly oriented and focusing out of the surface in 3CF@7BT composite, whereas the plates of BT got suppressed and covered with ferrite phase in case of 7BT@3CF composites. Density variations can be easily identified between two micrographs. The relative density of 7BT@3CF and 3CF@7BT was found to be nearly 75% and 90%, respectively. Grain sizes are about 5μm for the plate like $BaTO_3$ and between 1 μm - 2 μm for the polyhedral morphology of both $BaTiO_3$ and ferrite phases.

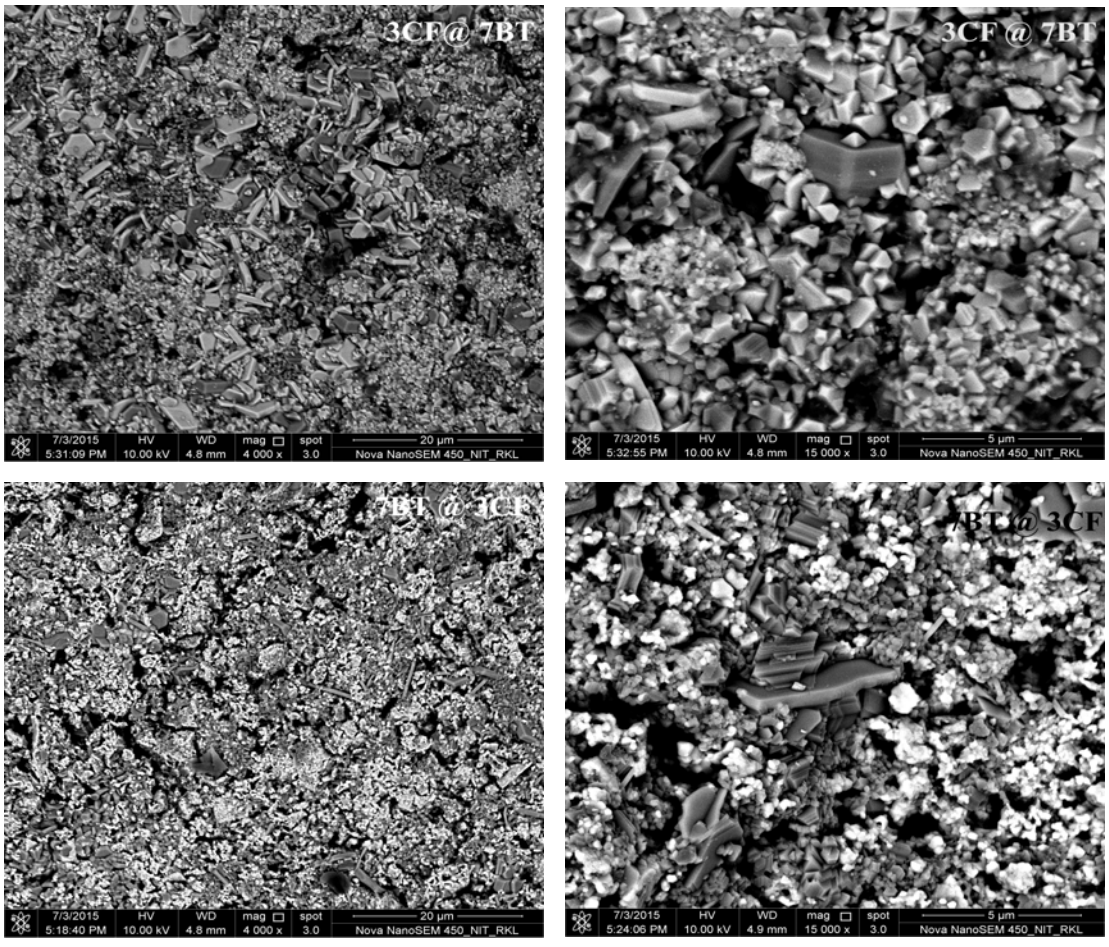

Fig. 7.2: FESEM micrographs of combustion derived ex-situ BT: CF composite having 30wt% ferrite

As the synthesis method effected for microstructure of ex-situ BT: CF composites, same appearance can be identified in the case of ex-situ BT: ZF system also. Fig. 7.3 shows the FESEM micrographs of combustion derived ex-situ BT: CF composite having 30 wt% ferrite compositions. $BaTiO_3$ existence in two morphologies, as plate and nearly spherical shapes along with ferrite in polyhedral morphology can be identified. Plate like morphology in the 3ZF@7BT appeared clearly and plate morphology focusing out of surface. However, in the case 7BT@3ZF composites plate like morphology got suppressed and covered partially by ferrite phase, which clearly can be seen in the higher magnified FESEM images. Grain sizes of the plate like $BaTiO_3$ in the range of 5 µm - 7µm. polyhedral mixing of both $BaTiO_3$ and ferrite are in the range between 1 µm-2 µm. Synthesis methods has significant effect on the densification of composites. The theoretical densities of 7BT@3ZF and 3ZF@7BT composites are around 74 % and 89 %, respectively.

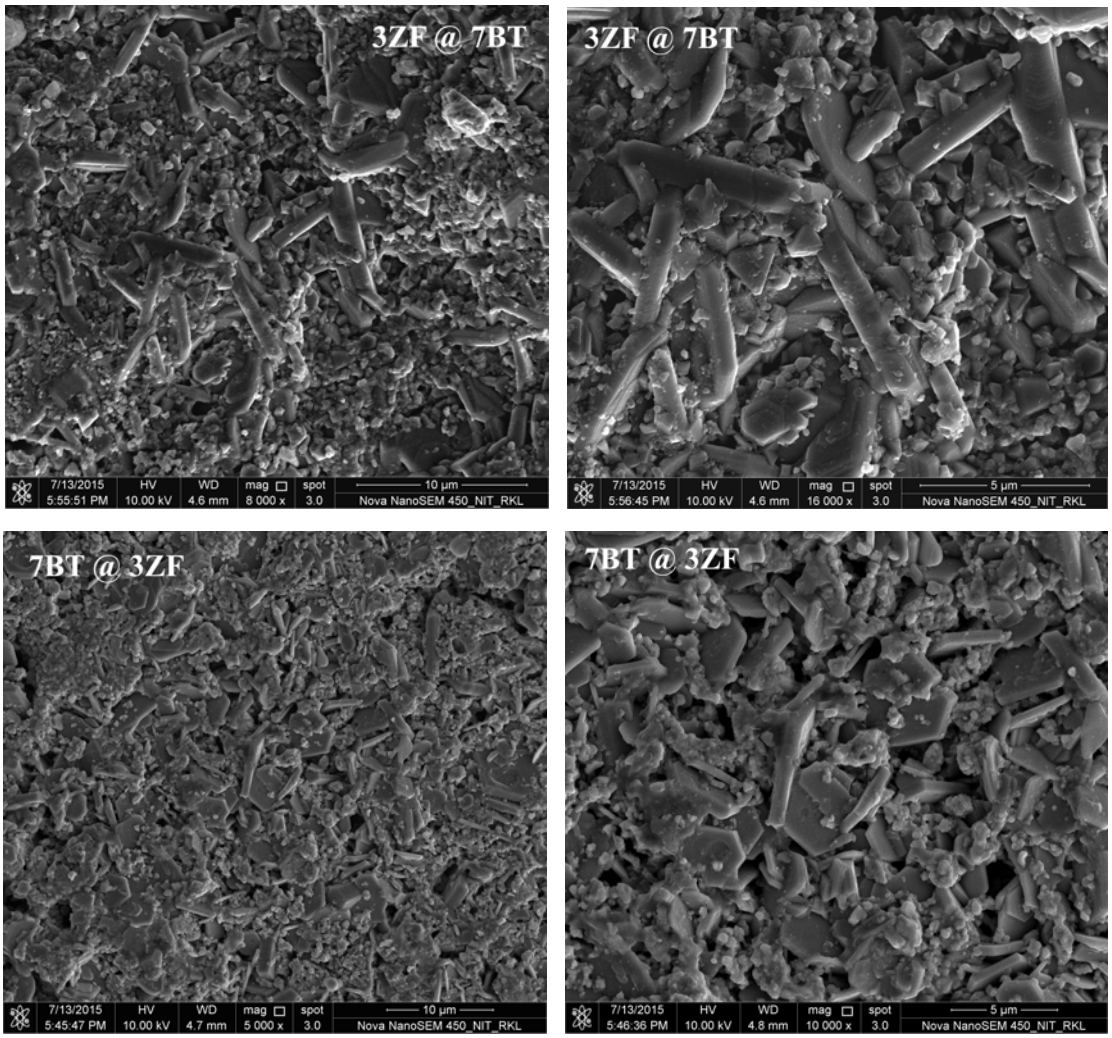

Fig. 7.3: FESEM micrographs of combustion derived ex-situ BT: ZF composite having composite having 30wt% ferrite

Similarly, FESEM micrographs of combustion derived ex-situ BT: CZF composite are shown in Fig. 7.4. The plate like morphology of BT is much prominent in 3CZF@7BT composite, which strongly focusing out of surface. But in 7BT@3CZF composites no such evidence of plate like morphology appeared on surface. It seems that ferrite phase was covered and BT phase was suppressed in7BT@3CZF composites. Comparing the morphology of BT in ex-situ derived both BT@CF / CF@BT and BT@ZF / ZF@BT, the grain size of BT was much larger and more thicker. Also BT phase was more exposed from the surface. The grain size of plate like $BaTiO_3$ exists in between 12 μm to 8μm having a thickness of nearly 2μm. Spherical shapes of $BaTiO_3$ and polyhedral shape of ferrite phases are nearly 1 μm -2 μm in size. The theoretical densities of 7BT@3CZF and 3CZF@7BT composites are found to be 80% and 86% respectively.

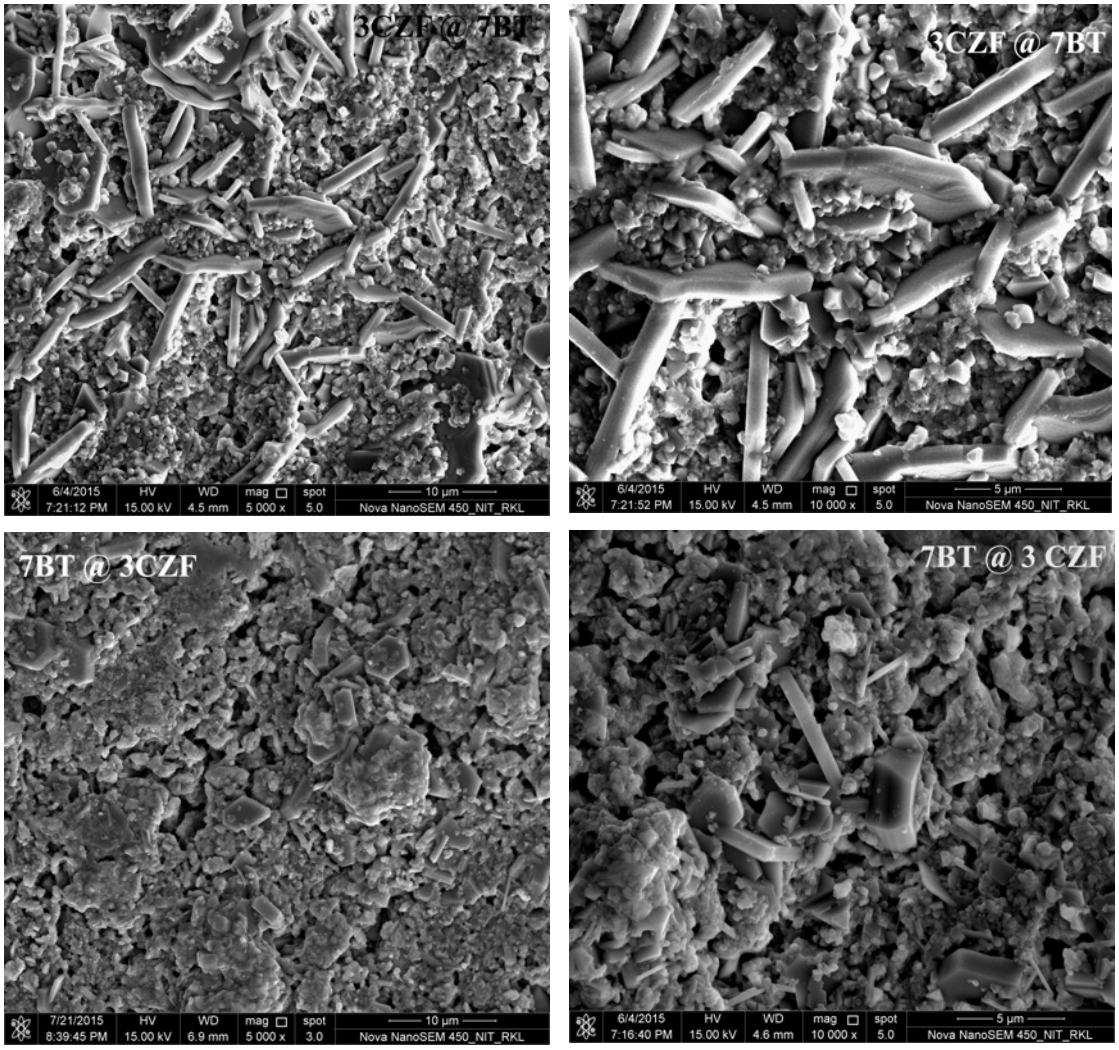

Fig. 7.4: FESEM micrographs of combustion derived ex-situ BT: CZF composite having 30wt% ferrite

7.3.3: Dielectric and magnetic properties of auto combustion derived ex-situ BT: ferrite composites

Permittivity measure is the one of the important parameter to estimate the capacitance of the dielectrics. In present ex-situ composite system, permittivity measure at room temperature. Fig.7.5 shows the Permittivity as a function of frequency for ex-situ derived composites. BT@ferrite composites show the frequency dependent response at lower frequency and got independent at higher frequency. In Ferrite@BT composite permittivity response look dependent hardly on the frequency and also slightly dependent type of ferrite. At lower frequency though BT@ferrite campsite has the higher permittivity both BT@ferrite and Ferrite@BT composites merged together and Ferrite@BT shows slightly higher permittivity at higher frequency. The high permittivity responses of the BT@ferrite at lower frequencies can be attributed to the Maxwell-wagner interfacial polarization [32, 34, 51, 53] between plate like $BaTiO_3$ and Ferrite. In present ex-situ composites percolation limit of the ferrite has changed with the synthesis method which became continuous in lower ferrite percentage only, so that permittivity has increased owing to hopping mechanism [33] and also significant effect of space charge polarization (due to porosity) can also because of high permittivity in 7BT@3ferrite , which have less density. [34] 6835, 4952 and 5912 are highest permittivity values observed for 7BT@3CF, 7BT@3ZF and 7BT@3CZF respectively at 42 Hz.

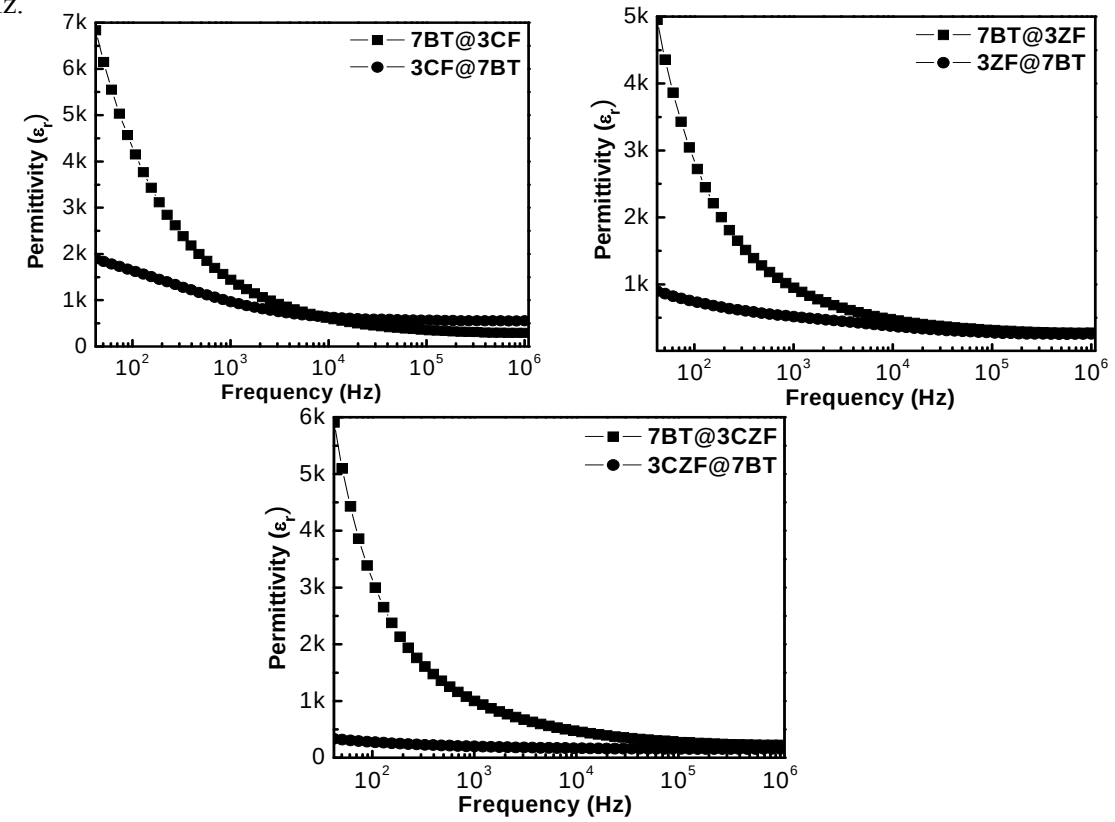

Fig.7.5: Permittivity as a function of frequency for combustion derived ex-situ composites.

The dielectric loss measurement of the composites gives the electric energy dissipation as loss angle tanδ. Fig.7.6 shows Dielectric loss as a function of frequency for ex-situ derived composites. Loss in the magneto-dielectric composites originates from both dielectric phase and magnetic phase. All the ex-situ derived composite shows the frequency dependent loss response at lower frequency and slowly became independent at higher frequency. BT@ferrite composites show the relatively higher loss than ferrite@BT composites at lower frequency and decreased with nearly exponential scale. Very slight humps can be identified in the loss response for the 3CF@7BT and 3ZF@7BT composites at 10^4 Hz frequency. Electron transfer between Fe^{2+} and Fe^{3+} usually gives the high loss [33], if that electron transfer (between Fe^{2+} and Fe^{3+}) frequency resonate with the applied frequency it gives the loss humps (at resonance frequency) These responses can be seen prominently in cobalt and zinc based composite systems, but not in cobalt-zinc ferrite system. Loss of about 3.16, 1.83 and 2.76 was observed in 7BT@3CF, 7BT@3ZF and 7BT@3CZF respectively at 42Hz frequency. Ferrite@BT composites have 4 times less loss compared to BT@Ferrite.

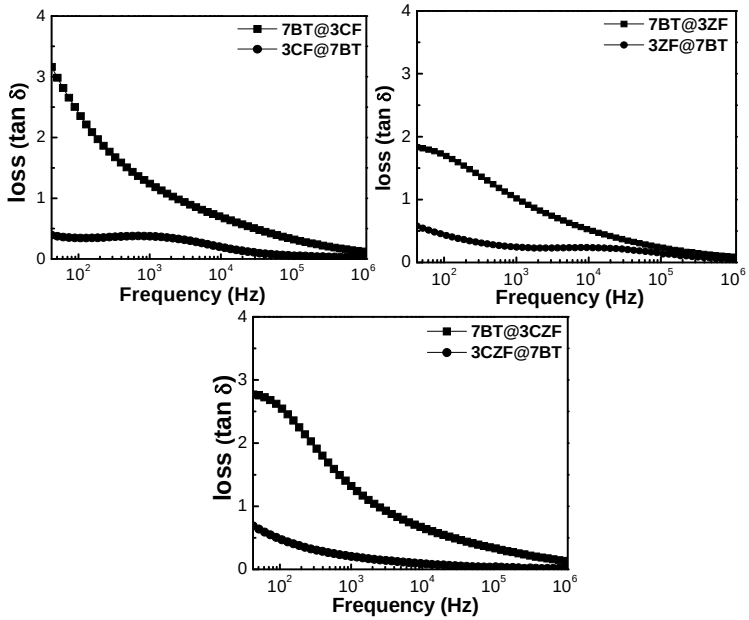

Fig.7.6: Dielectric loss as a function of frequency for combustion derived ex-situ BT: ZF composites.

Polarization responses of the magneto-dielectric due to applied field shows significant difference due to the synthesis method. Fig. 7.7 shows the polarization response of Ex-situ derived BT: ferrite composites as function of electric field. Effect of synthesis method and phase connectivity shows noticeable difference in the PE loops. The polarization from the magnetic phase can also be contributed to PE loop, which arises from the dipodic interaction between Fe^{2+} and Fe^{3+} ions. Composites synthesized with BT@Ferrite method has took the shape of the lossy dielectric.

Which indicates the high loss in composites, and proportional to the area enclosed in the loop. However Ferrite@BT synthesized composites has less loss compared to BT@Ferrite composites. This change in the PE loops can originated from the connectivity of $BaTiO_3$ phase in the Ex-situ composites, which has good connectivity between $BaTiO_3$ grains in Ferrite@BT composites than BT@Ferrite composites. Remanent polarization (Pr) and polarization (P) at maximum field decreased with the change in synthesis method from Bt@ferrite to Ferrite@BT, but coercivity responded inversely. Detailed values regarding remanent polarization, coercivity and polarization are tabulated in table no 7.1.

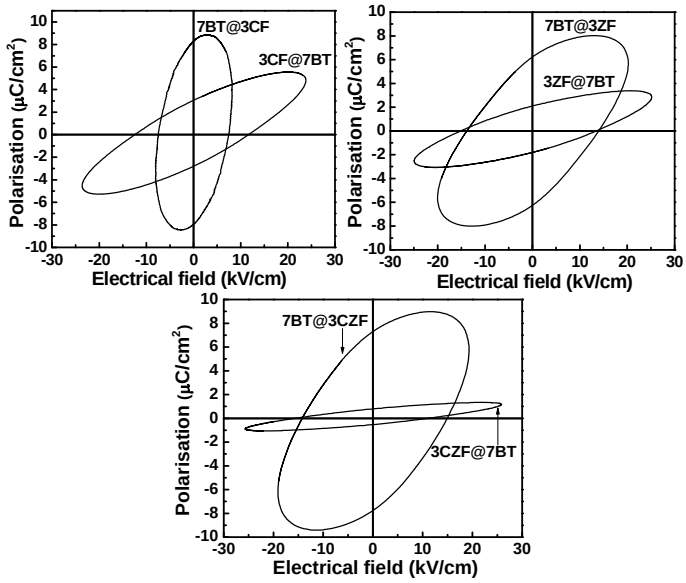

Fig. 7.7: polarization as function of electric field combustion derived ex-situ BT: ferrite composites

Table 7.1: Remanent polarization, coercivity and polarization (at maximum field) of ex-situ derived BT: ferrite composites.

Composites	Remanent Polarization $P_r(\mu C/cm^2)$	Coercivity Ec(kV/cm)	Polarization $P(\mu C/cm^2)$
7BT@3CF	8.2	7.4	8.9
3CF@7BT	3.0	12	5.6
7BT@3ZF	6.2	13	8.0
3ZF@7BT	2.0	15	3.6
7BT@3CZF	7.2	14	9.0
3CZF@7BT	0.8	15	1.29

M-H loop magnetic characterization of the composite gives the understanding on the magnetic dipole movement in the magnetic phase in the presence of the dielectric phase in the

composite. In present magneto-diacritic composite system hard and soft magnets were selected as a part of magnetic phase. Cobalt-zinc ferrite shows relatively soft magnetic nature up on cobalt ferrite which can be confirmed by less coercivity in soft magnetic material. Zinc ferrite by nature it is a nonmagnetic material. In Ex-situ composite system we took 30 wt % ferrite for synthesizing both BT@ferrite and Ferrite@BT composites. Fig. 7.8 shows M-H loop of Ex-situ derived 30 wt % ferrite based BT: ferrite composites measured at room temperature. In present magneto-dielectric composites MH loop responses seems deviated from ideal MH loops. This deviation from ideal nature can be attributed to the presence of dielectric phase in the composite and very less magnetic phase present. Froth MH loop response it can be conclude that cobalt and cobalt zinc responses are in ferromagnetic nature, but not zinc based composite. Cobalt zinc ferrite based composite look more effective in ferromagnetic nature. Coercivity is more in ferrite@BT composite than ferrite@BT, because the prescience plates like BT in ferrite@BT. Average coercive values of cobalt ferrite (0.33kOe) and cobalt zinc ferrite (0.185kOe) based composites reveals relatively soft magnetic nature of the cobalt-zinc ferrite. By nature Zinc ferrite is nonmagnetic (no net magnetic movement due to dia-magnetic nature of Zn atom) material, but in our composite it responded to the field by showing remanent magnetization and coercivity. By care full observation of the X-ray diffraction pattern of the Ex-situ derived BT: zinc ferrite composites, it has barium haxa ferrite ($BaFe_{12}O_{19}$) as the impurity, which formed in the process of sintering of pellets. (CF/ZF)ferrite@BT composites have slightly lower magnetization than (CF/ZF)Ferrite@BT. In the case of cobalt-zinc based Ex-situ composites 3CZF@7BT has high magentization than 7BT@3CZF. Details of MH loop characteristics for Ex-situ composites are given in Table 7.2.

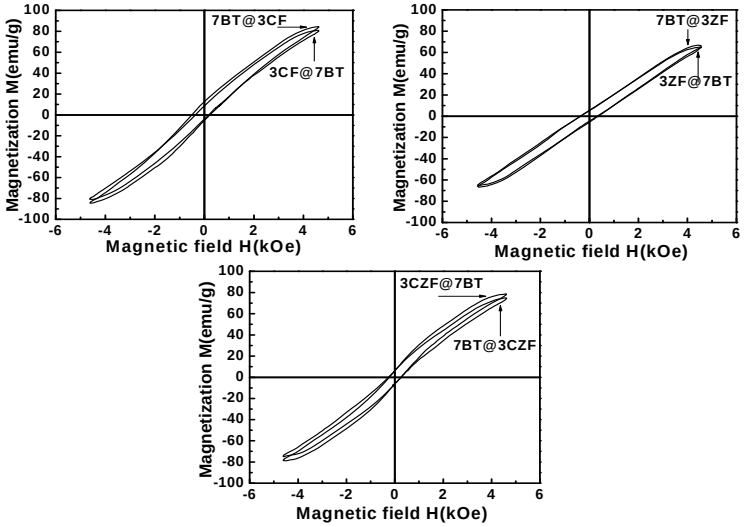

Fig. 7.8: M-H loop of combustion derived ex-situ 30 wt % ferrite based BT: ferrite composites.

Table 7.2: Remanent magnetization, coercivity and magnetization (at 4.5 kOe) of ex-situ derived BT: ferrite composites.

Composites	Remanent magnetization Mr(emu/g)	Coercivity Hc(kOe)	Magnetization M(emu/g)
7BT@3CF	7.75	0.37	84
3CF@7BT	6.25	0.29	80
7BT@3ZF	3.76	0.39	66
3ZF@7BT	3.37	0.32	65
7BT@3CZF	4.25	0.19	75
3CZF@7BT	3.93	0.18	78

The important property of the magneto-dielectric composite is magneto capacitance. The change in percentage the permittivity of the composite in varying DC magnetic field to the no magnetic field gives the magneto capacitance percent change. From this data, the interaction between magnetic and dielectric phase can be determined. As it has been observed from previous chapters, synthesis method plays an important role in tuning the magneto-dielectric response in magneto-dielectric composite which effected by microstructure [56]. Fig.7.9 shows the Magneto-capacitance response as function of magnetic field for ex-situ derived composites. The responses from the 7Bt@3ferrite(CF/ZF/CZF) are in the positive direction and 3ferrite(CF/ZF)@7BT responses are in negative direction, but 3CZF@7BT composite shows positive response. Apart from the sign of response ex-situ synthesis method gave the highest magneto-capacitance percentage change among in-situ and solid-state mixing methods. Ex-situ synthesis method shows a great difference in magneto-dielectric response. The both negative and positive magneto-capacitance response observed in the cobalt ferrite based composite system, which is absence in the either of solid state and in-situ synthesis process prepared composites. Zinc ferrite also shows both negative and positive magneto-capacitances. Though the magnetostriction has the direction anomalies from the point of ferrite type used in the composite, present results are contradictory to magnetostriction.[57,58] Strong microstructural differences aroused due to plate like BT in the composites are responsible for divergent results. Similarly magneto-resistance in the composite varied by method adopted to synthesize the composite with same ferrite percentage. The core and interfacial magneto resistances along with Maxwell –Wagner polarization has given both positive and negative responses respectively in the present magneto-dielectric composites. [51] Though same percentage of ferrite exists in 7BT@3ferrite and 3Ferrite@7BT composites, microstructural difference gave different capacitance response in magnetic field. 9.91%, 19.67% and 19.9% are the magneto-capacitance for 7BT@3CF, 7BT@3ZF and 7BT@3CZF respectively in respective

magnetic type. In all (CF/ZF/CZF)Ferrite@BT magneto dielectric composites 3CZF@7BT gave highest response of 10.63% magneto-capacitance.

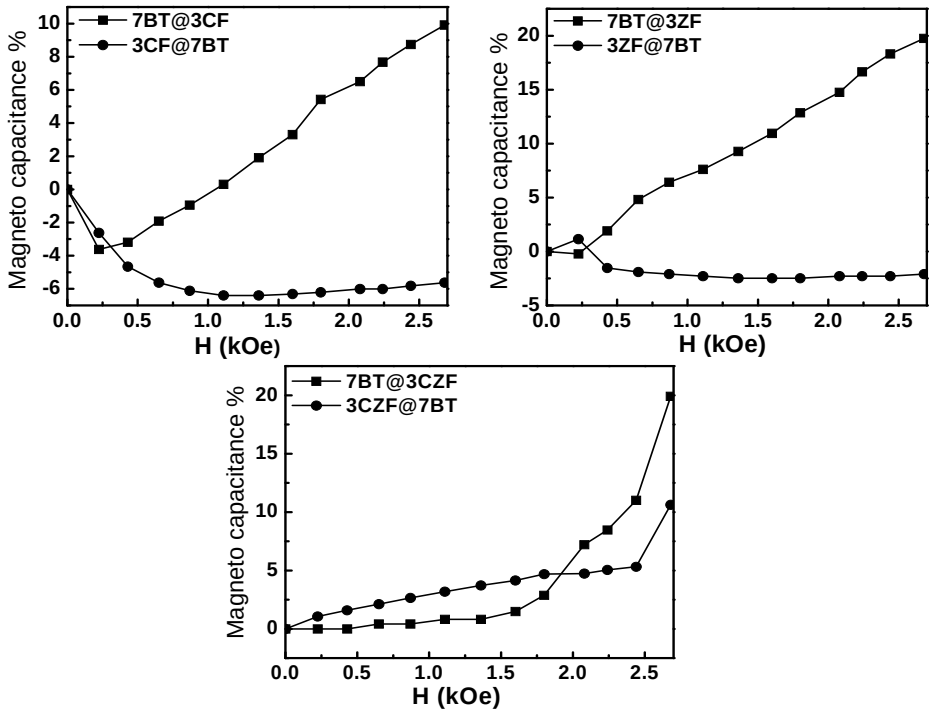

Fig.7.9: Magneto-capacitance as function of magnetic field for ex-situ derived composites

7.4 Remarks:

$BaTiO_3$ and ferrite based magneto-dielectric composites have been prepared via ex-situ auto-combustion synthesis method. Composite prepared in ferrite@ BT method has the both hexagonal and tetragonal $BaTiO_3$ phases. Permittivity and loss response are found frequency dependent. Composite prepared in ferrite@BT shows nearly ferroelectric PE loop, but BT@ferrite composite shows lossy loop behavior. CF and CZF based composites shows the ferromagnetic behavior in MH hysteresis loop. Both positive and negative magneto-capacitances are observed in the cobalt and zinc based composites, and only positive responses are observed in the cobalt-zinc ferrite based composite system.

CONCLUSIONS

BT: ferrite magneto dielectric composite were successfully prepared using auto-combustion derived solid-state mixing, in-situ and ex-situ synthesis methods. Structure, microstructure and magneto-dielectric characterizations were performed. Results were discussed and conclusions of this research work are as follows.

Phase analysis:

- $BaTiO_3$, $CoFe_2O_4$/$ZnFe_2O_4$/$Co_{0.5}Zn_{0.5}Fe_2O_4$ detected as major phases in composites along with the traces of $BaFe_{12}O_{19}$ in all composites.
- Hexagonal $BaTiO_3$ found in 40 wt% CZF composite prepared via in-situ synthesis method. Similarly (CF/ZF/CZF)ferrite@BT composites prepared via ex-situ method also shows the hexagonal $BaTiO_3$ along with tetragonal $BaTiO_3$.

Microstructure of BT: ferrite composites:

- $BaTiO_3$ found in two types of morphologies, which is plate and agglomerated nearly spherical-like shapes. Plate-like morphology is much prominent in 30 % ferrite composites. In these particular composites, the plate-like BT phase was randomly oriented and the plates in vertical position resembling rod-like morphology. However, the plate-like BT phase was also present but orientated in one direction for other composite systems.
- The growth of polyhedral ferrite in 20 wt % ferrite based composites is lower and not sufficient enough to orient the plate-like morphology of BT phase and thus plate-like BT phase orient in one direction in 8BT: 2 CF/ZF/CZF composite systems. As the percentage of ferrite increases to 30 wt%, the polyhedral ferrite phase is prominent and its growth is sufficient to orient the plate-like BT phase in random way. Further increase of ferrite to 40 wt%, the growth of polyhedral ferrite phase increases and also partially covers the plate-like BT phase. So, in 6BT: 4 CF/ZF/CZF composite systems unidirectional plate like BT and polyhedral ferrite phases are with nearly same size and distribute undistinguished.
- The size of BT plates was ~5 μm with a thickness ~1 μm, whereas polyhedral ferrite was in between 0.5-2.5 μm. Both BT and ferrite phases were well packed and seem to be highly dense. The density of these composites increases with ferrite content and varies in between 89-91%
- In-situ combustion synthesis, composite shows homogeneous and narrow grain distribution of agglomerated nearly spherical shape of BT phase and polyhedral shapes of ferrites.
- The grain size of BT varies from 1 μm to 5 μm, whereas particle size of CF was around 2 μm. Both BT and CF were well packed and seem to be highly dense. The theoretical density of these composites were found to be around in the range of 90-94 %.
- Plate like morphology of $BaTiO_3$ found in the composites (CF/ZF/CZF)3ferrite@7BT prepared by ex-situ synthesis method, which are focusing out of surface. Plates of $BaTiO_3$ phase shows unidirectional look and the orientation was suppressed by ferrite phase in 7BT@3ferrite(CF/ZF/CZF) based composites.

- The grain size of plate like $BaTiO_3$ exists in between 12 μm to 8μm having a thickness of nearly 2μm. Spherical shapes of $BaTiO_3$ and polyhedral shape of ferrite phases are nearly 1 μm -2 μm in size.
- The theoretical densities of 7BT@3(CF/ZFCZF) varies in between 75 to 86 % and 3(CF/ZFCZF)@7BT composites are found to be in the range of 86% and 90%.

Dielectric and magnetic behavior of BT: ferrite composites:

- Permittivity and loss responses are independent of frequency in 20 wt% ferrite and dependent of frequency for 30 and 40 wt % ferrite based solid state derived composites.
- Composites prepared via in-situ and ex-situ synthesis methods shows frequency dependent permittivity and dielectric loss.
- In slid state derived composites 20 wt % ferrite systems shows nearly ferroelectric PE loop. But 30 and 40 wt% ferrites shows the lossy loop behavior.
- 20 wt% ferrite composites prepared via in-situ synthesis method shows the better ferroelectric loops. But, 30 and 40 wt% ferrites composites shows nearly ferroelectric loop. Comparatively in-situ derived composites shows better PE loops than solid-state derived composites.
- Composites i.e.,ferrite@BT which was prepared via ex-situ synthesis method show nearly ferroelectric type PE loop, but BT@ferite composites shows lossy PE loop.
- All ferrite based composites prepared via solid-state, in-situ and ex-situ methods show nearly ferromagnetic as observed from M-H loop.

Magneto-capacitance behavior of BT: ferrite composites

- Magneto-capacitance behavior in the solid-state mixed composites shows both positive and negative response. The magneto-capacitance behavior found to be dependent type of ferrite, percentage of ferrite, morphologies of individual phases. Cobalt and zinc ferrite based composites shows the negative magneto-capacitance response in all there wt% of ferrites and saturated at ~2 kOe. Also cobalt-ferrite based composite shows the highest magneto-capacitance among the selected ferrites at respective wt% of ferrite in the composites. Cobalt zinc ferrite based composite show the both positive (20 and 40 wt% ferrite composites) and negative (30 wt% ferrite composite) magneto capacitance response. Directions of magneto-capacitance response are dependent on both the magnetostriction and magneto-resistance of ferrite along with morphologies of individual phases in the microstructure. Microstructural effects on the magneto capacitance are dominated in the 30% cobalt-zinc ferrite composite, which was modified from positive to negative due to prominent plate like $BaTiO_3$ in the composite.
- In-situ derived magneto-dielectric composites show both positive and negative response depending on the ferrite type and percentage in the composites. Saturation in magneto-capacitance response of the in-situ derived composites is dependent on the both percentage and type of ferrite. Cobalt ferrite based composite shows the negative response, having 30wt% ferrite composite at higher value. Both cobalt and cobalt-zinc ferrite based

composite shows the positive and negative magneto-capacitance response. Though the grains in the in-situ derived composites distributed evenly with nearby same size, intrinsic properties like magnetostriction and magneto-resistance plays important role in magneto-capacitance behavior. Cobalt ferrite based composite shows the highest magneto-capacitance among the ferrite used in the in-situ derived composites at 30wt% ferrite in composite.

- Ex-situ derived magneto-dielectric composites show both positive and negative magneto-capacitance responses. Cobalt and zinc ferrite based composites shows the both positive and negative responses, particularly 7BT@3(CF/ZF) composites. Magneto resistance along with the microstructure effect plays important role in the magneto-capacitance behavior of ex-situ derived composites, which positive and negative magneto-capacitance (in BT@CF/ZF) behavior from core dominant and interfacial magneto resistances respectively. Cobalt-zinc-ferrite based ex-situ derived composite shows only positive magneto-capacitance response in both 7BT@3CZF and 3CZF@7BT. Magnetostriction effect is prominent in the cobalt-zinc ferrite based composites. Ex-situ derived magneto-dielectric composites show the highest magneto-capacitance among the synthesis methods used.

The plate-like morphology of BT and polyhedral shape of ferrite explore a new direction in modifying the magnetic, dielectric properties as well as enhancing the magneto-capacitance response of BT: ferrite based composite systems, which have potential applications in the field of sensors, actuators, and devices.

Scope for future work

- Wide range of ferrite percentages in composite can give clear understanding about origins of magneto-capacitance response.
- Different ferroelectric and ferromagnetic combinations should be studied to enhance the magneto-capacitance response.
- Study of temperature dependent dielectric, magnetic and magnetodielctric properties in magnetodielctric composites will be use full to understand interaction between the phases.

List of publications

1. Sreenivasulu Pachari, Swadesh K. Pratihar, Bibhuti B. Nayak **"**E*nhanced magneto-capacitance response in $BaTiO_3$–Ferrite composite systems***",** RSC Advances (Accepted).
2. Sreenivasulu Pachari, Swadesh K. Pratihar, Bibhuti B. Nayak **"**Improved magneto-capacitance response in combustion derived $BaTiO_3$-($CoFe_2O_4$/$ZnFe_2O_4$/$Co_{0.5}Zn_{0.5}Fe_2O_4$) composites**"** (Revised manuscript to be submitted in Journal of Alloys and Compounds).

References:

1. Y. Huan, X. Wang, J. Fang, L. Li, "*Grain size effect on piezoelectric and ferroelectric properties of $BaTiO_3$ceramics*", J. Eur. Ceram. Soc., **34**, (2014), 1445–1448.
2. H. Xu, L. Gao, J. Guo, "*Preparation and characterizations of tetragonal barium titanate powders by hydrothermal method*", J. Eur. Ceram. Soc., **22** (2002) 1163–1170.
3. S. K. Lee, T. J. Park, G. J. Choi, K. K. Koo, Sang Woo Kim, "*Effects of KOH/BaTi and Ba/Ti ratios on synthesis of $BaTiO_3$ powder by co-precipitation/hydrothermal reaction*", Mater. Chem. Phy., **82** (2003) 742–749.
4. C. Chena, Y. Wei, X. Jiao, D. Chen, "*Hydrothermal synthesis of $BaTiO_3$: Crystal phase and the Ba^{2+} ions leaching behavior in aqueous medium*", Mater. Chem. Phys., **110** (2008) 186–191.
5. S. Moon, H.W. Lee, C.-H. Choi, D. K. Kim, "*Influence of Ammonia on Properties of Nanocrystalline Barium Titanate Particles Prepared by a Hydrothermal Method*", J Am. Ceram. Soc., 95, (2012) 2248-2253.
6. M. Boulosa, S. G. Fritscha, T. F. Mathieua, B. Duranda, T. Lebeyb, V. Bley, "*Hydrothermal synthesis of nanosized $BaTiO_3$ powders and dielectric properties of corresponding ceramics*" Solid State Ionics **176** (2005) 1301 – 1309.
7. S. H. Jhunga, J.H. Leea, J.W. Yoona, Y. K. Hwanga, J.-S. Hwanga, S.-E. Parkb, J.-S. Chang, "*Effects of reaction conditions in microwave synthesis of nanocrystalline barium titanate*", Mater. Lett., **58** (2004) 3161–3165.
8. B. L. Newalkara, S. Komarnenia, H. Katsuki, "*Microwave hydrothermal synthesis and characterization of barium titanate powders*", Mater. Res. Bull., **36** (2001) 2347–2355.
9. T. V. Anuradha, S. Ranganathan, T. Mimani, K. C. Patil, "*Combustion synthesis of nanostructured barium titanate*", Scripta Mater., **44** (2001) 2237–224.
10. D. Rathore, R. Kurchania, R. K. Pandey, "*Influence of particle size and temperature on the dielectric properties of $CoFe_2O_4$ nanoparticles*", Int. J. Min. Metal. Mater., **21-4** (2014) 408.
11. K. Sinko, E. Manek, A. Meiszterics, K. Havancsa´k, U. Vainio, H. Peterlik, "*Liquid-phase syntheses of cobalt ferrite nanoparticles*" J. Nano Part. Res., **14** (2012), 894
12. I. Sharifi, H. Shokrollahi, M. Doroodmand, R. Safi, "*Magnetic andstructuralstudieson $CoFe_2O_4$ nanoparticles synthesized by co-precipitation, normalmicelles and reversemicelles methods*" J. Magn. Magn. Mater., **324** (2012) 1854–1861.
13. S. A. Khorrami, Q. S. Manuchehri, "*Magnetic Properties of Cobalt Ferrite synthesized by Hydrothermal and Co precipitation Methods: A Comparative Study*", J. Appl. Chem. Res., **7** (2013) 15-23.
14. F. Bensebaa, F. Zavaliche, P. L'Ecuyer, R.W. Cochrane, T. Veres, "*Microwave synthesis and characterization of Co–ferrite nanoparticles*", J. Coll. Inter. Sci., **277** (2004) 104–110.
15. C.K. Kima, J.-H. Lee, S. Katoh, R. Murakami, M. Yoshimur, "*Synthesis of Co-, Co-Zn and Ni-Zn ferrite powders by the microwave-hydrothermal method*", Mater. Res. Bull., **36** (2001) 2241–2250.

16. S. Hajarpour, K. Gheisari, A. H. Raouf, "*Characterization of nanocrystalline Mg0.6Zn0.4Fe2O4 soft ferrites synthesized by glycine-nitrate combustion process*", J. Magn. Magn. Mater., **329** (2013) 165–169.
17. G. Vaidyanathan, S. Sendhilnathanb, R. Arulmurugan, "*Structural and magnetic properties of $Co_{1-x}Zn_xFe2O4$ nanoparticles by co-precipitation method*", J. Magn. Magn. Mater., **313** (2007) 293–299.
18. A.V. Raut, R.S. Barkule, D.R. Shengule, K.M. Jadhav, "*Synthesis, structural investigation and magnetic properties of Zn^{2+}substituted cobalt ferrite nanoparticles prepared by the sol–gel auto-combustion technique*", J. Magn. Magn. Mater., **358-359**, (2014) 87-92.
19. P. Sivakumar, R. Ramesh, A. Ramanand, S. Ponnusamy, C. Muthamizhchelvan, "*Synthesis and characterization of nickel ferrite magnetic nanoparticles*", Mater. Res. Bull., **46** (2011) 2208–2211.
20. D. Bahadur, S. Rajakumar, A. Kumar, "*Influence of fuel ratios on auto combustion synthesis of barium ferrite nano particles*", J. Chem. Sci., **118** (2006) 15–21.
21. Y.Q. Dai, J.M. Dai , X.W. Tang, K.J. Zhang, X.B. Zhu, J. Yang, Y.P. Sun, "*Thickness effect on the properties of $BaTiO_3$–$CoFe_2O_4$ multilayer thin films prepared by chemical solution deposition*", J. Alloys Comp., **587**, (2014) 681-687.
22. L. Zhang, J. Zhai, W. Mo, X. Yao, "*Electrical and dielectric behaviors of composite $CoFe_2O_4$–$BaTiO_3$ thick films*", Mater. Chem. Phys., **118** (2009) 208–212.
23. D. Zhou, G. Jian, Y. Hu, Y. Zheng, S. Gong, H. Liu, "*Electrophoretic deposition of multiferroic $BaTiO_3/CoFe_2O_4$ bilayer films*", Mater. Chem. Phys., **127** (2011) 316–321.
24. D. Zhou, G. Jian, Y. Zheng, S. Gong, F. Shi, "*Electrophoretic deposition of $BaTiO_3/CoFe_2O_4$ multiferroic composite films"*, Appl. Sur. Sci., **257** (2011) 7621–7626.
25. F. Aguesse, A.-K. Axelsson, M. Valant, N. M. Alford, "*Enhanced magnetic performance of $CoFe_2O_4/BaTiO_3$ multilayer nanostructures with a $SrTiO_3$ ultra-thin barrier layer*", Scripta Mater., **67** (2012) 249–252.
26. K. S. Kim, S. H. Han, J. S. Kim, H. G. Kim, C. I. Cheon, "*Effect of working pressure on the properties of $BaTiO_3$–$CoFe_2O_4$ composite films deposited on STO (100) by PLD*", Mater. Lett., **64** (2010) 1738–1741.
27. L.V. Leonel, A. Righi, W.N. Mussel, J.B. Silva, N.D.S. Mohallem, "*Structural characterization of barium titanate–cobalt ferrite composite powders*" Ceram. Inter., **37** (2011) 1259–1264.
28. A. Khamkongkaeo, P. Jantaratana, C. Sirisathitkul, T. Yamwong, S. Maensiri, "*Frequency-dependent magnetoelectricity of $CoFe_2O_4$−$BaTiO_3$ particulate composites*", Trans. Nonferr. Met. Soc. China, **21** (2011) 2438-2442.
29. S. Agarwal, O. F.Caltun, K. Sreenivas, "*Magneto electric effects in $BaTiO_3$–$CoFe_2O_4$ bulk composites*", Solid State Comm., **152** (2012) 1951–1955.
30. I. Fina, N. Dix, L. Fàbrega, F. Sánchez, J. Fontcuberta, *"Magnetocapacitance in $BaTiO_3$–$CoFe_2O_4$ nanocomposites"*, Thin Solid Films **518**, (2010), 4634–4636.

31. M. Rafiquea, S. Q. Hassana, M.S.Awanb, S. Manzoor, *"Dependence of magnetoelectric properties on the magnetostrictive content in 0–3 composites"*, Cer. Int, **39**, (2013), S213–S216.
32. H. Yang, H. Wang, L. Hea, X. Yaoa, *"Hexagonal $BaTiO_3/Ni_{0.8}Zn_{0.2}Fe_2O_4$ composites with giant dielectric constant and high permeability",* Mat. Chem. Phy. **134**, (2012), 777-782.
33. H. Zheng, Lu Li, Z. Xu, W. Weng, G. Han, N. Ma, and P. Du, *"Ferroelectric/ferromagnetic ceramic composite and its hybrid permittivity stemming from hopping charge and conductivity inhomogeneity"*, J. App. Phy, **113**, (2013), 044101.
34. H. Zhenga, W.J. Wenga, G.R. Hana, P.Y. Du, *"Crucial role of percolation transition on the formation and electromagnetic properties of $BaTiO_3/Ni_{0.5}Zn_{0.47}Fe_2O_4$ ceramic composites*", Cer. Int, **41**, (2015), 1511–1519.
35. J. Nie, G. Xua, Y. Yang, C. Cheng, *"Strong magnetoelectric coupling in $CoFe_2O_4$–$BaTiO_3$ composites prepared by molten-salt synthesis method"*, Mat. Chem. and Phy **115**, (2009), 400–403.
36. S. Q. Ren, L. Q. WEeng, S.-H. Song, F. LI*, "$BaTiO_3/CoFe_2O_4$ particulate composites with large high frequency magnetoelectric response"*, J. mat. Sci, **40**, (2005), 4375 – 4378.
37. Yu Deng, J. Zhou, DiWuc, Y. Du, M. Zhang, D. Wang, H. Yu, S. Tang, Y. Du,*"Three-dimensional phases-connectivity and strong magnetoelectric response of self-assembled feather-like $CoFe_2O_4$–$BaTiO_3$ nanostructures",* Chem. Phy. Let, **496**, (2010), 301–305.
38. M.A. Ahmed. N. Okasha, N.G. Imam, *"Modification of composite ceramics properties via different preparation techniques",* J. Mag. Mag. Mat, **324**, (2012), 4136–4142.
39. A.R. Iordan, M. Airimioaiei, M.N. Palamaru, C. Galassi, A.V. Sandu, C.E. Ciomagad, F. Prihor, L. Mitoseriu, A. Ianculescu*, "In situ preparation of $CoFe_2O_4$–$Pb(ZrTi)O_3$ multiferroic composites by gel-combustion technique",* J. Eur. Cera. Soc., **29**. (2009) 807–2813.
40. C. Harnagea , L. Mitoseriu, V. Buscaglia, I. Pallecchi, P. Nanni, *"Magnetic and ferroelectric domain structures in $BaTiO_3$–$(Ni_{0.5}Zn_{0.5})Fe_2O_4$ multiferroic ceramics"* J. Eur. Cer. Soc. **27**, (2007), 3947–3950.
41. M. T. Buscaglia, V. Buscaglia, L. Curecheriu, P. Postolache, L. Mitoseriu, A. C. Ianculescu, Bogdan S. Vasile, Z. Zhe, and P. Nanni, *"Fe_2O_3@$BaTiO_3$ Core-Shell Particles as Reactive Precursors for the Preparation of Multifunctional Composites Containing Different Magnetic Phases"*, Chem. Mater. **22**, (2010) 4740–4748.
42. J. Chen , Z. Xu, S. Qu, X. Wei, X. Liu, *"Electromagnetic properties of ferroelectric-ferrite ceramic composites"*, Cer. Int, **34**, (2008) 803–807.
43. P.Penga, Y. Hua, Y. Liua, S. Chenb, J. Shia, R. Xionga, Y. Zhang, *"Magnetoelectric effect of $CoFe_2O_4/Pb(Zr,Ti)O_3$ composite ceramics sintered via spark plasma sintering technology",* Cer. Int, **41, (**2015) 6676–6682.
44. J. Peng, M. Hojamberdiev, H. Li, D. Mao, Y. Zhao, P. Liu, J. Zhou, G. Zhu, *"Electrical, magnetic, and direct and converse magnetoelectric properties of $(1-x)Pb(Zr_{0.52}Ti_{0.48})O_3$-$(x)CoFe_2O_4$ (PZT–CFO) magnetoelectric composites"*, J. Mag. Mag. Mat, **378** (2015) 298–305.

45. M. AzizarRahman, M.A.Gafur, A.K.M.AktherHossain, *"Structural, magnetic and transport properties of magnetoelectric composites"*, J. Mag. Mag. Mat, **345**, (2013) 89–95.
46. J. Rani, K.L. Yadav, S. Prakash, *"Dielectric and magnetic properties of* $xCoFe_2O_4$*–(1-x)[0.5*$Ba(Zr_{0.2}Ti_{0.8})O_3$*–0.5*$(Ba_{0.7}Ca_{0.3})TiO_3$*] composites"*, Mat. Res. Bul, **60**, (2014) 367–375.
47. B. Mojić-Lanté, J. Vukmirović, Konstantinos P. Giannakopoulos, D. Gautam, A. Kukovecz, V. V. Srdić, *"Influence of synthesis conditions on formation of core–shell titanate–ferrite particles and processing of composite ceramics",* Ceram. Inter, **41**, (2015) 1437–1445.
48. S. R. Jain and K. C. Adiga, *"A New Approach to Thermochemical Calculations of Condensed Fuel-Oxidizer Mixtures"*, Comb. Flames **40**, (1981) 71-79.
49. B. D. Cullity, *Elements of X-Ray diffraction*, Second edition ed., (1978).
50. A.B. Salunkhe, V.M. Khot, M.R. Phadatare, S.H. Pawar, *"Combustion synthesis of cobalt ferrite nanoparticles—Influence of fuel to oxidizer ratio"*, J. Alloy. Com, **514**, (2012) 91–96.
51. G. Catalana, *"Magneto-capacitance without magnetoelectric coupling",* Appl. Phy. Let, **88**, (2006) 102902.
52. R. Zhang, C. Deng, L. Ren, Z. Li, J. Zhou, *"Dielectric, ferromagnetic and maganetoelectric properties of* $BaTiO_3$*–*$Ni_{0.7}Zn_{0.3}Fe_2O_4$ *composite ceramics"*, Mat. Res. Bull, **48**, (2013) 4100–4104
53. Z. Yu, C. Ang, "*Maxwell–Wagner polarization in ceramic composites* $BaTiO_3$ *–* $(Ni_{0.3}Zn_{0.7})Fe_{2.1}O_4$", J. Appl. Phys., 91 (2002) 794-797.
54. A. Testino, L. Mitoseriu, V. Buscaglia, M.T. Buscaglia, I. Pallecchi A.S. Albuquerque e, V. Calzona, D. Marr´e, A.S. Siri, P. Nanni, *"Preparation of multiferroic composites of* $BaTiO_3$*–* $Ni_{0.5}Zn_{0.5}Fe_2O_4$ *ceramics"* J. Eur. Cer. Soc. **26**, (2006) 3031–3036.
55. L. Mitoseriu, I. Pallecchi, V. Buscaglia, A. Testino, C.E. Ciomaga, A. Stancu*, "Magnetic properties of the* $BaTiO_3$*–*$(Ni,Zn)Fe_2O_4$ *multiferroic composites"*, J. Mag. Mag. Mat **316** , (2007) e603–e606.
56. K. Raidongia, A. Nag, A. Sundaresan, and C. N. R. Rao, *"Multiferroic and magnetoelectric properties of core-shell* $CoFe_2O_4$*@*$BaTiO_3$ *Nanocomposites",* App. Phy Let, **97**, (2010) 062904
57. P.R. Mandal, T.K. Nath, *"Enhanced magnetocapacitance and dielectric property of* $Co_{0.65}Zn_{0.35}Fe_2O_4$*–*$PbZr_{0.52}Ti_{0.48}O_3$ *magnetodielectric composites",* J. Alloy. Comp. **599**, (2014) 71–77.
58. G. Srinivasan, E. T. Rasmussen, and R. Hayes*, "Magnetoelectric effects in ferrite-lead zirconate titanate layered composites: The influence of zinc substitution in ferrites",* Phy. rev. B **67**, (2003) 014418.
59. Y. Shen, J. Sun, L. Li, Y. Yao, C. Zhou, R. Sua and Y. Yang, *"The enhanced magnetodielectric interaction of (1-x)*$BaTiO_3$*–*$xCoFe_2O_4$ *multiferroic composites"*, J. Mater. Chem. C, (2014) **2**, 2545.
60. S. Singh, N. Kumar, R. Bhargava, M. Sahni, K. Sung, J.H. Jung, *"Magnetodielectric effect in* $BaTiO_3/ZnFe_2O_4$ *core/shell nanoparticles"*, J. Alloys and Comp, **587**, (2014) 437–44.